VALIDATION AND USE OF SATELLITE REMOTE SENSING DERIVED EVAPOTRANSPIRATION ESTIMATES IN SEMI-ARID REGIONS OF SOUTH AFRICA

Nobuhle Patience Majozi

VALIDATION AND USE OF SATELLITE REMOTE SENSING DERIVED EVAPOTRANSPIRATION ESTIMATES IN SEMI-ARID REGIONS OF SOUTH AFRICA

DISSERTATION

to obtain
the degree of doctor at the University of Twente,
on the authority of the rector magnificus,
prof.dr. T.T.M. Palstra
on account of the decision of the Doctorate Board,
to be publicly defended
on Friday 20 March 2020 at 14.45 hrs

by
Nobuhle Patience Majozi
born on 29 March 1981
in Mount Frere, South Africa

This dissertation has been approved by:

Supervisors
Prof.dr.ing. W. Verhoef
A/Prof.dr.ir. C.M.M. Mannaerts

Dissertation number 380

ISBN 978-90-365-4984-4
DOI 10.3990/1.9789036549844

Cover designed by Nobuhle Patience Majozi
Printed by ITC printing department

Graduation committee

Chair

Prof.dr.ir. A. Veldkamp

Supervisors

Prof.dr.ing. W. Verhoef

A/Prof.dr.ir. C.M.M. Mannaerts

Members

Prof.dr. A.D. Nelson	University of Twente
Dr.ir. C. van der Tol	University of Twente
Prof.dr.ir. P. van der Zaag	UN-IHE & TU Delft
Prof.dr.ir. Z. Bargaoui	ENIT - Universite El Manar, Tunis
Dr. A.S. Ramoelo	SanParks, Pretoria, SA
Dr. R. Mathieu	IRRI, Philippines

In loving memory of
my dearest mum, Agnes
Mamase Hiyashe

Summary

Evapotranspiration is a key component of the hydrological cycle and has been identified as an Essential Climate Variable (ECV). It plays a critical role in the carbon-energy-water nexus, with latent heat flux being the largest heat sink in the atmosphere. In semi-arid regions, actual evapotranspiration (ET) is almost equal to precipitation, and potential evapotranspiration exceeds precipitation. This prompts the importance of accurate estimation of this variable for improved water resource management in dry regions. However, estimation of ET from ground-based station data is challenged by the poor state of hydro-meteorological networks and low capital investment to maintain them in many countries.

Remote sensing technology is a critical tool in mapping evapotranspiration, especially in data-scarce and remote regions. This thesis evaluated the performance of remote sensing-based evapotranspiration estimates in semi-arid eco-climates. It also assessed the water productivity of different land use and land cover classes in South Africa, using remote sensing-based products of evapotranspiration, biomass, and precipitation.

A comprehensive analysis of the surface energy balance closure (SEBC) and partitioning of a 15-year (2000-2014) eddy covariance dataset from the Skukuza FLUXNET site was done in Chapter 2, to quantify and understand the quality of these data. With an overall surface energy ratio (EBR) of 0.93, the results showed the years of low and acceptable EBR and therefore were used to discard data of low quality. They also highlighted the variation of the surface energy balance closure per season, per year, including the climatic effects of wind speed, vapour pressure deficit and net solar radiation on the diurnal variations of the surface energy balance closure. The EBR analysis results were used to select periods of high-quality eddy covariance data that were used for evaluating the performance of the remote sensing-based ET models. Meanwhile, as characteristic of semi-arid regions, the energy partitioning analysis showed that sensible heat flux is the more dominant portion of net radiation during periods of little or no precipitation (low water availability) between March and October, than latent heat flux, and during the wet season latent heat was the more dominant flux. Water availability is a controlling factor in surface energy partitioning in tropical semi-arid ecoclimates.

In Chapter 3, we investigated the performance of two satellite-based ET retrieval methods and two large-scale ET products in two contrasting eco-climatic regions in South Africa. These were the Priestley-Taylor based land surface temperature/vegetation index (TsVI), the satellite-based Penman-Monteith (PM-Mu) model, and the large-scale ET products being the regional Meteosat

Second Generation ET (MET) and the Global Land-surface Evaporation: the Amsterdam Methodology (GLEAM)datasets. Our results were a reflection of previous ET model intercomparison studies, showing that no one model outperformed the others at the two sites across time. However, the PM-Mu model performed significantly better during periods of high evapotranspiration compared to periods of low evapotranspiration. For the large-scale and global evapotranspiration products, the biggest challenge was the spatial scale (10 to 25 km^2) which was compared against an average 1-km^2 ground measurement scale. In essence, our results conclude that further investigation of the PM-Mu model is possible to improve its estimation of ET measurements under dry conditions in South Africa.

Chapter 4 analysed uncertainty and sensitivity of core and intermediate input variables of a remote sensing data based version of the Penman-Monteith (PM-Mu) evapotranspiration (ET) model. This is a necessary step in environmental modelling, although it is often ignored in evapotranspiration modelling. The Welgegund FLUXNET site was used in this study, in addition to the Skukuza flux site due to data availability during the time of analysis. Absolute and relative uncertainties of the core meteorological and remote sensing-based, atmosphere and land surface input variables and parameters of the PM-Mu model were derived, and propagated through the intermediate parameters of net radiation and aerodynamic and surface resistances, to the final evapotranspiration uncertainty. Our analysis indicated relatively high uncertainties associated with relative humidity (RH), and hence, all the intermediate variables associated with RH, like vapour pressure deficit (VPD) and the surface and aerodynamic resistances in contrast to other studies who reported LAI uncertainty as the most significant. The semi-arid conditions and seasonality of the regional South African climate and high temporal frequency of the variations in VPD, air and land surface temperatures could explain observed uncertainties in this study. Moreover, the results also showed the ET algorithm to be most sensitive to the air - land surface temperature difference. Accurate assessment of those in situ and remotely sensed variables is required in order to achieve reliable evapotranspiration model estimates in these generally dry regions and climates. Apart from showing the most important input variables in PM-Mu model evapotranspiration estimation, these results give an indication of the effect of climate and land-use/ land cover change on evapotranspiration in this semi-arid region.

Finally, an assessment of remote sensing-based water use and productivity of different land use/ land cover classes was done, based on data from the FAO WaPOR platform. An accuracy assessment of the WaPOR precipitation and ET products showed a reasonable performance of the evapotranspiration product,

whereas the precipitation accuracy was quite low. The variability of biomass, water use and productivity was captured across the different land-use and land cover classes. However, a proper assessment of biomass production and water productivity for individual crops was not yet achieved, because the individual growth cycles for specific crops in all the regions need to be determined and are not yet available for South Africa from WaPOR. The biomass data are also available for C3 and C4 crops, and require conversion to estimate biomass for other crop and vegetation types.

Samenvatting

Verdamping is een belangrijk onderdeel van de hydrologische cyclus en is erkend als een essentiële klimaatvariabele (ECV). Verdamping speelt een cruciale en verbindende rol in de koolstof, energie en water cycli op aarde. Met name de latente warmteopslag en uitwisselingen zijn de grootste bron van energie in de atmosfeer. In semi-aride gebieden is actuele verdamping bijna gelijk aan neerslag, en potentiële evapotranspiratie aanzienlijk hoger. Dit duidt het belang van een nauwkeurige schatting van verdamping ter verbetering van het waterbeheer met name in droge gebieden. De bepaling van verdamping middels conventionele metingen van meteorologische stations, wordt gehinderd door de gemiddeld slechte staat en beperkte ruimtelijke dichtheid van hydro-meteorologische netwerken en lage kapitaalinvesteringen om deze te onderhouden in vele landen.

Aardobservatie technologie kan een cruciaal hulpmiddel zijn voor het bepalen en in kaart brengen van verdamping, vooral in afgelegen gebieden met weinig of geen grondgegevens. Dit proefschrift evalueerde de prestaties van berekeningen van verdamping door middel van aardobservatie in semi-aride ecosystemen in Zuid-Afrika. Het evalueerde ook de waterproductiviteit, afgeleid met behulp van aardobservatie, van verschillende landgebruik en bodembedekking klassen, in Zuid Afrika.

Een uitgebreide analyse van de straling- en energiebalans van het landoppervlak, alsmede het balansoverschot en de verdeling (partitie) van zonnestraling in andere energie componenten, van een 15-jarige (2000-2014) eddy covariantie dataset van de Skukuza Fluxnet-site werd behandeld in hoofdstuk 2. Dit om de kwaliteit van deze meetgegevens te kwantificeren en beter te begrijpen. De energie balans ratio (EBR) of de verhouding tussen, a> zonnestraling minus grond opwarming door warmte geleiding en b> de convectieve en latente warmte stromingscomponenten werd gebruikt om gegevens van lage kwaliteit te verwijderen. Ze benadrukten ook de variatie van het energiebalans overschot aan het landoppervlak per seizoen, per jaar, inclusief de weer invloeden zoals windsnelheid, waterdampdruk deficit en netto zonnestraling, op de dagelijkse variaties van de energiebalans aan het landoppervlak. De EBR analyseresultaten werden gebruikt om perioden van hoogwaardige eddy-covariantie gegevens te selecteren die werden gebruikt voor het evalueren van de prestaties van op satelliet data gebaseerde ET-modellen. Ondertussen, als kenmerk voor semi-aride gebieden, toonde de analyse van de energieverdeling aan, dat de voelbare of convectieve warmteflux de meest dominante omzetting vormt van de netto zonnestraling tijdens

perioden van weinig of geen neerslag (lage waterbeschikbaarheid) tussen maart en oktober. Tijdens het natte seizoen was de latente warmte uitwisseling of verdampingswarmte dan weer de meest dominante energieomzetting. De beschikbaarheid van water (neerslag en bodemvocht) bleek een bepalende factor bij de verdeling van zonnestralingsenergie aan het landoppevlak in tropische semi-aride ecoklimaten.

In hoofdstuk 3 hebben we de prestaties onderzocht van twee op satelliet gebaseerde berekeningsmethoden voor verdampings (ET) en twee globale of regionale ET-data producten in twee contrasterende ecoregio's in Zuid-Afrika. Dit waren de op het Priestley-Taylor model gebaseerde landoppervlakte temperatuur / vegetatie-index (TsVI), en een op satelliet data gebaseerde Penman-Monteith (PM-Mu) model. De ET- data producten zijn de Meteosat Second Generation ET (MET) en de Global Land-oppervlakte-verdamping: Amsterdam Methodology (GLEAM). Onze resultaten waren een weerspiegeling van eerdere onderzoeken naar de toepassing van ET-modellen, die aantoonden dat geen enkel model op jaarbasis beter presteerde dan de andere op de twee locaties. Het PM-Mu-model presteerde echter significant beter tijdens perioden van hoge verdamping in vergelijking met perioden van lage verdamping. Voor de wereldwijde evapotranspiratieproducten was de grootste uitdaging de ruimtelijke schaal (e.g. 10 km^2) die werd vergeleken met een gemiddelde meetschaal aan de grond van ongeveer 1 km^2. Onze resultaten toonden aan dat verder onderzoek van het PM-Mu model mogelijk is om de schatting van lage ET-metingen onder droge onstandigheden en dus in semi-aride gebieden in Zuid-Afrika te verbeteren.

Hoofdstuk 4 analyseerde de onzekerheid en gevoeligheid van basis- en intermediaire input variabelen van een op satelliet data gebaseerde versie van het Penman-Monteith (PM-Mu) verdampings (ET)-model. Onzekerheid- en gevoeligheidsanalyse is een noodzakelijke stap in elke wiskundige modellering, hoewel het vaak wordt genegeerd bij verdampingsmodelleren. De Welgegund Fluxnet site werd mede gebruikt in deze studie, naast de Skukuza flux-site vanwege de beschikbaarheid van gegevens tijdens de analyse periode. Absolute en relatieve onzekerheden van de meteorologische en op satelliet data gebaseerde variabelen en parameters voor de input van de atmosferische- en landoppervlakte gegevens van het PM-Mu-model werden afgeleid. De propagatie van fouten en onzekerheden, via de tussenliggende variabelen, o.a. netto zonnestraling en aerodynamische- en oppervlakte weerstandsvariabelen, werd ook uitgevoerd om tot de uiteindelijke totale onzekerheid van verdamping te komen. Onze analyse wees op relatief hoge onzekerheden geassocieerd met relatieve vochtigheid (RH), en dus alle intermediaire variabelen geassocieerd

met RH, zoals het waterdampdruk deficit (VPD) en de oppervlakte- en aerodynamische luchtweerstanden. Dit in tegenstelling tot vele andere studies die de “leaf area index” (LAI) of blad oppervlakte index als grootste onzekerheid en als meest significant rapporteerden. De semi-aride omstandigheden en grote seizoensgebondenheid van o.a. neerslag van het regionale Zuid-Afrikaanse klimaat en de zeer hoge tijdvariaties in luchtvochtigheid, lucht- en landoppervlaktetemperaturen kunnen de waargenomen onzekerheden in deze studie verklaren. Bovendien toonden de resultaten ook aan dat het PM-Mu ET-algoritme het meest gevoelig was voor het temperatuurverschil tussen lucht en het landoppervlak. Een nauwkeurige beoordeling van deze “in situ” en op afstand door satelliet waargenomen temperatuur variabelen is vereist om betrouwbare schattingen van een verdampingsmodel te verkrijgen in deze droge regio's en klimaten. Naast het aantonen van onzekerheden van de belangrijkste model variabelen in de schatting van verdamping met het PM-Mu-model, geven deze resultaten ook een goede indicatie van het effect van klimaatverandering en veranderingen in landgebruik en bodembedekking op verdamping in deze semi-aride regio’s van Zuid Afrika.

Ten slotte is een evaluatie gemaakt van op satelliet data gebaseerde watergebruik en productiviteit schattingen van verschillende landgebruiks- en bodembedekking klassen, gebruik makend van data van het FAO WaPOR-data platform. Een nauwkeurigheidsbeoordeling van de WaPOR-neerslag en ET-producten toonde een redelijke prestatie van het verdampingsproduct, terwijl de neerslagnauwkeurigheid vrij laag was. De variabiliteit van biomassa, verdamping en waterproductiviteit werd geanalyzeerd voor de verschillende klassen van landgebruik en bodembedekking. Een volledige beoordeling van biomassaproductie en waterproductiviteit voor individuele gewassen was op dit moment nog niet mogelijk, omdat de gegevens over de groeicyclus van vele gewassen in de regio’s, vooral jaarlijks beschikbaar zijn voor Zuid-Afrika. De biomassagegevens zijn ook beschikbaar voor C3- en C4-gewassen en vereisen een goede conversie om biomassa correct in te schatten voor andere gewassen en vegetatie.

Acknowledgements

When I completed my MSc in 2011, I shared that I would like to further my studies after a two-year break. Little did I know that this wish would be granted at the appointed time. This Ph.D. journey has truly been a life-changing experience for me and it would not have been possible without the support and guidance that I received from a number of people and institutions.

I begin with acknowledging the Council for Scientific and Industrial Research, and the National Research Foundation (under the then Department of Science and Technology), without whose funding and resources I would not have been able to do this Ph.D.; and the ITC Faculty of the University of Twente who afforded me the opportunity to study under their tutelage. Special appreciation goes to my supervisors Prof. Wouter Verhoef, Dr. Chris Mannaerts, and Dr. Renaud Mathieu. Wouter and Chris, thank you for believing in my potential and accepting me into this Ph.D. program. Chris, your patience and guidance kept me going, even when the journey became too tough for me. Our regular meetings, face to face when I was at ITC, and via Skype, helped give focus and direction to my research work. Thank you for encouraging my research and allowing me to grow as a research scientist. Renaud, each manuscript I submitted to you was dealt with a critical and thorough review. Also, your advice on research and career development has been insurmountable, much appreciation. Dr. Abel Ramoelo, my mentor and friend, those long discussions we had, on how to pen each chapter, running the models, advice on research and life, in general, helped a lot, especially when the going was really tough. Colleagues and friends in the corridors of CSIR and the ITC, the experiences we shared during our regular conversations, encouraging one another, are appreciated.

Last but not least, my family. My gratitude goes to you for being my pillar during the long years trying to complete this journey. To my daughter Lindelwa Grace, you inspired me to give it my all to finish this Ph.D. I always looked forward to the refreshing smile and warm hug that awaited me after a long, exhausting day.

All glory is to God.

Table of Contents

List of Figures

List of Tables

Nomenclature

Symbols

α	surface albedo	
A	available energy	Wm^{-2}
Ac	available energy in the canopy	Wm^{-2}
As	available energy at the soil surface	Wm^{-2}
Cc	bulk canopy conductance	sm^{-1}
CL	biome-specific mean potential stomatal conductance	sm^{-1}
Cι	leaf scale stomatal conductance	sm^{-1}
Cρ	specific heat capacity of air	$Jkg^{-1}K^{-1}$
λE (LE)	latent heat flux or evapotranspiration	Wm^{-2} or mm
ε	surface emissivity	
e	actual vapor pressure	Pa
es	saturation vapor pressure	Pa
Go	ground heat flux	Wm^{-2}
H	sensible heat flux	
Rnet	net radiation	Wm^{-2}
ρ	density of moist air	kgm^{-3}
ra	aerodynamic resistance	sm^{-1}
r_a^s	aerodynamic resistance to soil evaporation	sm^{-1}
r_a^t	aerodynamic resistance to canopy transpiration	sm^{-1}
r_a^{wc}	aerodynamic resistance to wet canopy evaporation	sm^{-1}
rs	surface resistance	sm^{-1}
r_s^{tot}	surface resistance to soil evaporation	sm^{-1}
r_s^t	surface resistance to canopy transpiration	sm^{-1}
r_s^{wc}	surface resistance to wet canopy evaporation	sm^{-1}
s	slope of the saturation vapor pressure versus temperature	PaK^{-1}
Tair	air temperature	K
u	wind speed	ms^{-1}
VPD	Vapor Pressure Deficit	Pa
ϕ	Priestley-Taylor coefficient	
λ	latent heat of vaporization	Jkg^{-1}
γ	psychrometric constant	PaK^{-1}

Abbreviations

AGBP	Above Ground Biomass Production
ALEXI	Atmosphere-Land EXchange Inverse
DOY	day of year
DTD	Dual Temperature Difference
EBR	energy balance closure
EC	eddy covariance
EF	evaporative fraction
ETp	potential evapotranspiration
ETo	reference evapotranspiration
ETEML	Enhanced Two-Source Evapotranspiration Model for Land
EVI	Enhanced Vegetation Index
ECV	essential climate variables
EUMETSAT	European Organisation for the Exploitation of Meteorological Satellites
FAO	FAO Food and Agriculture Organization of the United Nations
FPAR	fraction of photosynthetically active radiation
GBWP	Gross Biomass Water Productivity
GCOS	Global Climate Observing System
GEO	Group on Earth Observation
GEOS-5	Goddard Earth Observing System Data Assimilation System Version 5
GLEAM	Global Land Evaporation Amsterdam Model
GLDAS	Global Land Data Assimilation System
GMAO	Global Modelling and Assimilation Office
GSA	global sensitivity analysis
H-TESSEL	Hydrology Tiled ECMWF Scheme for Surface Exchanges over Land
IWMI	Institute for Water Education and the International Water Management Institute
ISO GUM	International Organisation for Standardisation, Guides to the expression of Uncertainty in Measurement
JPL	Jet Propulsion Laboratory
KNP	Kruger National Park
LAI	Leaf Area Index
LSA	local sensitivity analysis
LSA-SAF	Satellite Application Facility on Land Surface Analysis

LST	land surface temperature
METRIC	Mapping EvapoTranspiration at high Resolution with Internalized Calibration
MODIS	Moderate Resolution Imaging Spectroradiometer
NBWP	Net Biomass Water Productivity
NDVI	Normalized Differenced Vegetation Index
NPP	Net Primary Production
OLS	ordinary least squares
PM	Penman-Monteith
PT	Priestley-Taylor
PCR-GLOBWB	PCRaster Global Water Balance
RH	Relative Humidity
RMSE	Root-Mean-Squared Difference
RS	remote sensing
SA	sensitivity analysis
SAFARI	Southern African Regional Science Initiative
SBA	societal benefit area
SEB	surface energy balance
SEBAL	Surface Energy Balance Algorithm over Land
SEBC	surface energy balance ratio
SEBI	Simplified Surface Energy Balance Index
SEBS	Surface Energy Balance System
S-SEBI	Simplified Surface Energy Balance Index
SSEBop	Operational Simplified Surface Energy Balance
TSEB	two source energy balance model
TSM	Two-Source Model
TSTIM	Two-Source Time Integrated Model
UA	uncertainty analysis
UNESCO	United Nations Educational, Scientific and Cultural Organization
WP	water productivity

1 INTRODUCTION

1.1 Background

Water is the most abundant element on the Earth's surface (about 71%); however, 96.5% is held in oceans, and therefore not fit for human consumption. Of the remaining 3.5%, 87% is inaccessible, locked in either polar icecaps or deep underground aquifers. Therefore, only 0.4% is available as renewable freshwater for human consumption (Cap-Net, 2014). Water constantly changes from one state to another, reaching the land as precipitation (liquid or snow) and returning to the atmosphere through evapotranspiration (ET) in gaseous form, and some is available as runoff and groundwater storage. Global estimates of evapotranspiration are 60-65% of precipitation Rockström & Gordon, 2001; Trenberth et al., 2007). In semi-arid regions (with an Aridity Index of 0.2 to 0.5) (Middleton and Thomas 1997), however, precipitation is highly variable and unpredictable, with ET almost equal to, and potential ET (ET_p) being significantly higher than precipitation (Kurc & Small, 2004; Sala et al., 1992). These areas cover over 40% of the terrestrial surface and are expected to be highly sensitive to climate and land-use change (Asner et al., 2003; Jia et al., 2014). This, combined with the spatial and temporal variability of each hydrological cycle component and/or process, makes water resources planning and management complex. Despite the importance of establishing water resources management principles and practices at operational scale, there is insufficient information on water use by different land uses (UNESCO & Earthscan, 2009). In sub-Saharan Africa particularly, this is further aggravated by the poor state of hydro-meteorological networks and low capital investment to maintain them.

Evapotranspiration is a key component of the hydrological cycle. It is listed as one of the 48 observation priorities of water societal benefit area (Water SBA) by the Group on Earth Observation (GEO) (GEO, 2010), as well as one of the essential climate variables (ECV) (GCOS, 2009). It is a critical nexus between the energy, water and carbon cycles, with latent heat of vapourisation serving as the largest heat sink in the atmosphere (Trenberth et al., 2009). It facilitates the continuation of precipitation by replacing the vapour lost through condensation (Brutsaert, 2009), and is crucial for the transportation of minerals and nutrients required for plant growth as well as creating a beneficial cooling process to plant canopies in many climates. Consequently, it plays an important role in hydrology, agriculture, meteorology, and climatology.

Accurate estimates of ET contribute to confidence in the quantification of the catchment water balance and facilitate a variety of operational and management actions in sustainable water resources management (Allen et al., 2007; Mu et al., 2007; Su, 2002). The accurate ET estimates also improve how we understand the state, spatial and temporal variability of this

significant component of the water cycle at different scales. Managing the evaporative water use from various landscapes and at different scales is important to researchers, water resource managers, and policymakers. To do so, the relationship between land use, water resources, and their use needs to be described quantitatively and accurately (Jewitt, 2006). However, quantifying this variable comes with a number of challenges because of its high spatio-temporal variability, and the uncertainties that originate from the indirect nature of its measurement.

Semi-arid regions, for instance in Southern Africa, are characterised by abundant sunshine, high rainfall variability, frequent droughts, low soil moisture and extreme events such as flash floods. These conditions provide the foundation for climatic and water vulnerability of communities in these areas, which can ultimately threaten community health and food security. Improving the water resources management of semi-arid regions requires accurate knowledge of the hydrological processes involved. Indeed, data scarcity is still a major bottleneck for improving sustainable water use and water resources management. Worldwide, river flow monitoring networks are in decline and other hydrometeorological measurements tend to follow the same fate, due to lack of maintenance (Maidment et al., 2014; Pegram & Bárdossy, 2013). On the other hand, advances in remote sensing and numerous recent satellite missions have generated a wealth of potentially relevant data that may lead to improved water resources management.

1.2 Problem statement

Evapotranspiration is one of the major hydrologic processes, and is responsible for regulating the water and energy balance of the Earth's atmosphere, biosphere, and hydrosphere; hence, it has been under significant investigation for over a century (Bowen, 1926; Dalton, 1802; Rohwer, 1931). ET is a challenging variable to measure due to its high spatial and temporal variability, and the complexity of the associated hydrometeorological processes. In (semi-) arid regions, this is exacerbated by the fact that a large proportion of the low and sporadic precipitation is returned to the atmosphere via ET. These regions face water scarcity, which is a major constraint on economic welfare and sustainable development. Techniques have been developed to measure and estimate ET at different scales. They are categorised into methods based on i) direct measurements with porometry or lysimeters (Allen et al., 1991; Gebler et al., 2015; López-Urrea et al., 2006), and soil moisture depletion measurements (Hillel, 1982); and ii) atmospheric measurements, including micrometeorological and energy balance techniques like Bowen ratio (Bowen, 1926; Peacock & Hess, 2004; Perez et al., 1999), eddy correlation (D. Baldocchi et al., 2001; R Leuning et al., 1982; John L. Monteith & Unsworth, 2013; Stull,

2012), and scintillometry (Hemakumara et al., 2003; S. M. Liu et al., 2013a; Meijninger et al., 2006). The high cost of establishing and maintaining these (in)direct measurement systems through field networks continues to present an obvious limitation in understanding and monitoring ET dynamics. Hence, models were also developed to estimate this variable from routinely available meteorological and land surface characteristics data (Bouchet, 1963; Hargreaves & Samani, 1982; J. Monteith, 1963; J. L. Monteith; Penman, 1948; Priestley & Taylor, 1972). These techniques and methods mainly estimate ET at local, field-scale or as an average over a large area. However, the spatial averaging of ET presents inaccuracies because of its high spatial variability and complexity of the associated hydrometeorological processes.

The emergence of remote sensing (RS) technology, consequently, presented the research community with the opportunity to map ET and investigate its use and dynamics at larger spatial scales. RS provides spatially explicit and relatively frequent measurements of biophysical variables that affect ET, such as land cover type, surface albedo (α), emissivity (ε) and density, hence it provides inputs to ET models. Research has been conducted to develop RS based ET mapping models. Based on their structural complexities, theories and underlying assumptions, parameterisations, and uncertainties and limitations, these models are categorised under: (i) empirical methods that use statistically-derived relationships between ET and vegetation indices such as the normalised difference vegetation index (NDVI) or the enhanced vegetation index (EVI), or between ET and the difference between surface and air temperatures; (ii) residual surface energy balance methods, including the Surface Energy Balance Algorithm over Land (SEBAL), Mapping EvapoTranspiration at high Resolution with Internalized Calibration (METRIC), Surface Energy Balance System (SEBS), Atmosphere-Land EXchange Inverse (ALEXI); (iii) physically-based methods involving the Penman-Monteith (PM) and the simpler Priestley–Taylor (PT) equations; and (iv) data assimilation methods applied to the heat diffusion equation and radiometric surface temperature sequences.

Remote sensing-based ET models are under constant refinement to improve their accuracies, especially in non-water stressed climates where there are more established, long-term calibration and validation (cal/val) ET measurement and weather stations, including eddy covariance systems, lysimeters, and large aperture scintillometers. The refinements also include the models evolving from single-source energy balance models, where vegetation and soil are analysed in a combined energy budget, to dual-source models, where vegetation and soil energy budgets are analysed separately, and multi-source and multi-layer models where vegetation, soil and intercepted precipitation are analysed separately. A number of issues and/or challenges are, however, presented in

semi-arid regions, especially Sub-Saharan Africa, which has fewer hydrological measurement networks for rigorous cal/val of ET models. These regions are also water-scarce, which is an additional constraint when applying models that were initially developed for non-water strained environments.

The issues which will be discussed in this thesis (and more in-depth literature review from Chapter 2 to Chapter 4) include, although not limited to, the ones detailed in Section 1.3.

1.3 Literature review

1.3.1 Eddy covariance flux data quality and surface energy partitioning

Turbulent fluxes, i.e. sensible and latent heat fluxes, are key variables of the energy and water exchanges in the land-atmosphere interactions. They are responsible for the dynamics of the energy, water, and biogeochemical cycles while driving the evolution and characteristics of the planetary boundary layer, such as its depth, thermodynamic behaviour, surface-air temperature, and humidity. The partitioning of available solar radiation into turbulent fluxes impacts the hydrological cycle, planetary boundary layer characteristics, cloud development, and climate. How the partitioning varies across different climates is a function of, among others, water availability, solar radiation, and land surface/ vegetation characteristics. Studies on surface energy partitioning have been covered under different climates with varying results.

To measure these fluxes, techniques like the scintillometer, lysimeter, and eddy covariance (EC) systems have been developed. So far, the EC technique is considered the most reliable method for measuring carbon, energy and water fluxes, and has become a standard measurement technique in the study of the surface-atmosphere boundary layer. Combined with measurements of solar radiation and soil heat flux, this technique provides detailed data for the estimation of the terrestrial water, energy, and carbon balances, and for the understanding of the related physical and biological processes (Aubinet et al., 1999; Baldocchi et al., 2001; Law et al., 2002). They play a critical role in the calibration and validation of ecosystem, climate, and land-surface models. More details on its practical and theoretical aspects are given by Leuning et al. (1982), Goulden et al. (1996), Finnigan et al. (2003), Baldocchi et al. (2001), and Gash and Dolman (2003). Many EC systems have been established across the globe for long-term monitoring of the different fluxes under the FLUXNET network. However, most of the stations are deployed in the Northern Hemisphere than the Southern Hemisphere, especially Sub-Saharan Africa (Baldocchi, 2008; Baldocchi, 2003; Schmid, 1994; Wofsy et al., 1993). The lack of instrumentation in these regions means there are limited long-term flux measurements to study

the energy flux partitioning and its control, to support comprehensive analyses of the land surface exchange processes and to advance model development and validation (Kurc & Small, 2004; Saux-Picart et al., 2009).

As much as EC systems are the most reliable, they pose a number of challenges in terms of data processing methods and quality, especially under complex conditions (such as heterogeneous topography and unfavourable weather, like high turbulence and low wind speed). These result in surface energy imbalance, where available energy (A), i.e. net radiation less soil heat flux (Rnet-G), does not equal the sum of turbulent fluxes (sensible heat flux (H) plus latent heat flux (λE)). This lack of surface energy balance closure has significant implications on how energy flux measurements are interpreted and their use in cal/ val of land surface and climate models. Extensive research done to assess this issue has shown a closure error of 20 – 30% (Barr et al., 2012; Chen et al., 2009; Foken et al., 2010; Mauder et al., 2007), with the surface energy balance closure (SEBC) assessment being a standard performance criterion of EC flux data (Twine et al., 2000; Wilson et al., 2002). The non-closure of the SEB has been documented to be a result of a number of factors, such as the exclusion of soil and canopy heat storage, low and high-frequency turbulence in the computation of the turbulent fluxes, advective flux divergence, and inadequate sampling of large-scale, land surface heterogeneities, systematic measurement and sampling errors.

As a standard for quality assessment of eddy covariance data, the SEB closure will be investigated. Furthermore, how the solar radiation is partitioned into the two fluxes in a semi-arid FLUXNET site will be addressed in this thesis.

1.3.2 Performance of remote sensing-based ET models

Using the fundamentals of ET estimation, such as the surface energy balance, great strides have been made on developing models to estimate ET using remote sensing techniques. These models incorporate meteorological and land surface parameters retrieved quantitatively from satellite remote sensing data to estimate ET. Until recently, these models have been calibrated and rigorously validated in temperate regions due to the availability of in situ networks that have provided long-term data. The emergence of remote sensing technology has proven invaluable in providing routine data that cannot be represented by point measurements, and due to its relative accuracy and cost-effectiveness. Intensive reviews have been done on the different RS based ET models, resulting in them being categorised as shown in Section 1.2 (Carlson, 2007; Kalma et al., 2008; Liou & Kar, 2014; Vinukollu et al., 2011a; Wang & Dickinson, 2012; Zhang et al., 2016). A recent review examines issues beyond the already tried and tested ET models, and highlights , need for new paradigms in ET estimation (McCabe et al., 2019). Prior to reviewing the intercomparison studies of the

different ET methods that have been done, a brief look at each category of the models will be done.

Surface energy balance (SEB) models were the earliest to be used to estimate ET using RS data as inputs. In this approach, latent heat flux (λE) is estimated as a residual of the surface energy budget and heat transfer equation. The main difference in these methods is the estimation of sensible heat flux (H). In single-source SEB models, like the Surface Energy Balance Algorithm for Land (SEBAL; Bastiaanssen et al. (1998a); W. G. M. Bastiaanssen et al. (1998b)), Simplified Surface Energy Balance Index (S-SEBI; Roerink et al. (2000), Surface Energy Balance System (SEBS; Su (1999, 2002)), Mapping Evapotranspiration at High Resolution with Internalized Calibration (METRIC; Allen et al. (2007)), and Operational Simplified Surface Energy Balance (SSEBop; Senay et al. (2014)), H estimation is based on how the dry (maximum H and minimum λE) and wet (maximum λE and minimum H) limits are defined, as well as interpolating between the defined lower and upper limits of H and λE for a given set of parameters. One major assumption of the single source models is that there are little or no changes to the surface available energy in space, with sufficient land surface variation to allow for dry and wet limits to be identified within the study area. SEBS was evaluated in this thesis, however, due to calibration difficulties around model stability, it was not reported on in Chapter 3. Dual-source SEB models, on the other hand, estimate soil evaporation and transpiration separately by using different resistances for the two surfaces. These models include the two source energy balance model (TSEB), Two-Source Model (TSM; (Norman et al., 2000), Two-Source Time Integrated Model (TSTIM; (Anderson et al., 1997)), Atmosphere-Land Exchange Inverse (ALEXI; (Anderson et al., 2007)), Dual Temperature Difference (DTD; (Norman et al., 2000)), and Enhanced Two-Source Evapotranspiration Model for Land (ETEML; Yang et al., 2015b)).

Combination type models, like the Penman-Monteith (PM) (Monteith, 1965; Penman, 1948) incorporate the energy (i.e. the energy required to maintain evapotranspiration) and aerodynamic terms (for the atmosphere's ability to remove water vapour from the surface). Deemed as the standard for ET estimation, the PM model has been adopted by the Food and Agriculture Organization of the United Nations (FAO) in crop ET modelling, as well as a basis in the development of the SEB models. The use of remote sensing data as inputs to this algorithm has also been studied intensively (Cleugh et al., 2007; Leuning et al., 2008; Mu et al., 2007). The initial single-source PM model has been adapted into a multi-source model that estimates transpiration, soil and intercepted evaporation separately (Mu et al., 2011). Also, different versions of PM, for instance, those that include soil moisture to constrain surface conductance, instead of using vapour pressure deficit as a proxy, and

modifications in the parameterisation of the resistances, are also available (Bai et al., 2017; Chang et al., 2018; Di et al., 2015; Sun et al., 2013). Meanwhile, Priestley-Taylor (Priestley & Taylor, 1972), which is a simplified version of PM, has also been applied to estimate ET using remote sensing data. Modifications to the PT include adaptations to estimate the evaporative fraction (EF) using the PT parameter (α_{PT}) and the triangle feature space between NDVI and LST (land surface temperature) (Ts-VI ET estimation method), surface albedo and vegetation fraction cover; and incorporating ecophysiological constraint functions (Jet Propulsion Laboratory PT (JPL-PT) method), and the rainfall interception loss (Fisher et al., 2008; Jiang & Islam, 1999, 2001; Miralles et al., 2011; Song et al., 2016; Wang et al., 2006; Yao et al., 2013; Yao et al., 2014).

Furthermore, efforts have been made to generate global RS based ET products by employing the described methods. The Penman-Monteith based (MOD16 ET) product is derived using MODIS land surface characteristics products and meteorological data generated by the Global Modelling and Assimilation Office (GMAO) Goddard Earth Observing System Data Assimilation System Version 5 (GEOS-5), as inputs (Mu et al., 2007; Mu et al., 2011). On the other hand, the EUMETSAT Satellite Application Facility on Land Surface Analysis (LSA-SAF) derived Meteosat Second Generation geostationary satellites ET product (MET) using the SEVIRI products, based on the Hydrology Tiled ECMWF Scheme for Surface Exchanges over Land (H-TESSEL) scheme (Ghilain et al., 2011; Ghilain et al., 2012; Ghilain et al., 2014). The MET product also uses a version of PM in its estimation of latent heat flux. The Global Land Evaporation Amsterdam Model (GLEAM) model is made up of different algorithms, the base being the PT equation, then a soil water module, stress module, and the interception module. All these modules are driven by remote sensing data to estimate different components of ET (Martens et al., 2017; Miralles et al., 2011).

Validating these remote sensing ET models is essential for them to be used confidently under different eco-climates. Although validation exercises have commonly focused on single models, ET model intercomparison studies have been done to rank their performance across different eco-climates. In other instances, ET models have been intercompared to gain a better understanding of their differences and possible disparities between the models. In other cases, these are done to understand the effect of energy and moisture exchange and transport processes on climate feedback. Finally, studies were done to select the best performing models for water management, use and application purposes. Despite that they cover different eco-climates, most intercomparison studies have mainly concentrated in the Northern Hemisphere and the Australian region. For instance, as much as their evaluation covered arid and semi-arid regions, Michel et al. (2015) evaluated PT-JPL, PM-Mu, SEBS and the

GLEAM in 24 FLUXNET sites in Australia, Europe, and North America. Their results showed good performances of PT-based models (PT-JPL and GLEAM), while PM-Mu mostly underestimated and SEBS showed a systematic overestimation of ET. They also reported on the low performances of the ET models in dry regions. Similarly, Miralles et al. (2016) assessed global ET products derived using the same models (except SEBS) against catchment water balance estimated ET in 837 catchments. PM generally underestimated ET throughout the continents. PT-based models show overestimations in Europe and Amazonia and lower than average ET in North America, but disagree in water-stressed regions of Africa and Australia due to the model representation of evaporativestress. McCabe et al. (2015) also reported the poor performance of the same models in water-stressed regions. Chirouze et al. (2014) intercompared four SEB models (S-SEBI, TSEB, SEBS and a modified triangle method, VIT) in irrigated semi-arid Yaqui Valley of Mexico. They reported poor performance of the models during senescence, which they attribute to poor partitioning of turbulent fluxes and of the ET components of evaporation and transpiration. In the African continent, Trambauer et al. (2014) intercompared the MOD16 and GLEAM ET products against water balance based PCR-GLOBWB modelled ET by subdividing the continent into regions based on aridity and precipitation. They mention the challenges of deriving ET products calibrated using input data validated across the African continent, and more importantly the validation of ET outputs with field datasets acquired in various ecoregions in Africa. Poor calibration and validation of modelled ET present a huge challenge in studies investigating the intensification of the hydrological cycle and climate change in Sub-Saharan Africa (Marshall et al., 2013). This consequently makes extensive evaluation of remote sensing ET models and products still valid and necessary in the sub-Sahara African context.

1.3.3 Uncertainty and sensitivity in evapotranspiration estimation

Evapotranspiration is influenced by a number of biological and environmental factors, making it a complex process to measure. It is therefore often estimated using models based on weather and land surface data, which on their own are highly variable and carry uncertainties of their own. These models carry different errors and uncertainty that are propagated to the final output. The errors and uncertainties are attributed to i) the model structure, which reflects lack of understanding of the process, hence presenting simplified descriptions of the modelled process compared to the reality, ii) input variables, both measured and derived, and iii) study site characteristics.

The terms uncertainty analysis (UA) and sensitivity analysis (SA) are often used interchangeably. However, UA assesses the degree of confidence of the model

output and system performance indices by identifying possible model input errors, whereas SA quantifies the effect of input error and uncertainties on model output (Saltelli et al., 2004). SA also allows in ranking the influence of input variables on the models' output, thus identifying the critical model inputs and in some cases helps in removing insignificant inputs from the model, resulting in model simplification. These methods have become critical parts of the modelling process, especially in fields like hydrological, ecological and crop modelling. They are the first steps towards model development and calibration as they answer questions like where data collection efforts should focus, what degree of care should be taken for parameter estimation and the relative importance of various parameters (Brugnach et al., 2008). SA methods of varying complexity exist, from simple local (LSA) to global SA (GSA) techniques, from differential to Monte Carlo analysis, from measures of importance to sensitivity indices, and from regression or correlation methods to variance - based techniques (Frey & Patil, 2002; Hamby, 1994, 1995; Lilburne & Tarantola, 2009; Saint-Geours & Lilburne).

Most studies have focused on analysing the sensitivity of reference ET (ETo) and potential ET (PET) models to climatic input variables across different biomes and climates (Ambas & Baltas, 2012; Estévez et al., 2009; Gong et al., 2006; Guo et al., 2017b; Paparrizos et al., 2017), with a few assessing actual ET model sensitivity. In these studies, different SA methods were applied, from simple local SA methods where sensitivity indices are estimated by changing a single variable at a time whilst holding the rest constant to more sophisticated global SA methods (DeJonge et al., 2015; Su, 2002). Apart from being done to identify the most critical input variables in ET modelling, SA of ET models has been conducted to in order to understand the potential implications of climate change on the catchment water balance (Goyal, 2004; Tabari & Hosseinzadeh Talaee, 2014), with few analysing the impact of climatic inputs on actual ET. These studies have shown varying results, for example, Gong et al. (2006) showed that the PM derived ET0 was most sensitive to RH, followed by solar shortwave radiation (Rsd), Tair and u, and that these sensitivities were season dependent in the Yangtze River Catchment.

The emergence of RS based ET modelling presents another opportunity to assess, not only the reaction of the ET models to climatic input variables but also to land surface parameters, which culminates to how land-use change impacts on ET. Few studies have investigated the sensitivity of ET models to remote sensing input parameters (Van der Kwast et al., 2009; Wang et al., 2009). This indicates that more work still needs to be done to understand the sensitivity of ET models to remote sensing land surface parameters, especially considering

the number of remote sensing-based ET models that have been extensively evaluated across different bioclimates.

Uncertainty analysis is mostly used interchangeably with SA, while other studies have used the term when evaluating the performance of ET models. For instance, Westerhoff (2015) showed that PM estimated ETo is most sensitive to temperature, followed by solar radiation, RH and cloudiness, in several locations in New Zealand. Also, Paparrizos et al. (2017) analysed the sensitivity of several PET models to climatic inputs in different Greek locations, to come up with the best model suited for each area. However, few studies have explicitly explored UA of ET models. Khan et al. (2018) tested the performance of three actual ET products (MOD16, GLEAM, and GLDAS) against eddy covariance system measurements from different land covers. Hofreiter and Jirka used the International Organisation for Standardisation, Guides to the expression of Uncertainty in Measurement (ISO GUM) method to evaluate the uncertainty of the PM to uncertainty associated with net radiation measurements. Using the same method, Chen et al. (2018) analysed the uncertainty of the Stanghhellini and Baille ET equations to error associated with instruments used to measure input variables. An uncertainty analysis study of the PM model to both climate variables and land surface parameters is necessary to determine the degree of confidence of the model in relation to input error and/ uncertainty. Also, this will give an indication of how the model reacts to any change in climatic variables, such as air temperature, net radiation, and water availability. Furthermore, through this section, an analysis of how land use/ land cover change impacts on ET variation.

1.3.4 Using remote sensing products to monitor water use and water productivity

In semi-arid regions, water is a critical scarce resource that requires sustainable use and management. Meanwhile, population expansion is resulting in increased competition for the scarce water resources between urbanisation, domestic water use, agriculture, mining, industrialisation and the need to maintain a safe ecological reserve. Agriculture water use, which is already the largest, will continue to rise as the population grows and diets change due to improved, prosperity. Moreover, climate and global change continue to add to the already existing pressure on water resources. This implies there is need to produce more food with the same or even reduced amount of water from existing and sometimes reduced croplands. Indeed, expanding croplands may not be a viable option due to the negative environmental effect of cropland extension. After alleviating other food production stresses like nutrient deficiency, pest and weed infestations, improving water productivity through

better water resource management remains the only feasible option, especially in water-scarce regions.

Water productivity, sometimes loosely interchanged with water use efficiency, has been defined differently based on the required outcome, but the fundamental being the output produced per unit of water consumed. A review by Zwart and Bastiaanssen (2004) reveals different values of WP of major crops across the globe based on the different climatic and biome regions. Mapping WP at various spatial scales allows for the identification of areas with good and / or poor water management practices. Hence, with the maturity of remote sensing-based evapotranspiration and biomass estimation, tools are being developed to assess and monitor water use and water productivity at larger than farm spatial scales (Zwart et al., 2010a; Zwart et al., 2010b; Zwart & Leclert, 2010). The main focus of these studies has been wheat since it is a recognised global staple food. Global crop water productivity maps assist in identifying where water productivity gaps exist to show understanding where systems perform well, and where improvements are necessary. Furthermore, they serve as a base to spatially analyse and explain the underlying reasons for a gap in WP by combining it with other datasets like soils, agronomic practices, and climate.

FAO, in conjunction with UNESCO-IHE Institute for Water Education and the International Water Management Institute (IWMI), under the 'Remote sensing for water productivity' programme, has developed an open-access platform to assess and monitor WP, as well as identify WP gaps, using remote sensing data. The ultimate goal of this programme is to identify ways of closing these gaps by increasing agricultural WP sustainably. WP of different land use classes derived from this platform needs to be evaluated against existing literature values and *in situ* data like EC flux data so that this dataset can be used with confidence from farm to policy level.

1.4 Thesis objectives

Based on the literature review and previous work done, a number of issues have been identified, especially concerning remote sensing ET estimation in semi-arid (Sub-Saharan Africa) regions. The overall aim of this thesis is to

1. evaluate the performance of remote sensing-based evapotranspiration models in semi-arid biomes, and
2. assess the use of remote sensing-based ET model estimates for monitoring water use and water productivity of different land use/ land covers.

To achieve the aim of this work, the main objectives were subdivided into the following specific objectives:

i. To assess the surface energy balance closure and partitioning of the semi-arid Skukuza eddy covariance flux tower system

ii. To evaluate the performance of remote sensing-based ET models through comparison with flux tower data in order to identify the most appropriate model for South African dry ecosystems

iii. To analyse the uncertainty and sensitivity of a selected ET model to measured and remote sensing derived input variables

iv. To apply different remote sensing products to determine and monitor water use and productivity under different land cover types.

1.5 Thesis outline

This thesis comprises six chapters, which are organised according to the specific objectives. The chapters are structured as follows:

Chapter one introduces the scientific background and problem statement. The objectives of this study are listed in this chapter.

Chapter two presents an in-depth analysis of the tropical savanna Skukuza eddy covariance (EC) flux tower data, to be further used in this research, is done. This includes assessing these data for surface energy balance closure, an accepted quality assurance technique, and how the available energy is partitioned into turbulent fluxes. In this chapter, years with low-quality EC data are red-flagged and discarded from further analysis.

Chapter three evaluates the performance of two ET models, plus two global ET products. The models that were examined include the land surface temperature- vegetation index triangle method (Ts-VI), which is a modified version Priestley-Taylor model, and the multisource Mu modified Penman-Monteith (PM-Mu) model, and the LSA-SAF MET and GLEAM global ET products. The ET model outputs are tested against two natural vegetation ecosystems in South Africa, i.e. tropical savanna and Mediterranean fynbos.

Chapter four analyses the uncertainty and sensitivity of the PM-Mu model to both measured meteorological and remote sensing-based land surface parameters at two natural vegetation sites.

Given the extensive evaluation of remote sensing-based ET across different biomes and climates, as shown in the previous chapter, and similar advances in other areas, including aboveground biomass mapping, **chapter five** assesses the use of these Remote Sensing products from the FAO WaPOR platform, to estimate water use and productivity of different land use classes in South Africa.

Chapter six provides a synthesis of the findings of this study, giving general remarks and discussion on the contributions made by this work. Recommendations for further work to be done for further study are also mentioned.

2 SURFACE ENERGY BALANCECLOSURE AND PARTITIONING ASSESSMENT AT THE SKUKUZA FLUXNET SITE

2.1 ABSTRACT[1]

Eddy covariance flux tower systems provide essential terrestrial climate, water, and radiation budget information needed for environmental monitoring and evaluation of climate change impacts on ecosystems and society in general. They are also intended for calibration and validation of satellite-based Earth observation and monitoring efforts, such as assessment of evapotranspiration from land and vegetation surfaces using different modelling approaches.

In this paper, 15 years of Skukuza eddy covariance data, i.e. from 2000 to 2014, were analysed for surface energy balance closure (SEBC) and partitioning. The surface energy balance closure was evaluated using the ordinary least squares regression (OLS) of turbulent energy fluxes (sensible (H) and latent heat (λE)) against available energy (net radiation (Rnet) less soil heat (G)), and the energy balance ratio (EBR). Partitioning of the surface energy during the wet and dry seasons was also investigated, as well as how it is affected by atmospheric vapour pressure deficit (VPD) and net radiation. After filtering years with low-quality data (2004–2008), our results gave an overall mean EBR of 0.93. Seasonal variations of EBR also showed the wet season with 1.17 and spring (1.02) being closest to unity, with the dry season (0.70) having the highest imbalance. Nocturnal surface energy closure was very low at 0.26, and this was linked to low friction velocity during night-time, with results showing an increase in closure with an increase in friction velocity.

The energy partitioning analysis showed that sensible heat flux is the dominant portion of net radiation, especially between March and October, followed by latent heat flux, and lastly the soil heat flux, and during the wet season where latent heat flux dominated sensible heat flux. An increase in net radiation was characterised by an increase in both LE and H, with LE showing a higher rate of increase than H in the wet season, and the reverse happens during the dry season. An increase in VPD is correlated with a decrease in LE and an increase in H during the wet season, and an increase in both fluxes during the dry season.

[1] **This chapter is based on**:
Majozi N. P., Mannaerts C.M., Ramoelo A., Mathieu R.S.A., Nickless A., Verhoef W. Analysing surface energy balance closure and partitioning over a semi-arid FLUXNET site in Skukuza, Kruger National Park, South Africa, Hydrol. Earth Syst. Sci., 21, 3401–3415, 2017, https://doi.org/10.5194/hess-21-3401-2017.

2.2 Introduction

Net solar radiation (Rnet) reaching the Earth's surface determines the amount of energy available for latent (LE), sensible (H), and soil (G) heat fluxes, and heat stored by the canopy, the ground, and energy storage terms by photosynthesis. Energy partitioning on the Earth's surface is a function of interactions between biogeochemical cycling, plant physiology, the state of the atmospheric boundary layer, and climate (Wilson et al., 2002). How the turbulent fluxes (H and LE) are partitioned in an ecosystem plays a critical role in determining the hydrological cycle, boundary layer development, weather, and climate (Falge et al., 2005). Understanding the partitioning of energy, particularly the turbulent fluxes, is important for water resource management in (semi) arid regions, where reference evapotranspiration far exceeds precipitation.

Eddy covariance (EC) systems are currently the most reliable method for measuring carbon, energy, and water fluxes, and they have become a standard technique in the study of surface-atmosphere boundary layer interactions. They provide a distinct contribution to the study of environmental, biological and climatological controls of the net surface exchanges between the land surface including vegetation) and the atmosphere (Aubinet et al., 1999; Baldocchi et al., 2001). The accuracy of these data is very important because they are used to validate and assess the performance of land surface and climate models. However, the EC techniques have limitations in terms of data processing and quality control methods, especially under complex conditions (e.g. unfavourable weather, such as high turbulence and low wind speed, and heterogeneous topography). In EC measurements, the ideal situation is that available energy, i.e. net radiation minus soil heat flux, is equal to the sum of the turbulent fluxes (Rnet-G=LE+H); however, in most instances, the measured available energy is larger than the sum of the measured turbulent fluxes of sensible heat and latent heat. Extensive research on the issue of surface energy imbalance in EC observations has been done (Barr et al., 2012; S. Chen et al., 2009; Foken et al., 2010; Franssen et al., 2010; Mauder et al., 2007), and closure error (or imbalance) has been documented to be around 10–30% (Sánchez et al., 2010; Von Randow et al., 2004; Wilson et al., 2002).

Causes for non-closure, as extensively discussed, include unaccounted soil and canopy heat storage terms, non-inclusion of the low- and high-frequency turbulence in the computation of the turbulent fluxes, land surface heterogeneities, systematic measurement, and sampling errors. This imbalance has implications on how energy flux measurements should be interpreted and how these estimates should be compared with model simulations. The surface energy balance closure is an accepted performance criterion of EC flux data (Twine et al., 2000; Wilson et al., 2002), and different methods have been used

to assess the energy closure and partitioning, including ordinary least squares regression (OLS) method, i.e. a plot of turbulence fluxes (H+LE) against available energy (Rnet-G), the residual method, i.e. Rnet-G-H-LE, and the energy balance ratio, i.e. H+LE = Rnet-G. Several researchers have investigated surface energy partitioning and energy balance closure for different ecosystems, including savannas. Bagayoko et al. (2007) examined the seasonal variation of the energy balance in West African savannas and noted that latent heat flux played a major role in the wet season, whereas sensible heat flux was significant in the dry season. In the grassland Mongolian Plateau, Li et al. (2006) concluded that sensible heat flux dominated the energy partitioning, followed by ground heat flux, with the rainy season showing a slight increase in latent heat flux. Gu et al. (2006) used different ratios (Bowen ratio, G/Rnet, H/Rnet, and LE/Rnet) to investigate surface energy exchange in the Tibetan Plateau, and showed that during the vegetation growth period, LE was higher than H, and this was reversed during the post-growth period.

Research using the Skukuza EC system data has focused mainly on the carbon exchange, fire regimes, and in global analysis of the energy balance (Archibald et al., 2009; Kutsch et al., 2008; Williams et al., 2009). However, there has been no investigation of surface energy partitioning and energy balance closure in this ecosystem. In this study, we examined the surface energy balance partitioning into soil heat conduction, convection (sensible), and latent heat components and its energy balance closure using 15 years (2000–2014) of eddy covariance data from the Skukuza flux tower.

First, a multi-year surface energy balance closure (SEBC) analysis was done, including the seasonal and day-night SEBC evaluations, the role of G on SEBC, and an assessment of its error sources. This included investigating how friction velocity affects the closure and its link to low night-time SEBC. Then, we examined how the surface energy partitioning varies with time in this ecosystem, based on the weather conditions in the region, particularly, in relation to water availability (precipitation) and vegetation dynamics. The effect of vapour pressure deficit (VPD) and Rnet on the energy partitioning between turbulent fluxes during the wet and dry seasons was also examined. Through this study, we expect to contribute to the existing literature on the surface energy balance closure and partitioning, especially in semi-arid savanna areas.

2.3 Materials and methods

2.3.1 Site description

Established in early 2000 as part of the SAFARI 2000 campaign and experiment, the Skukuza flux tower (25.02° S, 31.50° E) was set up to understand the

interactions between the atmosphere and the land surface in Southern Africa by connecting ground data of carbon, water, and energy fluxes with remote sensing data generated by Earth-observing satellites (R. J. Scholes et al., 2001; Shugart et al., 2004).

The site is located in the Kruger National Park (South Africa) at 365m above sea level, and receives 550-160 mm precipitation per annum between November and April, with significant inter-annual variability. The year is generally divided into a hot, wet growing season and a warm, dry non-growing season. The soils are generally shallow, with coarse sandy to sandy loam textures (about 65% sand, 30% clay and 5% silt). The area is characterised by a catenal pattern of soils and vegetation, with broad-leaved *Combretum* savanna on the crests dominated by the small trees (*Combretum apiculatum*), and fine-leaved *Acacia* savanna in the valleys dominated by *Acacia nigrescen*s (Scholes et al., 2003; Scholes et al., 2001). The vegetation is mainly open woodland, with approximately 30% tree canopy cover of mixed *Acacia* and *Combretum* savanna types. Tree canopy height is 5–8m with occasional trees (mostly *Sclerocarya birrea*) reaching 10 m. The grassy and herbaceous understorey comprises grasses such as *Panicum maximum, Digitaria eriantha, Eragrostis rigidor,* and *Pogonarthria squarrosa*.

Eddy covariance system

Since 2000, ecosystem-level fluxes of water, heat, and carbon dioxide have been measured using an eddy covariance system mounted at 16m height of the 22m high flux tower. The measurements taken and the instruments used are summarised in Table 2-1.

Table 2-1: Measurements taken and instruments used at the Skukuza eddy covariance flux tower

Instrument	Model/ brand	Measurement
Sonic anemometer	Gill Instruments Solent R3, Hampshire, England	3-dimensional, orthogonal components of velocity (u, v, w (ms^{-1})), sonic temperature
Closed path gas analyser	IRGA, LI-COR 6262, LI-COR, Lincoln	Water vapour, carbon dioxide concentrations
Radiometer	Kipp & Zonen CNR1, Delft, The Netherlands	Incoming and outgoing longwave and shortwave radiation
HFT3 plates	Campbell Scientific	Soil heat flux at 5 cm depth with 3 replicates, i.e. two under tree canopies and one on open space
Frequency domain reflectometry probes	Campbell Scientific CS615, Logan, Utah	Volumetric soil moisture content with two in the Acacia-dominated soils downhill of the tower at 3, 7, 16, 30, and 50 cm, and another two at 5, 13, 29, and 61 cm in the Combretum-dominated soils uphill

From 2000 to 2005, H and LE were derived from a closed-path CO_2 /H_2O monitoring system, which was replaced by the open-path gas analyser in 2006. Also, from 2000 to 2008, incident and reflected shortwave radiation (i.e. 300-1100 nm, Wm^{-2}), incident and reflected near-infrared (600–1100 nm, Wm^{-2}) and incoming and emitted longwave radiation (>3.0 µm, Wm^{-2}) measurements were made using a two-component net radiometer (model CNR 2: Kipp & Zonen, Delft, the Netherlands) at 20-second intervals and then recorded in the data logger as 30-minute averages; this was replaced with the Kipp & Zonen NR-Lite net radiometer in 2009. Soil heat flux is measured using the HFT3 plates (Campbell Scientific) installed at 5 cm below the surface at three locations – two under tree canopies and one between canopies.

Ancillary meteorological measurements include air temperature and relative humidity, also measured at 16 m height, using a Campbell Scientific HMP50 probe; precipitation at the top of the flux tower using a Texas TR525M tipping bucket rain gauge; wind speed and direction using a Climatronics wind sensor; and soil temperature using Campbell Scientific 107 soil temperature probe.

Data pre-processing

The Eddysoft software was used to process the raw data collected from the eddy covariance system (Kolle & Rebmann, 2007). Post-processing of the raw high-frequency (10 Hz) data for calculation of half-hour periods of the turbulent fluxes and CO_2 (F_c; g CO_2 m^2 $time^{-1}$) involved standard spike filtering, planar rotation of velocities, and lag correction to CO_2 and *q* (Aubinet et al., 1999; Wilczak et al., 2001). Frequency response correction of some of the energy lost due to instrument separation, tube attenuation, and gas analyser response for LE and *Fc* was performed with empirical cospectral adjustment to match the H co-spectrum (Eugster & Senn, 1995; Su et al., 2004).

2.3.2 Data analysis

Half-hourly measurements of eddy covariance and climatological data from 2000 to 2014 were used to assess surface energy partitioning and closure. When measuring the different variables, instruments like the sonic anemometer and the net radiometer are affected by different phenomena, like rainfall events and wind gusts, resulting in faulty diagnostic signals, outliers and data gaps, which are sources of error and bias. Thus, cleaning, which involved screening, diagnosing and editing, of these half-hourly surface energy data, which was done to reduce bias and error, rejected (i) data from periods of sensor malfunction (i.e. when there was a faulty diagnostic signal), (ii) incomplete 30 minute data sets of Rnet, G, LE and H, and (iii) outliers. The data outliers were detected using the outlier detection procedure found in the Statistica software. After data screening, flux data with non-missing values of Rnet, G, LE, and H data

were arranged according to monthly and seasonal periods (summer (December-February), autumn (March-May), winter (June-August), and spring (September–November)), as well as into daytime and night-time. To be used in this study, soil heat flux was computed as a weighted mean of the three measurements, i.e. two taken under tree canopies and one on open space.

Surface energy balance assessment

The law of conservation of energy states that energy can neither be created nor destroyed, but is transformed from one form to another; hence, the ideal surface energy balance equation is written as

$$\boldsymbol{Rnet - G = H + LE} \quad 1$$

Energy imbalance occurs when both sides of the equation do not balance. The energy balance closure was evaluated at different levels, i.e. multi-year, seasonal, and day/night periods (the assumption being that daytime has positive Rnet and night-time has negative Rnet), using two methods:

i. The ordinary least squares (OLS) method, which is the regression between turbulent fluxes and available energy. Ideal closure is when the intercept is zero and slope and the coefficient of determination (R^2) are one. An assumption is made using this method, that there are no random errors in the independent variables, i.e. Rnet and G, which of course is a simplification.

ii. The energy balance ratio (EBR), which is the ratio of the sum of turbulent fluxes to the available energy, $\sum(LE + H) / \sum(Rnet - G)$.

The EBR gives an overall evaluation of energy balance closure at longer timescales by averaging over errors in the half-hour measurements, and the ideal closure is 1. EBR has the potential to remove biases in the half-hourly data, such as the tendency to overestimate positive fluxes during the day and underestimate negative fluxes at night. We did not account for the heat storage terms in the EBR, including soil and canopy heat storage, and energy storage by photosynthesis and respiration, in this study. The significance and uncertainty associated with neglecting particularly the soil heat storage term will be discussed.

To investigate the effect of friction velocity on EBR and how it is related to the time of day, using friction velocity, the half-hourly data were separated into four 25th percentiles, and the EBR and OLS evaluated. MATLAB was used to create the graphs.

Analysing surface energy partitioning

To evaluate solar radiation variation and partitioning into latent and sensible heat fluxes in this biome, EC surface energy data from 2000 to 2014 were used.

Violations in micrometeorological assumptions, instrument malfunction, and poor weather resulted in a proportion of the data being rejected. Yet, our aim was to construct continuous records of half-hourly fluxes measured by eddy covariance and compute monthly, seasonal and annual sums of surface energy fluxes. To fill the gaps in our data set, we used the Amelia II software, an R program designed to impute missing data using the expectation maximisation with bootstrapping (EMB) multiple imputation algorithm (Honaker et al., 2011). The original data set is resampled using bootstrapping, after which the missing data values are imputed using the EMB algorithm. Each complete imputed data set is in such a way that the observed values are the same as those in the original data set; only the missing values are different. The minimum, maximum and mean statistics of Rnet, H, LE, and G were then estimated. The monthly and seasonal trends of energy partitioning were assessed, and how each component is affected by vegetation dynamics at the site. Surface energy partitioning was also characterised as a direct function of VPD and Rnet during the wet and dry seasons, following Gu et al. (2006),

2.4 Results and Discussion

2.4.1 Meteorological conditions

Figure 2-1 shows the 15-year mean monthly anomalies of air temperature, VPD and rainfall totals at the Skukuza flux tower site. The annual average temperatures over the 15-year period ranged between 21.1°C in 2012 and 23.2 °C in 2003, with a 15-year average temperature of 22.9 °C. While the 2003 season being the hottest year, it was also the driest year, with an annual rainfall of 273 mm, with 2002 also recording very low rainfall of 325 mm, both receiving rainfall amounts below the recorded mean annual rainfall of 550±160 mm. The wettest years were 2013, 2000, 2014 and 2004 which received 1414, 1116, 1010 and 1006 mm, respectively. 2007 and 2008 had incomplete rainfall data records to assess their annuals. The annual daily average VPD was between 0.024 and 4.03 kPa, with an overall average of 1.28 ± 0.62 kPa. The daily average VPD decreased with rainy days and showed an increase during rain-free days. The wet years, i.e. 2000, 2013 and 2014 had low annual average VPD of 1.98, 1.34 and 1.83 kPa, respectively, whereas the drought years exhibited high VPDs with 2002 and 2003 with 2.77 and 2.97 kPa, respectively. The long-term weather records are comparable with the 1912–2001 and 1960–1999 climate analysis for the same area as reported by Kruger et al. (2002) and R. J. Scholes et al. (2001), showing a mean annual total precipitation of 547 mm and air temperature of 21.9 ºC. The low rainfall during the 2000-2003 seasons was also reported by Kutsch et al. (2008), who were investigating the connection between water relations and carbon fluxes during the mentioned period.

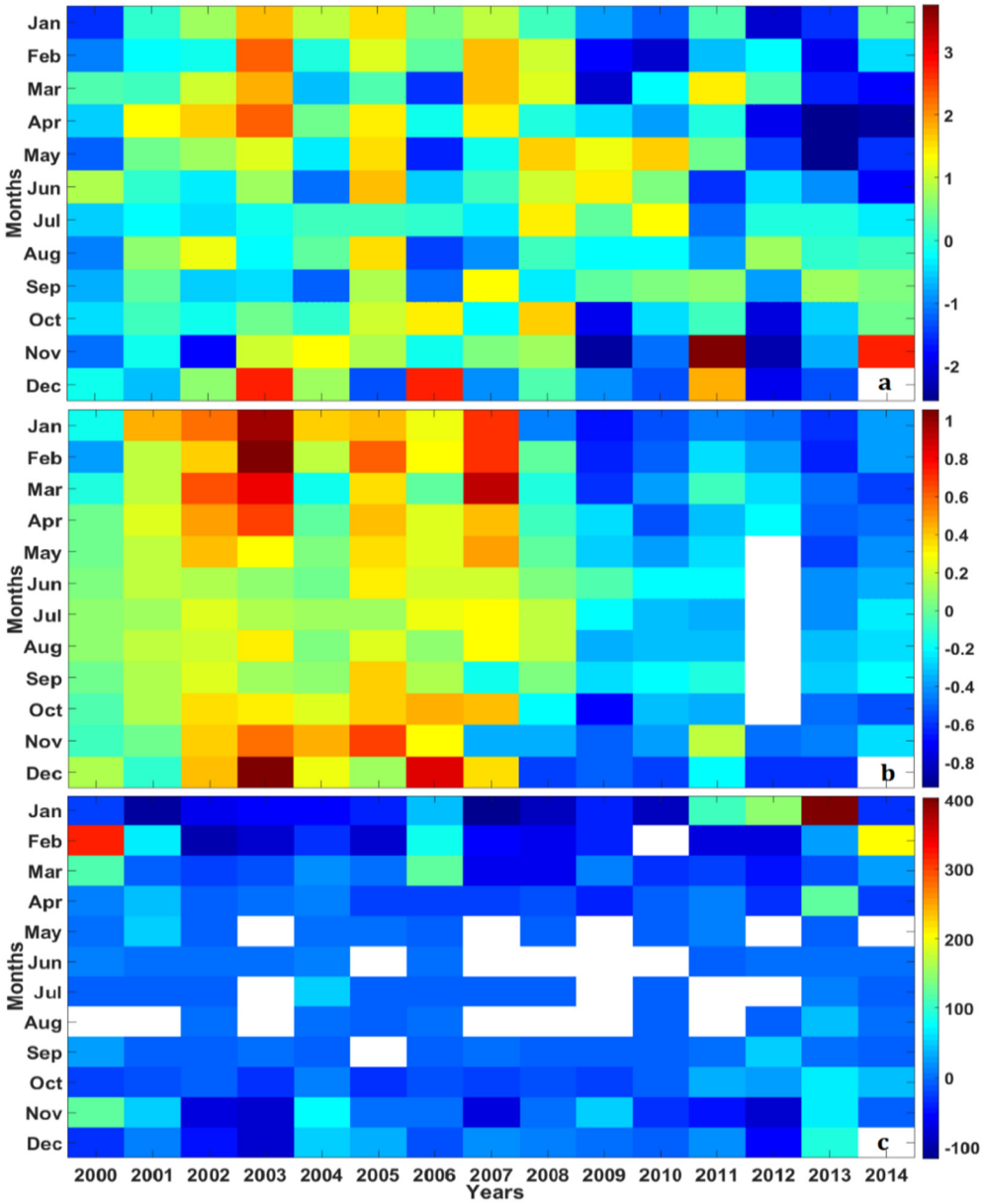

Figure 2-1: Summary of mean monthly anomalies of (a) air temperature, (b) VPD, and (c) rainfall from 2000 to 2014

2.4.2 Surface energy balance assessment

Data completeness varied largely 7.59% (2006) and 67.97% (2013), with a mean of 34.84%. The variation in data completeness is due to a number of factors

including instrument failures, changes and (re)calibration, and poor weather conditions.

Multi-year analysis of surface energy balance closure

Figure 2-2 summarises the results of the multi-year energy balance closure analysis for the Skukuza eddy covariance system from 2000 to 2014. The coefficient of determination (R^2) for the 15-years period varied between 0.74 and 0.92, with a mean value of 0.85±0.06. The slopes ranged between 0.56 and 1.25, with a mean of 0.77±0.19, while the intercepts varied from -23.73 to 26.28, with a mean of 1.03 and standard deviation of 18.20 Wm^{-2}. The annual energy balance ratio (EBR) for the 15 years extended between 0.44 in 2005 and 2007 and 1.09 in 2011, with a mean of 0.78±0.24. Between 2004 and 2008, EBR ranged between 0.44 and 0.53, whereas from 2000 to 2003 and 2009 to 2014, the EBR was between 0.76 and 1.09. The EBR for 2010 to 2012 was slightly greater than 1 (1.08, 1.09 and 1.01, respectively), indicating an overestimation of the turbulent fluxes (H+λE) compared to the available energy, this still giving the absolute imbalance values of within 30%. The remaining years, 2000-2003 and 2009, were less than 1, indicating that the turbulent fluxes were lower than the available energy. The further away the slope is from unity, the lower the EBR, as shown by the low slope values between 2004 and 2008. The period of low EBR between 2004 and 2008 is characterised by the absence of negative values of available energy (Rnet-G) as illustrated in Figure 2. Between 2000 and 2004, the CNR2 net radiometer was used to measure long and shortwave radiation, and these were combined to derive Rnet. However, when the pyrgeometer broke down in 2004, Rnet was derived from measured shortwave radiation and modelled longwave radiation until the CNR2 was replaced by the NRLite net radiometer in 2009. This was a significant source of error, as shown by the low EBR between 2004 and 2008. The closed-path gas analyser was also changed to the open-path gas analyser in 2006. An analysis of the 2006 data (which had very low data completeness of 7.59%) showed that there were no measurements recorded until September, possibly due to instrument failure. Further analysis and discussion of the EBR were done with the exclusion of years with low-quality data.

Our final mean multiyear EBR estimate, excluding the years with poor data quality (2004 to 2008), was therefore 0.93 ± 0.11, ranging between 0.76 and 1.09. The R^2 for these years varied between 0.77 and 0.92, with a mean value of 0.87±0.05. The slopes were from 0.7 to 1.25, with a mean of 0.87±0.17, while

the intercepts varied from -12.57 to 26.28, with a mean of 10.79 and standard deviation of 13.67 Wm^{-2}.

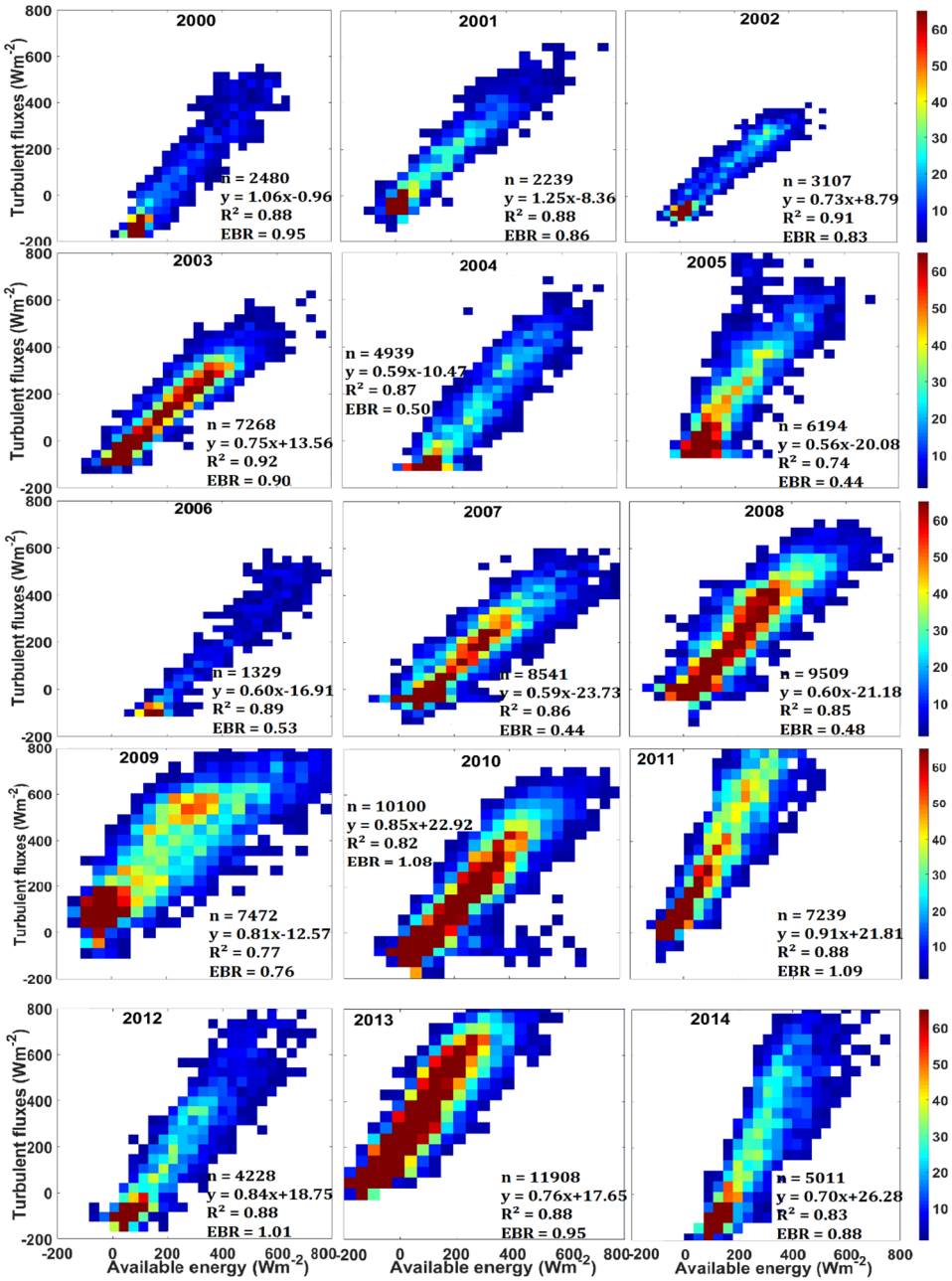

Figure 2-2: 15-year series of annual regression analysis of turbulent (sensible and latent) heat fluxes against available energy (net radiation minus ground heat flux) from 2000 to 2014 at Skukuza, (SA). The colour bars represent the count of EBR values

The EBR results for the Skukuza eddy covariance system, which vary between 0.76 and 1.09 with an annual mean of 0.93 (only the years with high-quality data), are generally within the reported accuracies as shown in most studies that report the surface energy balance closure error at 10–30%, across different ecosystems. For instance, Wilson et al. (2002) also reported an annual mean EBR of 0.84, ranging between 0.34 and 1.69 in an extensive study investigating 22 FLUXNET sites across the globe; EBR in ChinaFLUX sites ranged between 0.58 and 1.00, with a mean of 0.83 (Yuling, 2005); according to Were et al. (2007), EBR values of about 0.90 were found over shrub and herbaceous patches in a dry valley in southeast Spain, whereas Chen et al. (2009) showed a mean of 0.98 EBR for their study in the semi-arid region of Mongolia, and an EBR value of 0.80 was found by Xin and Liu (2010) in a maize crop in semi-arid conditions, in China. Using data from the Tibetan Observation and Research Platform (TORP), Liu et al. (2011) observed an EBR value of 0.85 in an alfalfa field in semi-arid China.

Seasonal variation of EBR

Figure 2-3 shows the seasonal OLS results for the 15 year period, excluding the years 2004 to 2008. The slopes ranged between 0.67 and 0.87, with a mean of 0.78±0.08, and the intercepts were a mean of 19.13± 6.30 Wm^{-2}. R^2 ranged between 0.81 and 0.88 with a mean of 0.84±0.04. The EBR for the different seasons ranged between 0.70 and 1.12, with a mean of 0.92 ± 0.19. The dry season had the lowest EBR of 0.70, while summer with an EBR of 1.02, and spring with an EBR of 1.12, were closest to unity, and autumn had EBR of 0.84. A large number of outliers are observed in summer due to cloudy weather conditions and rainfall events that make the thermopile surface wet, thus reducing the accuracy of the net radiometer. A study comparing different the performance of different net radiometers by Blonquist et al. (2009) shows that the NR-Lite is highly sensitive to precipitation and dew/ frost since the sensor is not protected.

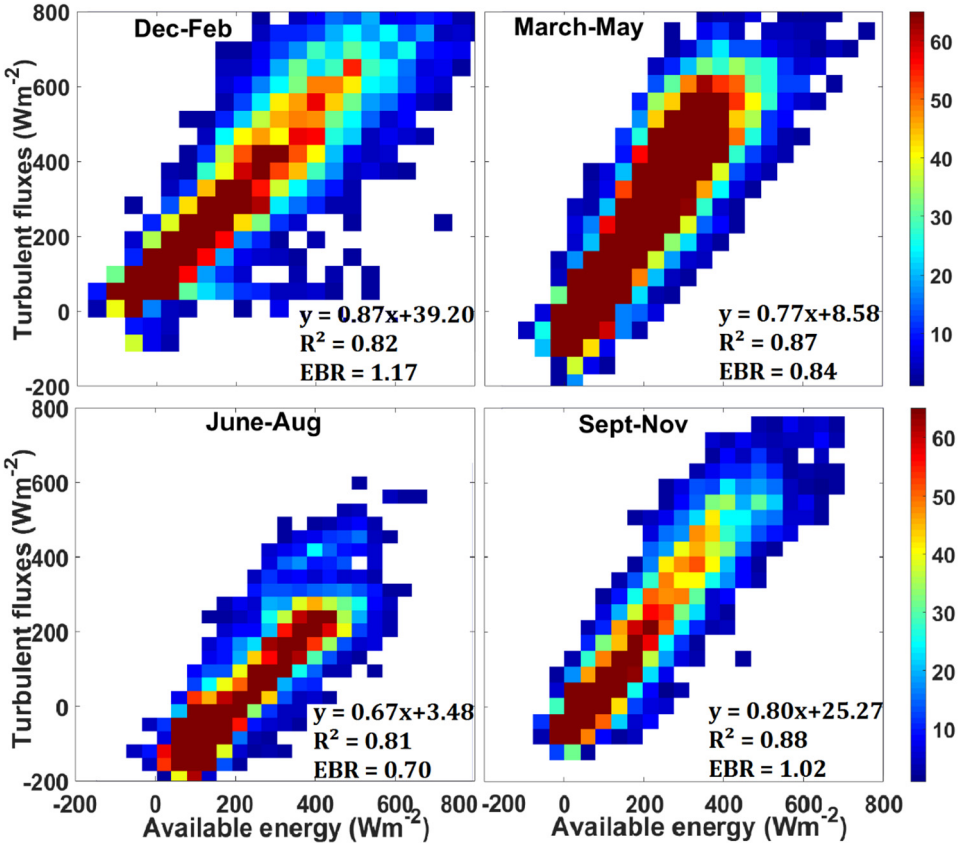

Figure 2-3: Seasonal turbulent fluxes (H+LE) correlation to available energy (Rnet-G) for Skukuza flux tower from summer(Dec-Feb), autumn (March-May), winter (June-Aug), spring (Sept-Nov). The colour bars represent the count of EBR values

The results of our study concur with similar studies that assessed the seasonal variation of EBR. For instance, Wilson et al. (2002) comprehensively investigated the energy closure of the summer and winter seasons for 22 FLUXNET sites for 50 site-years. They also reported higher energy balance correlation during the wet compared to the dry season, with the mean R^2 of 0.89 and 0.68, respectively. Whereas our results show significant differences between the wet (1.12) and dry (0.70), their EBR showed smaller differences between the two seasons, being 0.81 and 0.72, for summer and winter, respectively. Ma et al. (2009) reported an opposite result from the Skukuza results, showing energy closures of 0.70 in summer and 0.92 in winter over the flat prairie on the northern Tibetan Plateau.

Day- night-time effects

Figure 2-4 shows the daytime and nocturnal OLS regression results for the 15 year period. The daytime and nocturnal slopes were 0.99 and 0.11, with the intercepts being 76.76 and 1.74 Wm^{-2}, respectively. Daytime and nocturnal R^2 were 0.64 and 0.01, respectively. The EBR for the different times of day were 0.96 and 0.27, daytime and nocturnal, respectively.

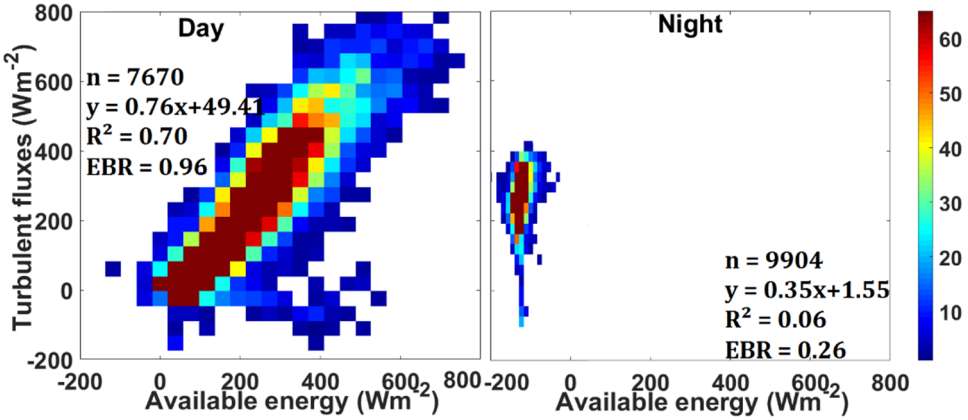

Figure 2-4: Turbulent fluxes correlation to available energy for daytime and night-time, using the full (2000-2014) 15-year available data series. The colour bars represent the count of EBR values

Other studies also reported a higher daytime surface energy balance closure. For instance, Wilson et al. (2002) showed that the mean annual daytime EBR was 0.8, whereas the nocturnal EBR was reported to be negative or was much less or much greater than 1.

To understand the effect of friction velocity on the energy balance closure, surface energy data which had corresponding friction velocity (u*) data, were analysed. Using friction velocity, the data were separated into four 25-percentiles, and the EBR and OLS evaluated. Results show that the first quartile, the EBR was 3.94, with the 50-percentile at 0.99, the third quartile at unity, and the fourth quartile at 1.03 (Figure 2-5). The slopes were between 1.01 and 1.12, with the intercepts ranging between -9.26 and -0.17 Wm^{-2}, whereas R^2 were 0.82, 0.86, 0.85 and 0.81 for the first to the fourth quartiles, respectively.

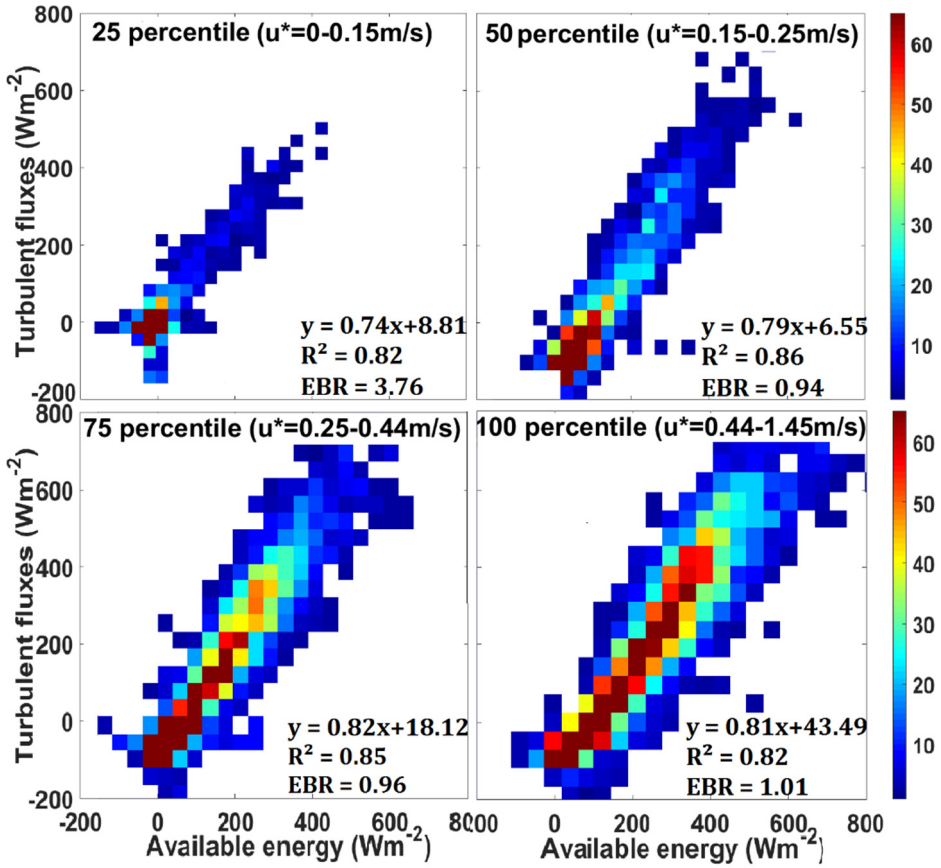

Figure 2-5: OLS and EBR evaluations at different friction velocity sorted at four quartiles. The colour bar represents the count of EBR values. The colour bars represent the count of EBR values

An assessment shows that the time associated with the low friction velocities, i.e. the first quartile are night-time data constituting 81% of the whole first quartile dataset, and the last quartile had the highest number of daytime values at 79.29% of the fourth quartile dataset. Lee and Hu (2002) hypothesised that the lack of energy balance closure during nocturnal periods was often the result of mean vertical advection, whereas Aubinet et al. (1999) and Blanken et al. (1997) showed that energy imbalance during nocturnal periods is usually greatest when friction velocity is small. Another source of error in the nocturnal EBR is the high uncertainty in night-time measurements of Rn. At night, the assumption is that there is no shortwave radiation, and Rnet is a product of longwave radiation. Studies show that night-time measurements of longwave radiation were less accurate than daytime measurements (Blonquist et al., 2009). The RN-Lite, for instance, has low sensitivity to longwave radiation, resulting in low accuracy in low measurements.

Soil heat flux (G) plays a significant role in the surface energy balance as it determined how much energy is available for the turbulent fluxes, especially in areas with limited vegetation cover. In this study, we examined how G, i.e., its presence or absence, impacts on the EBR. Our results revealed a decrease of up to 7%, with an annual mean of 3.13±2.70%, in EBR when G was not included in the calculation. During the daytime, the absence of G resulted in a decrease of approximately 10% of the initial EBR, while at nighttime EBR was as low as 50% of the initial EBR, showing that G has a greater impact on the surface energy balance at night. While G plays a significant role in the surface energy balance closure, our study ignored the different energy storage terms in determining the EBR, including the soil heat storage term. The exclusion of this storage term results in the underestimation of G, as the real value of G is a combination of the flux measured by the plate and the heat exchange between the ground and the depth of the plate. This, in turn, contributes to overestimating the available energy, which then lowers the SEBC. As reported by different studies, the omission of the soil heat storage results in the underestimation of the energy SEBC by up to 7%. For instance, Zuo et al. (2011) reported an improvement of 6 to 7% when they included the soil heat storage in their calculation of EBR, at the Semi-Arid Climate and Environment Observatory of Lan-Zhou University (SACOL) site in semi-arid grassland over the Loess Plateau of China. In their study in the three sites in the Badan Jaran desert, Li et al. (2014) analysed the effect of including soil heat storage derived by different methods in the energy balance closure; their EBR improved by between 1.5% and 4%. The improvement of the EBR in the study in a FLUXNET boreal site in Finland by Sánchez et al. (2010) was shown to be 3% when the soil heat storage was included, which increased to 6% when other storage terms (canopy air) were taken into account.

2.4.3 Surface energy partitioning

Surface energy measurements

The mean daily and annual measurements of the energy budget components from 2000 to 2014 are highlighted in Figure 2-6 and Table 2-2. The seasonal cycle of each component can be seen throughout the years, where at the beginning of each year the energy budget components are high, and as each year progresses they all decrease to reach a low during the middle of the year, which is the winter/ dry season, and a gradual increase being experienced during spring right to the summer at the end of each year. The multi-year daily means of Rnet, H, LE, and G were 139.1 Wm^{-2}, 57.70 Wm^{-2}, 42.81 Wm^{-2}, and 2.94 Wm^{-2}, with standard deviations of 239.75 Wm^{-2}, 104.15 Wm^{-2}, 70.58 Wm^{-2}, and 53.67 Wm^{-2}, respectively.

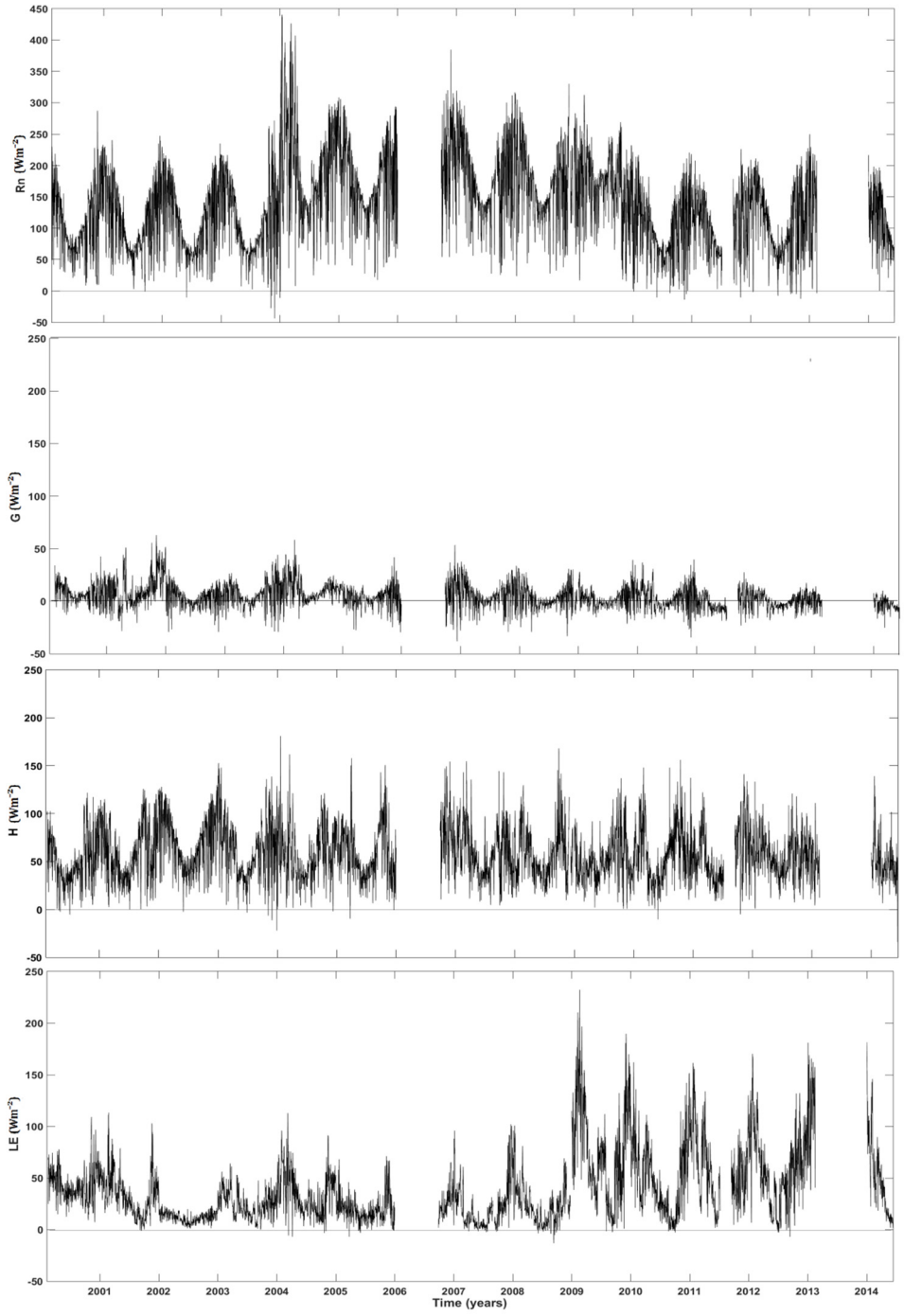

Figure 2-6: Time series of daily mean surface energy balance component fluxes from 2000 to 2014 at Skukuza flux tower site (SA)

The gaps in 2006 indicate the absence of the surface energy flux measurements in those years, which was a result of instrument failure. Between 2004 and 2008, the Rnet was calculated as a product of measured shortwave radiation and modelled longwave radiation, which was a high source of error in the estimation of Rnet. These years are also characterised by poor energy balance closure, as shown in Section 2.3.3 above.

Table 2-2: Statistical summary of annual values of the energy balance components

Year	% Data completion	Statistics	H	LE	G	Rnet
2000	14.16	Max	470.31	422.89	191.53	817.6
		Min	-139.77	-72.43	-61.6	-95.93
		Mean	45.82	36.11	5.32	91.46
2001	12.78	Max	790.82	513.09	292.87	899.9
		Min	-159.87	-85.95	-90.27	-116.58
		Mean	58.56	43.68	9.27	128.27
2002	17.77	Max	415.93	174.07	171.93	583.3
		Min	-117.66	-89.16	-86	-122.21
		Mean	61.35	10.29	4.1	90.72
2003	41.5	Max	556.21	308.71	217.6	879.3
		Min	-92.99	-97.81	-106.23	-116.04
		Mean	58.15	21.68	6.17	94.53
2004	28.21	Max	505.36	498.1	129.96	925.3
		Min	-150.08	-89.07	-69.76	-5.88
		Mean	56.46	17.99	7.97	156.1
2005	35.37	Max	606.28	737.43	288.2	933.2
		Min	-130.4	-97	-107.37	-4.92
		Mean	51.43	17.82	0.99	159.09
2006	7.59	Max	583.66	331.25	335.3	1003.3
		Min	-72.45	-119.09	-72.8	-6.56
		Mean	84.67	35.94	19.69	247.7
2007	48.77	Max	552.93	426.34	340.67	1011.3
		Min	-131.4	-130.79	-129.7	-6.71
		Mean	59.04	14.32	4.14	169.84
2008	54.3	Max	616.43	439.76	238.57	1038.5
		Min	-140.13	-144.97	-104.6	-5.91
		Mean	63.06	26.3	6.22	191.26
2009	42.69	Max	551.34	776.62	328.93	1060.5
		Min	-96.68	-135.43	-94.2	-155.9
		Mean	55.42	96.54	6.87	207.77

		Max	626.68	624.38	199.33	888
2010	57.65	Min	-173.11	-135.62	-66.35	-180.7
		Mean	57.23	52.54	3.74	105.1
		Max	591.16	688.46	171.27	832
2011	41.34	Min	-135.77	-127.02	-58.59	-96.5
		Mean	63.88	73.11	1.75	127.94
		Max	572.11	566.88	185.8	899
2012	27.62	Min	-171.83	-148.49	-50.92	-99.69
		Mean	59.25	52.49	2.16	111.31
		Max	570.79	665.48	146.03	845.58
2013	67.97	Min	-197.4	-149.1	-55.36	-107.7
		Mean	50.25	38.63	-1.22	92.8
		Max	533.46	726.31	89.5	893
2014	28.66	Min	-238.65	-134.39	-33.36	-89.7
		Mean	59.37	69.55	1.18	147.3

Influence of weather conditions and seasonality

In arid/semi-arid ecosystems, solar radiation is not a limiting factor for latent heat flux, instead, it is mainly limited by water availability. The seasonal fluctuations of energy fluxes are affected by the seasonal changes in the solar radiation, air temperature, precipitation and soil moisture (Arain et al., 2003; Baldocchi et al., 2001). These climatic variables influence vegetation dynamics in an ecosystem, as well as how solar radiation is partitioned. Hence, daily measurements of precipitation, air temperature, and VPD were evaluated to investigate the partitioning of the surface energy in the semi-arid savanna landscape of Skukuza.

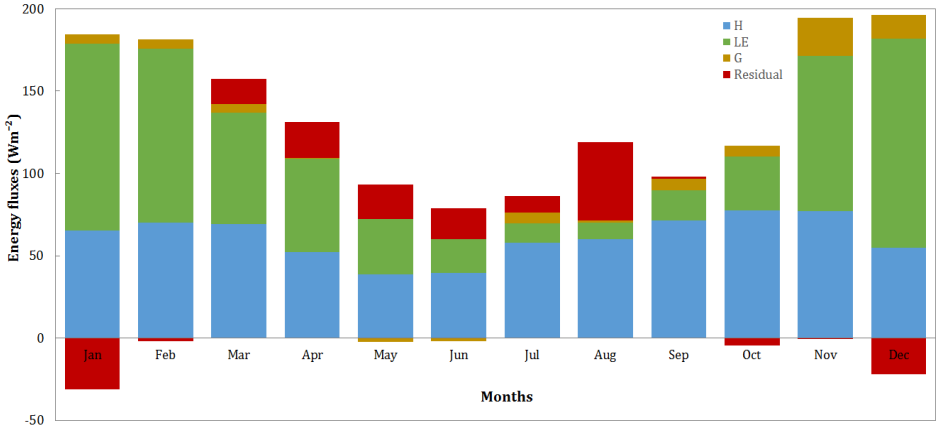

Figure 2-7: 15-year (2000-2014) monthly means of surface energy balance fluxes of Skukuza flux tower site (SA), highlighting the partitioning of Rnet

To illustrate the partitioning of solar radiation into the different fluxes throughout the year, Figure 2-7 presents the multi-year mean monthly variations of the surface energy components showing a general decrease of the components between February and June, which then gradually increases again until November. The multi-year monthly means of Rnet, H, LE, and G were 71.27 Wm^{-2} (June) and 197.33 Wm^{-2} (November), 37.11 Wm^{-2} (June) and 80.37 Wm^{-2} (November), 8.52 Wm^{-2} (August) and 127.17 Wm^{-2} (December), -2.28 Wm^{-2} (June) and 20.78 Wm^{-2} (November), respectively. The month of August had the highest BR of 6.42, whereas December had the least at 0.42. The residual accounted for between -19.69 and 34.74% of Rnet, and an average of 4.70%.

The general trend shows that sensible heat flux dominated the energy partitioning between May and October, followed by latent heat flux, and lastly the soil heat flux, except during the wet season where latent heat flux was larger than sensible heat flux. This is illustrated by the trend of BR, showing an increase from April, with the peak in August, then a steady decrease until it hits lowest in December. The period of low BR is characterised by high Rnet and high precipitation. As the season transitions into the dry season, it is characterised by reduced net radiation and low measurements H and LE.

Just before the first rains, i.e. between September and November, tree flowering and leaf emergence occur in the semi-arid savanna in the Skukuza area (S. Archibald & Scholes, 2007), and grasses shoot as soil moisture availability improves with the increasing rainfall (Scholes et al., 2003). This is characterised by a gradual increase in LE and a decrease in BR, which, when compared to the dry season, is significantly lower than the H, as illustrated in Figure 2-7. As the rainy season progresses, and vegetation development peaks, LE also reaches its maximum, becoming significantly higher than H, and hence, low BR. Between March and September, when leaf senescence occurs, the leaves gradually change colour to brown and grass to straw, and trees defoliate, H again gradually becomes significantly higher than LE.

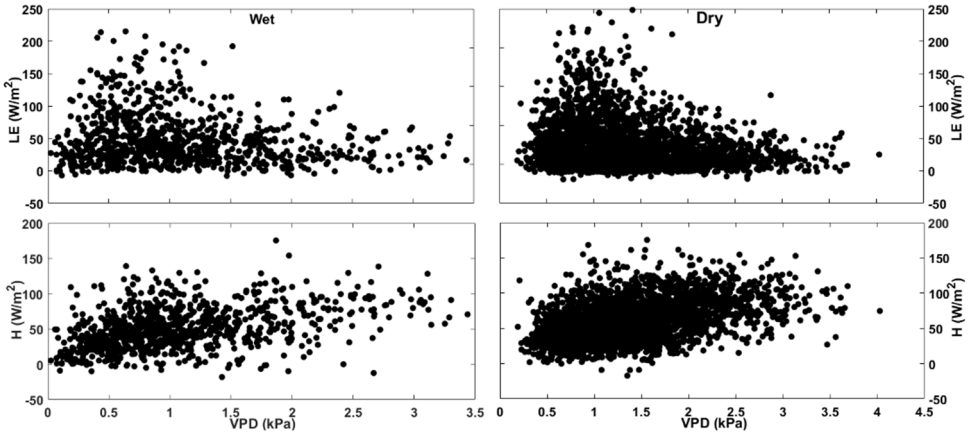

Figure 2-8: Relationship between the fluxes and VPD under wet and dry conditions

The influence of VPD and Rnet on surface energy partitioning was investigated during the wet and dry seasons. Results show that during both periods there is an increase in H and decrease in LE with an increase in VPD; although the gradient of LE decrease differs significantly during the two periods, H increases similarly during both the wet and dry periods (Figure 2-8). VPD is higher in times of little or no rain (low soil water availability), which explains the decrease in LE with a rise in VPD. In this instance, although the evaporative demand is high, the stomatal conductance is reduced due to the absence of water in the soil, resulting in smaller LE and higher H. Rnet, on the other hand, is partitioned into different fluxes, based on other climatic and vegetation physiological characteristics. Figure 2-9 illustrates that both LE and H increase with an increase in Rnet, although their increases are not in proportion, based on the season. During the wet season, the rate of increase of LE is higher than that of H, whereas in the dry season the reverse is true. The rate of increase of LE is controlled by the availability of soil water (precipitation), (also illustrated in Figure 2-6 (LE)), and during the wet season, it increases steadily with increasing Rnet, whereas the rate of increase of H is concave, showing saturation with an increase in Rnet. The opposite is true during the dry season, with limited water availability, where the rate of increase of LE slows down with an increase in Rnet, and a steady increase of H with Rnet increase.

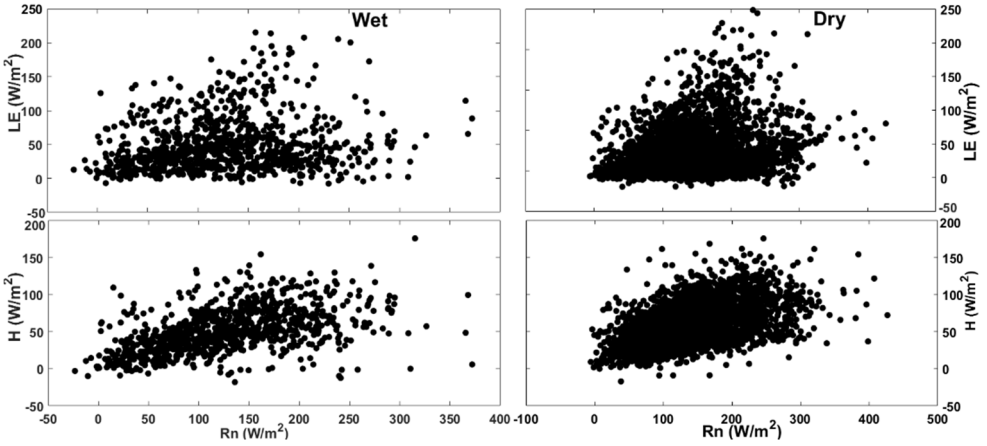

Figure 2-9: Effects of net radiation on LE and H under wet and dry conditions

Our study results are consistent with similar studies, for example, Gu et al. (2006), who examined how soil moisture, vapour pressure deficit (VPD) and net radiation control surface energy partitioning at a temperate deciduous forest site in central Missouri, USA. Both studies agree that with ample soil moisture, during the rainy season, latent heat flux dominates over sensible heat flux, and reduced soil water availability reversed the dominance of latent heat over sensible heat, because of its direct effect on stomatal conductance. An increase in net radiation, on the other hand, also increases both sensible and latent heat fluxes. The increase of either then becomes a function of soil moisture availability, since they cannot increase in the same proportion. However, whereas we found that a rise in VPD is characterised by a decrease in LE and an increase in H in both periods, their findings show a significant increase in LE and decrease in H with a rise in VPD during the non-drought period, with both components showing slight increases with increase in VPD in dry conditions. S.-G. Li et al. (2006) also investigated the partitioning of surface energy in the grazing lands of Mongolia, and concluded that the energy partitioning was also controlled by vegetation dynamics and soil moisture availability, although soil heat flux is reportedly higher than latent heat flux in most instances. In a temperate mountain grassland in Austria, Hammerle et al. (2008) found that the energy partitioning in this climatic region was dominated by latent heat flux, followed by sensible heat flux and lastly soil heat flux.

The consensus in all the above studies is that vegetation and climate dynamics play a critical role in energy partitioning. They note that during full vegetation cover, latent heat flux is the dominant portion of net radiation. However, depending on the climatic region, the limiting factors of energy partitioning vary between water availability and radiation. Our study confirms that in semi-arid

regions, sensible heat flux is the highest fraction of net radiation throughout the year, except during the wet period, when latent heat flux surpasses sensible heat flux. However, in regions and locations where water availability is not a limiting factor, latent heat flux may take the highest portion of net radiation.

2.5 Conclusion

This study investigated both surface energy balance and how it is partitioned into turbulent fluxes during the wet and dry seasons in a semi-arid savanna ecosystem in Skukuza using eddy covariance data from 2000 to 2014. The analysis revealed a mean multi-year energy balance ratio of 0.93, the variation of EBR based on season, time of day and as a function of friction velocity was explored. The seasonal EBR varied between 0.70 and 1.12, with the dry season recording the highest energy imbalance. Daytime EBR was as high as 0.96, with 0.27 EBR for the nighttime. The high energy imbalance at night was explained as a result of stable conditions, which limit turbulence that is essential for the creation of eddies. The assessment of the effect of friction velocity on EBR showed that EBR increased with an increase in friction velocity, with low friction velocity experienced mainly during night-time. Furthermore, the impact of G in this biome on EBR, with results showing a decrease of up to 7%, with an annual mean of 3.13±2.70, in EBR when G was excluded in the calculation of EBR.

The energy partition analysis revealed that sensible heat flux is the dominant portion of net radiation in this semi-arid region, except during the rainfall period. The results also show that water availability and vegetation dynamics play a critical role in energy partitioning, whereby when it rains, vegetation growth occurs, leading to an increase in latent heat flux / evapotranspiration. Clearly, an increase in Rnet results in a rise in H and LE, however, their increases are controlled by water availability. During the wet season, the rate of increase of LE is higher than that of H, whereas in the dry season the reverse is true. The rate of increase of LE is controlled by the availability of soil water (precipitation), and during the wet season, it increases steadily with increasing Rnet, whereas the rate of increase of H shows saturation with an increase in Rnet. The opposite is true during the dry season, with limited water availability, the rate of increase of LE reaches saturation with an increase in Rnet and a steady increase of H with Rnet increase. An increase in VPD, on the other hand, results in an increase in H and a decrease in LE, with higher VPD experienced during the dry season, which explains the high H, although the evaporativedemand is high.

3 PERFORMANCE OF SATELLITE REMOTE SENSING-BASED EVAPOTRANSPIRATION ESTIMATES

3.1 ABSTRACT[2]

Knowledge of evapotranspiration (ET) is essential for enhancing our understanding of the hydrological cycle, as well as for managing water resources, particularly in semi-arid regions. Remote sensing offers a comprehensive means of monitoring this phenomenon at different spatial and temporal intervals. Currently, several satellite methods exist and are used to assess ET at various spatial and temporal resolutions with various degrees of accuracy and precision. This research investigated the performance of three satellite-based ET algorithms and two global products, namely land surface temperature/vegetation index (TsVI), Penman-Monteith (PM), and the Meteosat Second Generation ET (MET) and the Global Land-surface Evaporation: the Amsterdam Methodology (GLEAM) global products, in two eco-regions of South Africa. Daily ET derived from the eddy covariance system from Skukuza, a sub-tropical, savanna biome, and large aperture boundary layer scintillometer system in Elandsberg, a Mediterranean, fynbos biome, during the dry and wet seasons, were used to evaluate the models. Low coefficients of determination (R^2) of between 0 and 0.45 were recorded on both sites, during both seasons. Although PM performed best during periods of high ET at both sites, results show it was outperformed by other models during low ET times. TsVI and MET were similarly accurate in the dry season in Skukuza, as GLEAM was the most accurate in Elandsberg during the wet season. The conclusion is that none of the models performed well, as shown by low R^2 and high errors in all the models. In essence, our results conclude that further investigation of the PM model is possible to improve its estimation of low ET measurements.

[2] **This chapter is based on**:
Majozi N. P., Mannaerts C.M., Ramoelo A., Mathieu R.S.A., Mudau A., Verhoef W. An intercomparison of satellite-based daily evapotranspiration estimates under different eco-climatic regions in South Africa, Remote Sensing 9 (4), 307.

3.2 Introduction

As an essential climate variable (ECV), evapotranspiration (ET) plays a critical role as a link of the energy, carbon and water cycles, with the latent heat of vapourisation serving as the largest sink of heat in the atmosphere. It is, therefore, important for disciplines such as agriculture, hydrology, meteorology, and climatology. Because of its high spatio-temporal variability, it is a challenge to directly measure this biophysical variable. Remote sensing remains the only feasible means of spatially estimating ET over varying spatial and temporal extents. Several authors have reviewed the remote sensing approaches used to estimate ET (Gibson et al., 2013; Li et al., 2009; Wang & Dickinson, 2012; Zhang et al., 2016) based on their structural complexities, theories and underlying assumptions, parameterisations, and uncertainties and limitations, and classified them as: i) empirical methods involving the use of statistically-derived relationships between ET and vegetation indices such as the normalised difference vegetation index (NDVI) or the enhanced vegetation index (EVI) (Glenn et al., 2007; Glenn et al., 2010; Nagler et al., 2005), ii) residual surface energy balance modelling (single- and dual-source models), which include the Surface Energy Balance Algorithm over Land (SEBAL)/ Mapping EvapoTranspiration at high Resolution with Internalized Calibration (METRIC) (Allen et al., 2011; Allen et al., 2007; Paul et al., 2014; Wang et al., 2014) , Surface Energy Balance System (SEBS) (W. Ma et al., 2014; Su, 1999, 2002), iii) physically-based methods involving the Penman-Monteith (PM) (Dhungel et al., 2014; Ershadi et al., 2015; Westerhoff, 2015) and Priestley-Taylor (PT) equations (Colaizzi et al., 2014; Priestley & Taylor, 1972; Szilagyi et al., 2014), and iv) data assimilation methods applied to the heat diffusion equation and radiometric surface temperature sequences. Global satellite-based ET products have been produced using these algorithms, like the MOD16 ET product that is estimated using the Penman - Monteith equation by Mu et al. (2007); Mu et al. (2011) , the Meteosat Second Generation ET product (MET) derived using the physically-based Soil-Vegetation-Atmosphere-Transfer (SVAT) model Tiled ECMWF (European Centre for Medium-Range Weather Forecasts) Surface Scheme of Exchange processes at the Land surface (TESSEL) that uses a combination of atmospheric model outputs and Meteosat Second Generation's Spinning Enhanced Visible and Infrared Imager MSG-SEVIRI remote sensing data (Arboleda et al.; Dutra et al., 2010; Ghilain et al., 2011) and the Global Land-surface Evaporation: the Amsterdam Methodology (GLEAM) based on the Priestley-Taylor equation and the Gash analytical model of forest rainfall interception (Miralles et al., 2011).

Validation and model comparison studies have been done at different locations, time steps and periods. Yuting Yang et al. (2015a) examined the performances

and model physics of three dual-source ET models, the Hybrid dual-source scheme and Trapezoid framework-based ET Model (HTEM), the Two-Source Energy Balance (TSEB) model, and the MOD16 ET (PM) algorithm in the Heihe River Basin in Northwest China. They reported that HTEM outperformed the other models, whereas PM performed least; and the reason for the poor performance of PM being that the model does not effectively capture soil moisture restriction on ET. Singh and Senay (2015) compared four models, i.e., METRIC, SEBAL, SEBS, and the Operational Simplified Surface Energy Balance (SSEBop) models at three AmeriFlux cropland sites in the Midwestern United States. Their results showed all models recorded R^2 of 0.81, with METRIC and SSEBop having low RMSE (<0.93 $mmday^{-1}$) and a high Nash–Sutcliffe coefficient of efficiency (>0.80), whereas SEBAL and SEBS gave relatively higher bias. ¯Index (S-SEBI)) at four sites (marsh, grass, and citrus surfaces), to identify the most appropriate for use in the humid southeastern United States. SEBS generally outperformed the other with RMSE of 0.74 $mmday^{-1}$, whereas SSEBop was consistently the worst performing model (RMSE = 1.67 $mmday^{-1}$). They observed that for short grass conditions, SEBAL, METRIC, and S-SEBI worked much better than SEBS. Ershadi et al. (2014) assessed the performance of four models, i.e. SEBS, PM, Priestley-Taylor Jet Propulsion Laboratory (PT-JPL), and Advection-Aridity (AA), in twenty FLUXNET towers covering different biomes that included grassland, cropland, deciduous broadleaf forest and evergreen needleleaf forest, mainly in Europe and North America, at half-hourly, hourly and monthly time steps. Their results showed that PT-JPL outperformed the other models, followed by SEBS, PM, and lastly AA. Their overall findings, however, were that there was no model that consistently performed well across all the biomes. A study by Ha et al. (2015) in semi-arid pine forests with variable disturbance history, over a period of 4 years and at monthly time steps, also showed that the PT model gave the best results, with the PM model and MOD16 ET product under predicting ET at all sites. Vinukollu et al. (2011b) tested SEBS, PT, and PM over 16 FLUXNET sites and concluded that PT outperformed the other models.

Many remote sensing-based ET estimation studies have been performed in different South African landscapes and land uses, as reviewed by Gibson et al., (2013). The review stresses the importance of validating the remotely sensed ET estimates to allow for confidence in their use and application in the various biomes. Jarmain et al., (2009b) used a large discontinuous *in situ* ET dataset, mainly from agricultural land, to evaluate remote sensing-based ET algorithms (SEBS, SEBAL, METRIC, and VIIT), and recorded poor performance of all the models. Evaporativefraction estimation by these models was the main source of error, which led to low accuracy in ET estimation. One of the challenges of this study was the limited data points at each site for substantive statistical analysis,

hence, no distinct conclusion could be made. Jovanovic et al. (2014) reported an R^2 of 0.72 and 0.75 in their validation of the 30 minutes and daily MET ET products for the fynbos vegetation of the Riverlands Nature Reserve. Ramoelo et al. (2014) validated the PM-derived MOD16 8-day ET product using multiyear eddy covariance-derived ET datasets for two flux towers in savannahs, Skukuza and Malopeni. Inconsistent results were attributed to various factors, including the parameterisation of the PM model, flux tower measurement errors, and flux tower footprint vs. MODIS pixel size. Furthermore, Sun et al. (2012) used the Skukuza flux tower data to evaluate a remote sensing - based continental ET product. The results were reasonable during the wet season, whereas low coefficients of determination were observed in the dry season. One example of remotely sensed ET applications in South Africa is the use of SEBAL by the eLEAF company, in collaboration with the Water Research Commission (WRC), the South African's Department of Agriculture (DAFF) and academic institutions, to provide information on water use efficiency of irrigated crops, inclusive of grapes, deciduous fruits, sugarcane and grain crops in the Western Cape Province of South Africa (Jarmain et al., 2009a; Klaasse et al., 2008; Klaasse & Jarmain, 2011). Overall, limited work has been done to assess and compare the performance of different ET models in different SA natural ecosystems.

There is still scope to extensively compare different models for different biomes in semi-arid ecosystems, which would result in the identification of the most accurate and robust model that could be used to map and monitor ET at national scale. Hence, this study intended to evaluate and compare the performance of daily ET estimates derived using TsVI and MOD16 Penman-Monteith-based models, and GLEAM and MET global products, under two different climatic regions, a subtropical, savannah, summer rainfall and a Mediterranean, fynbos, winter rainfall climates. From each climatic region, rainy and dry periods were selected to evaluate the performance of each model.

3.3 Materials and Methods

One of the challenges in evaluating evapotranspiration models is the availability of accurate and complete datasets. The comparisons were performed for two eco-regions in South Africa, Skukuza in the North-East of South Africa, an area characterised by summer rainfall, and Elandsberg in the South-West of the country, characterised by winter rainfall (Figure 3-1). A full description of the sites is given in Section 3.2.1 below.

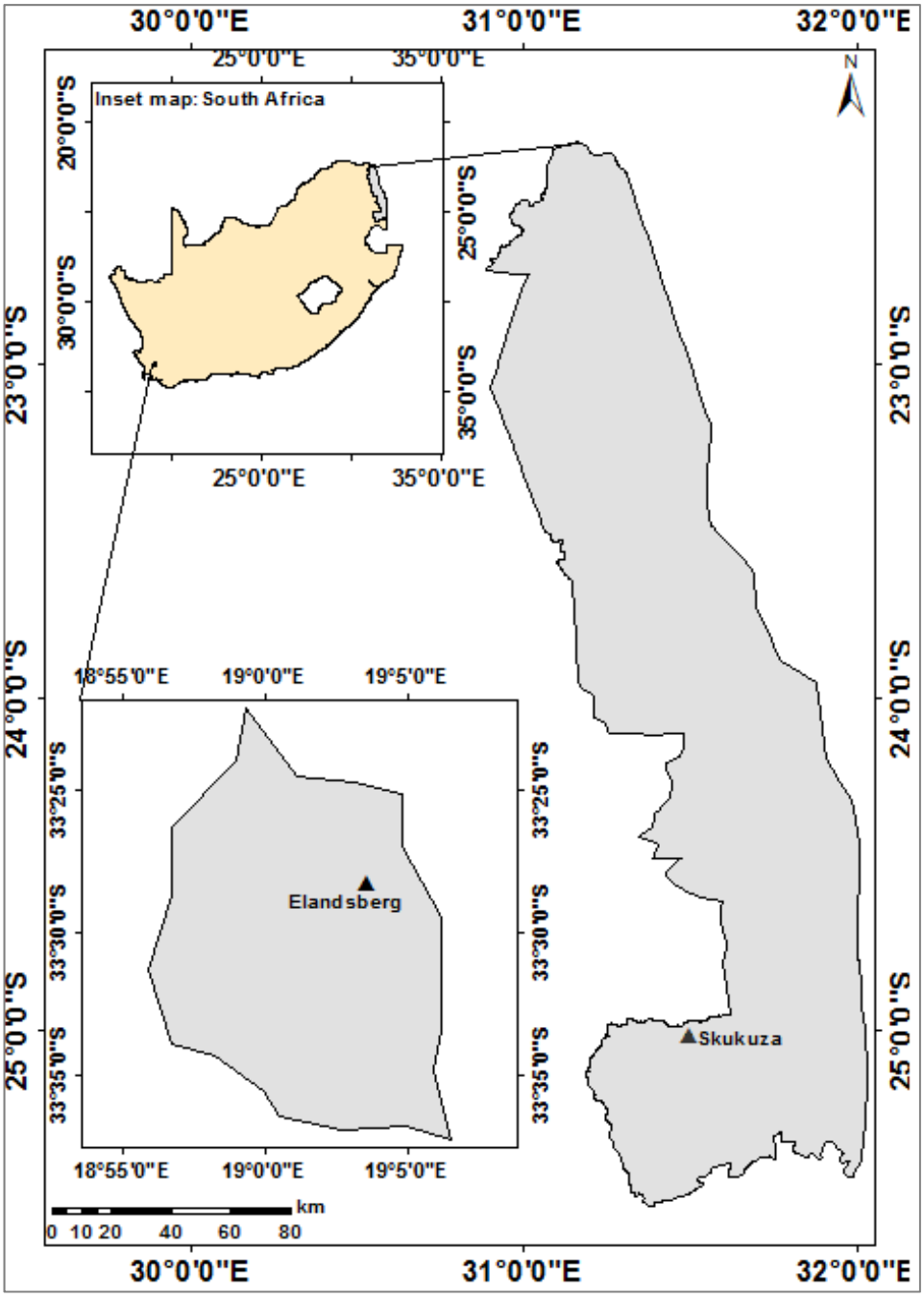

Figure 3-1: Location of Skukuza eddy covariance flux tower and Elandsberg LAS sites

3.3.1 Site description

Summer rainfall savannas and Skukuza flux tower

The Skukuza eddy covariance flux tower (25.02°S, 31.50°E) was established early 2000 as part of the SAFARI 2000 experiment, set up to understand the interactions between the atmosphere and the land surface in southern Africa (Scholes et al., 2001; Shugart et al., 2004).

The site is located in the Kruger National Park (South Africa) at 365 m above sea level, and receives 550 ± 160 mm precipitation per annum between November and April, with significant inter-annual variability. The soils are generally shallow, with coarse sandy to sandy loam textures. The area is characterised by a catenal pattern of soils and vegetation, with broad-leaved Combretum savanna on the crests dominated by *Combretum apiculatum*, and fine-leaved Acacia savanna in the valleys dominated by *Acacia nigrescens*. The vegetation is mainly open woodland, with approximately 30% tree canopy cover of mixed Acacia and Combretum savanna types. Tree canopy height is 5–8 m with occasional trees (mostly *Sclerocarya birrea*) reaching 10 m. The grassy and herbaceous understory comprises grasses such as *Panicum maximum, Digitaria eriantha, Eragrostis rigidor,* and *Pogonarthria squarrosa*. The flux tower was placed on a vegetation transition to measure fluxes from the different types (Scholes et al., 2001).

Figure 3-2: Skukuza eddy covariance flux tower station in Kruger National Park

Eddy covariance system

Since 2000, ecosystem-level fluxes of water, heat and carbon dioxide are measured using an eddy covariance system mounted at 16 m of the 22 m high flux tower (Figure 3-2). The measurements that were taken and the instruments used are summarised in Table 3-1.

Table 3-1: Measurements taken at Skukuza eddy covariance system and the instruments used

Instrument	Model/ brand	Measurement
Sonic anemometer	Gill Instruments Solent R3, Hampshire, England	3-dimensional, orthogonal components of wind velocity, u, v, w (ms^{-1})
Closed path gas analyser	IRGA, LiCOR 6262, LiCOR, Lincoln	Water vapour, carbon dioxide concentrations
Radiometer	Kipp and Zonen CNR1, Delft, The Netherlands	Incoming and outgoing longwave and shortwave radiation
HFT3 plates	Campbell Scientific	Soil heat flux at5 cm depth
Frequency domain reflectometry probes	Campbell Scientific CS615, Logan, Utah	Volumetric soil moisture content at different depths

Ancillary meteorological measurements include air temperature and relative humidity, also measured at 16 m, using a Campbell Scientific HMP50 probe, precipitation at the top of the tower using a Texas TR525M tipping bucket rain gauge; wind speed and direction using a Climatronics Wind Sensor, and soil temperature using Campbell Scientific 107 soil temperature probe.

Flux footprint modelling for the Skukuza tower was done using footprint models that are incorporated in the EddyPro software, i.e. the footprint parameterisation model of Kljun et al. (2004) and footprint model of Kormann and Meixner (2001). Depending on a number of factors, including wind direction and friction velocity, atmospheric stability, terrain homogeneity, and measurement height, either of the models is selected to compute the footprint. It was estimated that 90% of the fluxes originated from an average of 1.6 km upwind from the flux tower, as reported by Ramoelo et al. (2014). The shape of the flux source area is dependent on the wind velocity and direction and varies throughout the day. With a surface energy balance closure of 1.03, the LE fluxes were then corrected by:

$$\boldsymbol{LE_{corr} = LE + Res\left(\frac{LE}{H+LE}\right)} \quad 2$$

where LEcorr is corrected latent heat flux, Res is the residual (Res=Rnet-G-H-LE).

Winter rainfall fynbos and Elandsberg large aperture scintillometer

Elandsberg Private Nature Reserve (33.47°S; 19.06°E) is situated near Hermon in the valley of the Berg River, Western Cape Province. It is a South African National Heritage Site, and it is also a Contractual Nature Reserve, which gives it formal conservation status in terms of fauna and flora. This study area lies within the West Coast Renosterveld of the fynbos biome. The vegetation of this area is classified as the Swartland Shale Renosterveld in the form of discrete vegetation patches. The dominant vegetation types include shrubland and low fynbos, thicket, bushland, and high fynbos. This study area is in a winter rainfall region, with dry summers typical of Mediterranean type climate; it receives between 250 and 600 mm rainfall per annum.

Figure 3-3: Left- LAS transmitter of infrared radiation; right- Receiver of the optically modified infrared beam located about 900 m away from the transmitter

Along the 900 m transect of the scintillometer, the average vegetation height is 1 m, with the general land cover being shrubland and low fynbos (Figure 3-3).

Scintillometry system

Prior to selecting the Elandsberg site for LAS installation and ET validation, a study was conducted to ensure that the area selected meets a number of criteria as a suitable flux tower site, including land cover homogeneity (single land cover type within the image pixel, in this case, the MODIS pixel), vegetation height, topographic variability, and atmospheric stability (Jovanovic et al., 2013). The site for the scintillometer study of evapotranspiration was, therefore, selected based on the extent and uniformity of the natural vegetation, and also to ensure that the match between the selected pixel and the scintillometer transect would be accurate enough for the ground-truthing of ET from that pixel.

A mobile large aperture boundary layer scintillometer (LAS) (BLS 900, Scintec, AG, Germany) was installed in Elandsberg Nature Reserve in October 2012 and collected data until November 2013. The scintillometer transmitter was located at 33.47404 °S; 19.06239 °E, while the receiver was placed at approximately 900 m from the transmitter, at 33.47001 °S; 19.05526 °E.

Sensible heat flux was calculated from the changes in the refractive index of air between the scintillometer transmitter of monochromatic infrared radiation at 880 nm and the receiver. The net radiation was measured using a net radiometer (Kipp and Zonen, Delft, The Netherlands), installed at 2 m above the vegetation in the middle of the scintillometer transect. The soil heat flux (G_0) was measured using a cluster of four soil heat flux plates (REBS, Inc. Seattle, WA, USA), installed at a depth of 80 mm at various positions within the MODIS pixel.

An automatic weather station was also installed to record air temperature, relative humidity, wind speed and direction, solar irradiance, and rainfall.

Temperature and relative humidity were measured at 1.5 m using a CS500 probe (Vaisala, Helsinki, Finland), while windspeed and direction were measured at 2.5 m height using an RM Young wind sentry (Model 03001 – Campbell Scientific Ltd, USA), and solar irradiance was monitored using a pyranometer (Apogee, Instruments, USA). Rainfall was measured using a tipping rain gauge (Model TE 525WS – Campbell Scientific Ltd, USA). Soil water content was also measured at 30 min intervals in the depth range 0 - 20 cm using a CS616 capacitance probe (Campbell Scientific Ltd, USA). All the sensors were connected to a CR23X datalogger (Campbell Scientific Ltd, USA).

3.3.2 Model descriptions

TsVI method

The concept of the land surface temperature-vegetation index triangle (Ts-VI) method was discovered by Goward et al., (1985) and has been used to retrieve soil water content, analyse land use/ land cover change and monitor droughts with satellite data (Allen et al., 2007; Mallick et al., 2012; Wang et al., 2006). Using the Ts-VI feature space, Jiang and Islam (1999, 2001; 2003) adapted the PT equation to estimate regional evaporative fraction (EF) and ET. This method calculates ET as a function of available energy, i.e. net radiation minus soil heat flux. Its main assumption is that ET depends on soil moisture and vegetation cover, the method requires a large heterogeneous area with a varied range of values. The PT parameter φ, which accounts for the aerodynamic and canopy resistances in the PT formulation is replaced with ϕ in the proposed formula by Jiang and Islam (1999), which is determined using the triangular shape of the LST-VI feature space. ET is estimated using:

$$\boldsymbol{LE = \phi \left[\frac{\Delta}{\Delta + \gamma} (Rn - G) \right]} \quad 3$$

where ϕ is a combined-effect parameter accounting for aerodynamic resistance (dimensionless), Rnet is surface net radiation (Wm^{-2}), G is soil heat flux (Wm^{-2}), Δ is the slope of saturated vapour pressure versus air temperature ($kPa°C^{-1}$), γ is psychrometric constant ($kPa°C^{-1}$).

Defining the ϕ parameter

The TsVI triangle method proposed by Jiang and Islam (1999, 2001; 2003) has been applied at different scales to estimate the parameter ϕ in the PT method, and thus evaporativefraction (EF). Modifications have also been made to this method as shown by Wang et al. (2006) who combined the triangle method with thermal inertia and developed a day-night LST difference-NDVI triangle using MODIS land surface products to estimate EF. Stisen et al. (2008) also combined the triangle method with thermal inertia and developed a quadratic function of

NDVI to determine ϕ at the dry edge using MSG-SERVIRI data. Furthermore, Tang et al. (2010) replaced NDVI in the construction of the triangle with fractional cover (Fr) and developed an automatic algorithm to determine the wet and dry edges.

The wet and the dry edges of the two-dimensional triangular space for each vegetation class are determined first, where the wet/cold edge represents the potential evapotranspiration, and the dry/warm edge represents water-stressed conditions. This global ϕ_{min} and ϕ_{max} are set at zero for a dry bare soil surface, and 1.26 for a saturated or well vegetated surface, respectively. Assuming that ϕ increases linearly with a decrease in Ts between ϕ_{min} and ϕ_{max} for any given Fr, $\phi_{min,i}$ is then linearly interpolated between ϕ_{min} and ϕ_{max}, with $\phi_{i,max} = \phi_{max} = 1.26$ as:

$$\boldsymbol{\phi_{min.i}} = \boldsymbol{\phi_{max}} * \boldsymbol{F_r} \quad (4)$$

where

$$\boldsymbol{F_r} = \frac{\boldsymbol{NDVI - NDVI_{min}}}{\boldsymbol{NDVI_{max} - NDVI_{min}}} \quad (5)$$

Then for each pixel in the triangle, ϕ_i is then derived by using the normalised temperature:

$$\boldsymbol{\phi_i} = \left(\frac{\boldsymbol{T_{max} - T_i}}{\boldsymbol{T_{max} - T_{min}}}\right) * (\boldsymbol{\phi_{max}} - \boldsymbol{\phi_{min.i}}) + \boldsymbol{\phi_{min.i}} \quad (6)$$

where T_{max} and T_{min} are the corresponding maximum and minimum surface temperatures at the dry and wet edges, respectively.

The evaporativefraction (EF) is then calculated using:

$$\boldsymbol{EF} = \boldsymbol{\phi} * \frac{\boldsymbol{\Delta}}{\boldsymbol{\Delta + \gamma}} \quad (7)$$

Penman-Monteith based MOD16 ET model

The Penman-Monteith (PM) is a physically-based model that incorporates heat and water vapour mass transfer principles and is known as the combination equation. Developed and modified by Penman (1948) and Monteith (1965), this algorithm was initially designed as a single-source model, computing ET from a heterogeneous land surface as a single component. Modified versions of this model now include the separate estimation of different components of water loss from bare soil and canopy intercepted water (evaporation), and transpiration via the canopy. Following Cleugh et al. (2007) who employed MODIS data to estimate ET using the PM model, Mu et al. (2007) modified the model by adding vapour pressure deficit and minimum temperature to constrain

stomatal conductance, using enhanced vegetation index instead of NDVI to calculate vegetation cover fraction and included the separate calculation of soil evaporation. Further improvements were made to the algorithm, including calculating ET as a sum of day- and night-time ET, adding soil heat flux calculation, separating dry and wet (interception) canopy surfaces, and soil surface into saturated and moist surface, as well as improving stomatal conductance, aerodynamic resistance and boundary layer resistance estimates (Mu et al., 2011). Taking into account that relative humidity, and by extension, vapour pressure deficit were soil moisture stress proxies in Mu et al. (2007; 2011), Sun et al. (2013) used the soil moisture index estimated from the TsVI method to constraint soil evaporation.

Latent heat flux is estimated as:

$$\boldsymbol{\lambda E} = \frac{\boldsymbol{s}*\boldsymbol{A}+\boldsymbol{\rho}*\boldsymbol{Cp}*(\boldsymbol{e_{sat}}-\boldsymbol{e})/\boldsymbol{r_a}}{\boldsymbol{s}+\boldsymbol{\gamma}*(\mathbf{1}+{}^{\boldsymbol{r_s}}/_{\boldsymbol{r_a}})} \quad 8$$

where λE is the latent heat flux (Wm^{-2}) and λ is the heat of vapourisation (Jkg^{-1}), s is the slope of the curve relating saturated vapour pressure to temperature (PaK^{-1}), A is available energy (Wm^{-2}), ρ is the air density (kgm^{-3}), Cp is the specific heat capacity of air ($Jkg^{-1}K^{-1}$), γ (PaK^{-1}) is the psychrometric constant, e_{sat} is the saturation vapour pressure (Pa), e is the actual vapour pressure (Pa), where e_{sat} – e = vapour pressure deficit (VPD), r_a (sm^{-1}) is the aerodynamic resistance, and r_s (sm^{-1}) is the canopy resistance, which is the reciprocal of canopy conductance gc ($gc=1rc^{-1}$).

The MOD16 remote sensing-based ET algorithm predicts ET globally at 86% accuracy when compared with eddy measurements of ET over many sites in the AmeriFlux network. Building on previous algorithms, it uses a physically-based PM approach driven by MODIS-derived vegetation data. ET is calculated as a sum of daytime and night-time components using vapour pressure deficit and minimum temperature to control stomatal resistance. Stomatal resistance is scaled up to the canopy level using LAI to calculate canopy resistance for plant transpiration. The algorithm also models soil heat flux and separates evaporation from a wet canopy and transpiration from a dry canopy. Actual soil evaporation is also calculated from potential evaporation.

For arid and semi-arid regions like South Africa and the Nile Basin, the Mu et al. (2013) version of the MOD16 Penman-Monteith method was used.

Net radiation and soil heat flux estimation

Net radiation (Rnet) is the difference between incoming and outgoing long- and shortwave radiation fluxes on the Earth's surface. It plays a very important role in the exchange processes of water and heat over the land surface. It is a critical parameter in the estimation of ET, and all ET models require its estimation (R.

G. Allen et al., 2007; W. G. M. Bastiaanssen et al., 2005; Penman, 1948; Z. Su, 2002).

It is expressed in terms of its components:

$$\boldsymbol{Rn = R_s^{\downarrow} - R_s^{\uparrow} + R_l^{\downarrow} - R_l^{\uparrow} = (1-\alpha)R_s^{\downarrow} + \sigma\varepsilon_a T_a^4 - \sigma\varepsilon_s T_s^4} \quad 9$$

where α is the land surface albedo, $R_S^{\downarrow}$ is the incoming shortwave radiation (W/ m²), $R_l^{\downarrow}$ is the longwave incoming radiation (Wm^{-2}), $R_l^{\uparrow}$ is the outgoing longwave radiation(Wm^{-2}), σ is the Stephan-Botlzmann constant (5.670373*10-8 $Wm^{-2}K^{-4}$), εa is the atmospheric emissivity, εs is the surface emissivity, Tair and Ts are air and surface temperature (K), respectively.

For this study, the method of Shine (1984) was used to estimate $R_S^{\downarrow}$:

$$\boldsymbol{R_s^{\downarrow} = \frac{S_0 cos^2\theta}{1.2cos\theta + e(1+cos\theta)*10^{-2} + 0.0455d^2}} \quad 10$$

where S_o is the Solar constant (1367 W/ m^2), θ is the Solar zenith angle, e is the vapour pressure.

Soil heat flux (G) was computed

$$\boldsymbol{G = Rn\big(Tc + (1-Fr)(Ts - Tc)\big)} \quad 11$$

where Tc is the ratio of G to Rnet for full vegetation cover, and Ts is the ratio of G to Rnet for dry bare soil.

The results used in the estimation of ET from Rnet and G are estimated using the same set of equations and parameters for the PM and TsVI models, hence the study will also compare these parameters.

3.3.3 Global evapotranspiration products

Apart from evaluating the two ET methods, the performance of two global ET products, i.e. the Meteo-sat (MET) and the Global Land Evaporation: the Amsterdam Model (GLEAM) ET products, will also be assessed in this study.

LSA SAF Evapotranspiration product

The global ET product (MET) by the EUMETSAT Satellite Application Facility on Land Surface Analysis (LSA-SAF) based on the SEVIRI sensor on-board the Meteosat Second Generation geostationary satellites (MSG-SEVIRI), is in near-

real time, and also available at 30 minute and daily time intervals and 3 km spatial resolution. This product is derived using the physically-based TESSEL SVAT scheme that uses a combination of the European Centre for Medium-range Weather Forecasts (ECMWF) atmospheric model outputs (i.e. air and dew point temperature, humidity, wind speed, atmospheric pressure, and soil moisture) and MSG/ SERVIRI remote sensing data (Arboleda et al.; Dutra et al., 2010; Ghilain et al., 2011). This model divides the pixel into different tiles representing different land covers within the pixel, with some parameters defined at the pixel level and the data are extracted from the ECOCLIMAP database. The pixel ET is the sum of the weighted contribution of each tile. It can be downloaded from the Land Surface Analysis Satellite Applications Facility (LSA SAF) website, http://landsaf.meteo.pt/.

GLEAM Evapotranspiration product

The Global Land Evaporation: the Amsterdam Model (GLEAM) ET product is derived using the semi-empirical PT equation and the Gash analytical model of forest rainfall interception (Miralles et al., 2011). The model uses inputs from different satellites to estimate ET daily at 0.25° spatial resolution. The use of the simple PT equation means there is no parameterisation of stomatal and aerodynamic resistances. It estimates different evaporation components, including transpiration for three land cover types, i.e. tall canopies, short vegetation, interception loss, bare-soil evaporation, snow sublimation, and open-water evaporation. The potential ET estimates are then constrained by a multiplicative stress factor computed based on the content of water in vegetation and the root zone. The final ET estimate presented in a grid is then given as a weighted average from the three land covers.

3.3.4 Input data

The two models that were tested in this study require different inputs and parameterisations. Table 3-2 lists each model's inputs and their sources, i.e. whether satellite or meteorological based.

Table 3-2: A summary of the different ET algorithms and where they have been applied

Method	Inputs	
	Remote sensing	**Meteorological**
LST-VI triangle	LST, EVI, surface emissivity , albedo, LAI, solar zenith angle	Ta, Pa, RH
PM	LST, EVI, land cover, surface emissivity, albedo, LAI, solar zenith angle	Ta, Pa, RH

3.3.5 *In situ* and meteorological measurements

To select the ET validation periods, eddy covariance data were filtered based periods having extensive data with minimal gaps per day and per month, and the availability of all required input data used in the different models. For each site, two time periods were selected for the summer and the winter season, i.e. wet and dry periods. For Skukuza, the periods between 01 and 31 January 2012 (wet), and 05 May to 05 June 2012 (dry) were selected, whereas, for Elandsberg, 09 November to 09 December 2012 (dry), and 07 June to 06 July 2013 (wet) were selected.

Meteorological data used from each site included air temperature (Ta), precipitation, relative humidity (RH), atmospheric pressure (P) and wind speed (u) were used to calibrate the models. From these data, we calculated daily maximum and minimum air temperature, average daily, daytime and night-time temperatures, daily atmospheric pressure, wind speed, and relative humidity. The input variables at each site were measured using the instruments listed in Table 3-3.

Table 3-3: Summary of meteorological input variables and their measurement instruments for Skukuza and Elandsberg

	Measurement instrument used	
Input variable	**Skukuza**	**Elandsberg**
Air temperature (°C)	Campbell Scientific HMP50 probe	CS500 probe (Vaisala, Helsinki, Finland)
Relative humidity (%)	Campbell Scientific HMP50 probe	CS500 probe (Vaisala, Helsinki, Finland)
Wind speed (m/s)	Climatronics Wind Sensor	RM Young wind sentry (Model 03001 – Campbell Scientific Ltd, USA)

The 30-minute λE measurements from the Skukuza eddy covariance were converted to ET, which were summed up to daily ET measurements following Mu et al. (2011). From Elandsberg, LE was estimated using the energy balance equation, i.e. as a residual of the surface energy balance from measurements of Rnet, G and H (estimated with the LAS), and then converted to daily ET estimates.

3.3.6 Remote sensing data

This study made use of MODIS Terra/ Aqua products as data inputs. The following MODIS products were used as inputs for this study: daily 1 km MOD11A1 land surface temperature (LST) and emissivity, 8-day 1 km MOD15A2 leaf area index and FPAR, 16-day 1 km MOD13A2 vegetation indices (NDVI and

EVI), 16-day 1 km MCD43A3 albedo, and MOD03 geolocation for solar zenith. These datasets were downloaded from the NASA Land Processes Distributed Active Archive Centre (LP DAAC) website (https://lpdaac.usgs.gov/data_access).

For the 8-day datasets (i.e. LAI/ FPAR and surface albedo), images for Julian days 1, 9, 17, 25 and 33 (Skukuza rainy period), and 121, 129, 137, 145, 153 and 161 (Skukuza dry period); 313, 321, 329, 337 and 345 (Elandsberg dry period), and 145, 153, 161, 169, 177 and 185 (Elandsberg rainy period) were downloaded. For the 16-day datasets (i.e. vegetation indices) images for days 1, 17, 33, 113, 129, 145 and 161 (Skukuza 2012), and 305, 321, 337, 353 (Elandsberg 2012), 145, 161, 177, 193 (Elandsberg 2013), were downloaded. The inverse distance weighting interpolation technique was then applied on consecutive 8-day and 16-day MODIS datasets to estimate the daily values of each data input. Assumptions made here include that the change of vegetation and land characteristics over time is slow and systematic, depending on seasonal progression.

Other methods and techniques that compute ET at daily, monthly and seasonal scale have been developed. These include the integration of the feedback method that uses the complimentary relationship between actual ET and pan ET (Long & Singh, 2010), data fusion methods (i.e. combining different data sources) (Cammalleri et al., 2014; Semmens et al., 2016), and the backward-averaged iterative two-source surface temperature and energy balance solution (BAITSSS) algorithm (Dhungel et al., 2016).

3.3.7 Data analysis

The models described in Section 3.2 were run using the above data to estimate daily ET during the selected times, i.e. 01 and 31 January 2012 (wet), and 05 May to 05 June 2012 (dry) for Skukuza, and 09 November to 09 December 2012 (dry), and 07 June to 06 July 2013 (wet) for Elandsberg.

The accuracy of the ET estimates depends on a number of factors, including the algorithms and their parameterisations and the accuracy of the input datasets. The performance of each model was assessed using the coefficient of determination (R^2) a measure of goodness of fit, bias, mean absolute error (MAE), root mean square error (RMSE), and relative RMSE (rRMSE); the latter being measurements of error/ accuracy. RMSE provides information on the short-erm performance of a model by allowing a term by term comparison of the actual difference between the predicted value and the measured value, although it does not differentiate between under- and over- estimation; bias provides information on the long-term performance of a model. A positive value

gives the average amount of over-estimation in the estimated values and vice versa.

3.4 Results

3.4.1 Ground measurements of evapotranspiration and meteorological input variables

The first part of the results describes the meteorological input variations, i.e. daily mean air temperature (Ta), RH, Rnet and precipitation in relation to ET, between the two sites (Skukuza located in a rainy summer region, and Elandsberg characterized by dry summers).

Daily time series of Tair, RH, Rnet, ET and precipitation for Skukuza and Elandsberg for the validation periods are shown in Figure 3-4. For Skukuza, the daily ET for the rainy period (DOY 1-31) ranged between 0.96 and 6.24 mmday^{-1}, with an average of 4.06 mmday^{-1} and a standard deviation of 1.24 mmday^{-1}. Temperature varied between 22.16 °C and 30.93 °C, with a mean of 27.25.±2.24 °C, RH ranged between 91.54 and 58.27%, with an average of 69.95%, and the average Rnet for this period was 144. 32± 43.7 Wm-^{2}. A total of 280 mm precipitation was recorded within the same period. During the dry period (DOY 128-153), daily ET ranged between 0.53 and 1.47 mmday^{-1}, with an average of 0.99±0.26 mmday^{-1}, Rnet was between 40.15 and 91.92 Wm-^{2}, and mean air temperature of 18.68±1.44 °C was recorded; no precipitation was recorded during the same period.

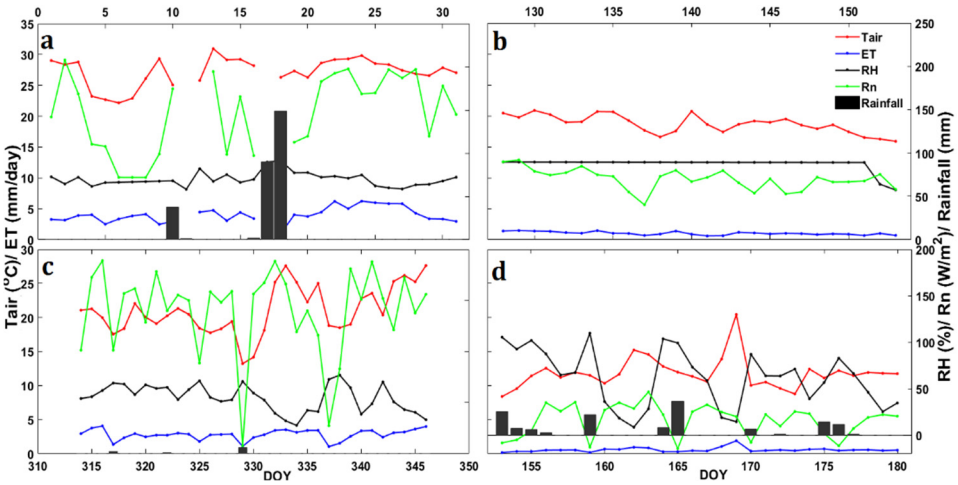

Figure 3-4: Meteorological data input measurements for DOY 1-31 (a) and DOY 128-153 (b) periods in Skukuza eddy covariance flux tower site; and DOY 314 - 346 (c) and DOY 153 and 180 (d) periods in Elandsberg LAS site

In Elandsberg, in the summer season (DOY 314-346), which is also the dry season, Tair recorded an average of 21±3.45 °C, whereas RH was between 27.76 and 77%, with Rnet ranging from 7.83 to 189 Wm^{-2}; ET ranged between 1.05 and 4.06 $mmday^{-1}$, with an average of 2.78 ± 0.76 $mmday^{-1}$, and a total precipitation of 9.2 mm. The wet, or winter period (DOY 153 and 180) recorded a total of 191 mm rainfall, and daily ET varied between 0.17 and 2.22 $mmday^{-1}$, with a mean of 0.65 $mmday^{-1}$ and standard deviation of 0.37 $mmday^{-1}$, Ta ranged from 8.39 to 20.45 °C, RH varied between 8.58 and 100%, whereas Rnet recorded daily averages between -14.47 and 46.52 Wm^{-2}.

3.4.2 ET models performance evaluation

In this sub-section, the performance of the evapotranspiration models, TsVI and MOD16-based Penman-Monteith, and MET and GLEAM global products estimates, against in situ measurements is analysed over two different seasons and ecosystems. This section will look at the performance of the models per location per season, and move on the intercompare the different locations per model per season. The results of the analysis are illustrated in Figures 3-5 and 3-6, and the statistical analyses summarised in Table 3-4. We also evaluated the modelled Rnet and against values that were measured at the sites.

Skukuza

Figure 3-5 a and b illustrate the temporal variation of the flux tower based and the modelled ET, Figure 3-6 a and b show the correlations between the flux tower and modelled ET, and Table 3-4 highlighting the statistics of the models comparisons. Generally, all the models underestimated ET on both seasons, as shown by the negative biases (Table 3-4) that ranged between -2.66 $mmday^{-1}$ (MET) and -0.79 $mmday^{-1}$ (PM) in the wet season, and -0.64 $mmday^{-1}$ (GLEAM) and -0.01 $mmday^{-1}$ (TsVI) during the dry season. The high underprediction of ET by MET and GLEAM during the wet period is also illustrated in Figure 3-5 a and Figure 3-6 a, whereas PM showed the least underprediction of ET. During the dry season, TsVI (-0.01 $mmday^{-1}$) had the lowest underestimation, and GLEAM (-0.64 $mmday^{-1}$) had the highest underestimation (Figure 3-5 b and 3-6 b). The slopes ranged between 0.19 (PM) and 0.66 (MET), and intercepts were between 1.23 $mmday^{-1}$ (MET) and 3.40 $mmday^{-1}$ (PM) in the wet season; in the dry season the slopes ranged from 0.20 (MET) to 3.35 (GLEAM), and the intercepts were between 0.02 $mmday^{-1}$ (GLEAM) and 0.66 $mmday^{-1}$ (MET). The correlations (R^2) of the modelled ET against the measured ET were relatively low, ranging between 0.05 (PM) and 0.45 (MET) during the wet season, and 0.07 (MET) and 0.42 (GLEAM) during the dry season. Although it had the lowest correlation, PM was the best performing model during the wet period, recording the lowest MAE, RMSE and rRMSE of 0.89 $mmday^{-1}$, 1.25 $mmday^{-1}$ and 27.34%,

respectively, followed by TsVI and GLEAM, which had comparable accuracies of 1.40 and 1.46 mmday^{-1}, 1.66 and 1.64 mmday^{-1}, and 36.46 and 40.44%, MAE, RMSE and rRMSE respectively. MET performed the least with MAE, RMSE and rRMSE of 2.66 mmday^{-1}, 2.85 mmday^{-1}and 67.5%, respectively. In the dry period, TsVI and MET had comparable accuracies of 0.23 and 0.25 mmday^{-1} (MAE), 0.29 and 0.32 mmday^{-1} (RMSE), 28.34 and 31.09% (rRMSE); GLEAM performed the least with MAE 0.64 mmday^{-1}, RMSE 0.67 mmday^{-1}, and rRMSE 65.96%.

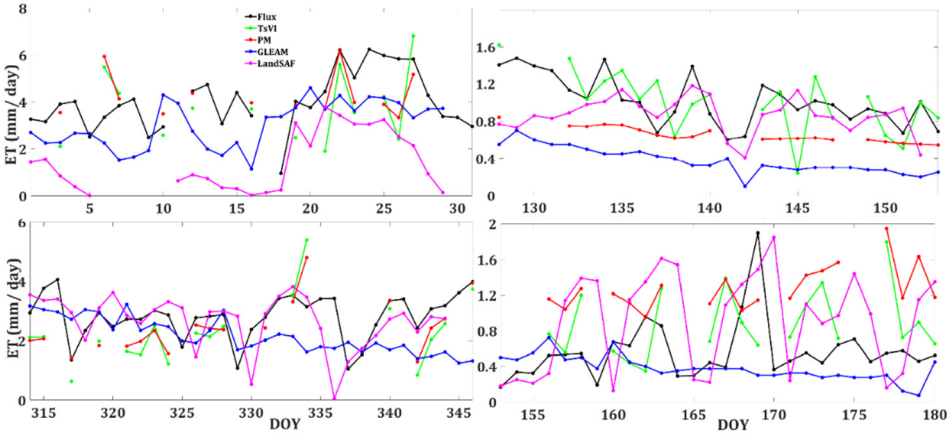

Figure 3-5: Time series of measured and modelled ET for the wet (a) and dry (b) periods in Skukuza eddy covariance flux tower site; and the dry (c) and wet (d) periods in Elandsberg LAS site

Elandsberg

Figures 3-5 c and d present the temporal variation of the LAS-derived ET and the modelled ET estimates, and Figures 3-6 c and d show the correlations between the measured and estimated ET. In the dry season, there is a general underprediction of ET by the models, as shown in Table 3-4 and Figures 3-5 c and d, and 3-6 c and d, whereas during the rainy season GLEAM underestimated ET. The slopes were between 0.012 (GLEAM) and 1.29 (TsVI), and intercepts ranged between -1.51 (MET) and 2.13 (GLEAM) in the dry season; during the wet season the slopes ranged from -0.27 (MET) and 0.57 (MET), and the intercepts were between 0.41 (GLEAM) and 1.41 (PM). The correlations of the modelled ET against the ground ET ranged between 0 (GLEAM) and 0.42 (TsVI) during the dry season, and lowly 0.01 (GLEAM) and 0.12 (MET) during the wet season (Table 3-4). Although it has higher absolute bias and MAE than MET (-0.09 and 0.65 mmday^{-1}), PM (-0.51 and 0.69 mmday^{-1}) was best performing with RMSE of 0.85 mmday^{-1}, and rRMSE of 28.73%, while MET had RMSE 0.96 mmday^{-1} and rRMSE 35.03%, which was close to TsVI, having recorded RMSE 1.05 mmday^{-1} and rRMSE 35.42%. The least accurate in this instance was GLEAM, which also had comparable results of bias -0.65 mmday^{-1}, MAE 0.94 mmday^{-1}, RMSE 1.15

mmday^{-1}, and rRMSE 40.73%. In the wet season, the performance of all the models was very poor, with all of them recording rRMSE of over 70%. The best performing model, GLEAM had rRMSE 73.02%, RMSE 0.42 mmday^{-1}, MAE 0.28 mmday^{-1} and bias -0.19 mmday^{-1}. Although the rRMSE for TsVI and MET were 88.91 and 119.55%, respectively, they generally performed very close to each other, with MAE and RMSE of 0.46 and 0.52 mmday^{-1}, 0.60 and 0.63 mmday^{-1}, respectively. The lowest performing model, PM, had a bias, MAE, RMSE and rRMSE of 0.61, 0.69, 0.77 mmday^{-1}, and 114.64%, respectively.

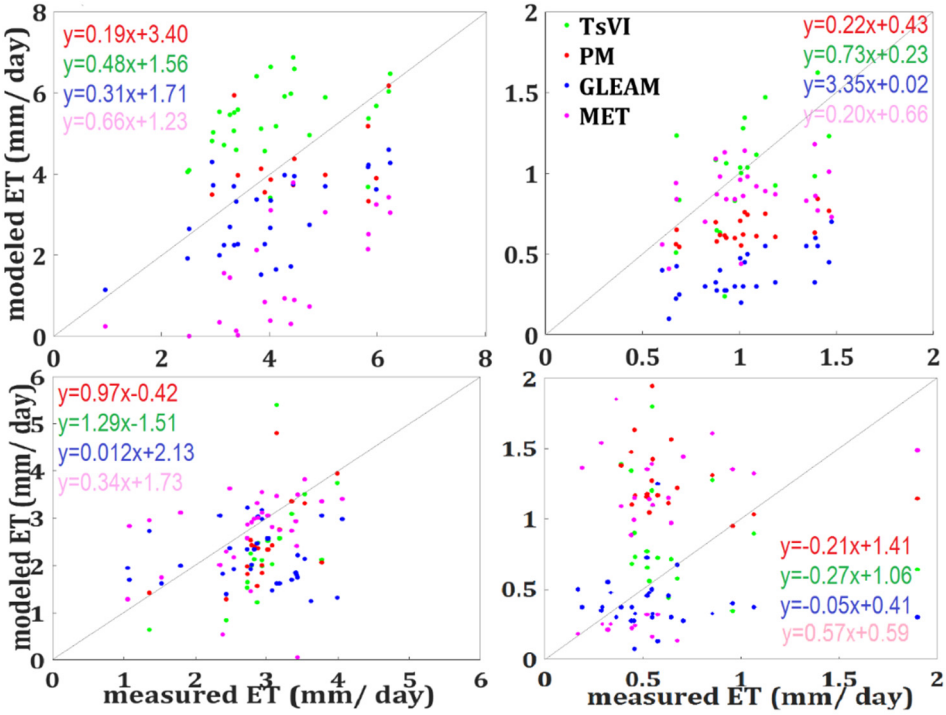

Figure 3-6: Scatterplots of daily measured vs modelled ET for Skukuza (a-wet and b-dry) and Elandsberg (c-dry and d-wet)

3.4.3 Net Radiation Estimations

Rnet and G were computed using the same formulae described above for both ET models at Skukuza and Elandsberg. These were estimated using both meteorological and remote sensing data inputs. In Skukuza, the results show that in the wet season the modelled Rnet was more the measured values. During the wet season Rnet had exhibited higher accuracies, as shown by R^2 of 0.46, rRMSE of 37.07%, whereas in the dry season the R^2 was extremely low, and rRMSE of 22%. On the other hand, the estimation of G was comparably poor at both times. The estimation of Rnet and G in Elandsberg was also characterised

by a low coefficient of determination (R^2) at both periods, with the wet period giving worse results. To improve the modelling ET using remote sensing-based ET models, it is critical to first ensure that intermediate input parameters like Rnet and G are accurately estimated.

Table 3-4: Statistics of estimated daily ET against measured ET for Skukuza flux and Elandsberg LAS

	Skukuza									
	Wet				Dry					
	TsVI	PM	MET	GLEAM	TsVI	PM	MET	GLEAM	TsVI	PM
R^2	0.13	0.05	0.45	0.15	0.24	0.34	0.07	0.42	0.42	0.36
Bias ($mmday^{-1}$)	-0.79	-0.28	-2.66	-1.08	-0.01	-0.36	-0.17	-0.64	-0.65	-0.51
MAE ($mmday^{-1}$)	1.40	0.89	2.66	1.46	0.23	0.36	0.25	0.64	0.89	0.69
RMSE ($mmday^{-1}$)	1.66	1.25	2.85	1.64	0.29	0.40	0.32	0.67	1.05	0.85
rRMSE (%)	36.46	27.34	67.50	40.44	28.34	39.86	31.09	65.96	35.42	28.73

3.5 Discussion

Figure 3-4 shows high evapotranspiration for both sites during the summer season despite that Elandsberg is located in a winter rainfall region and receives

higher rainfall in winter. With higher water availability in Elandsberg in winter, evapotranspiration is expected to be higher, however, low ET is recorded (Figure 3-4 d). In this instance, water availability is not a limiting factor in the process of evapotranspiration in Elandsberg, solar radiation is. Although different times were used for the two sites, this simply illustrates the general climatic trends in the two regions, which experience precipitation at different seasons.

Daily estimates of ET from two models and two products, TsVI, PM, MET, and GLEAM, of varying structural complexities, assumptions, and parameterisations were compared with ground measurements at two different ecoclimatic regions and times. These models gave differing results, mainly due to algorithm structural errors and input uncertainties and different model sensitivity to the different inputs. Our study shows that no model clearly outperformed the others on both sites and times. In Skukuza, PM gave the least error ET estimates in the wet season, whereas during the dry period TsVI and MET gave relatively comparable results, although TsVI estimates were slightly better. In Elandsberg also, no model distinctly outperformed the others during the dry season, as evidenced by the interchange in hierarchy of the statistics between PM and MET; during the wet season, GLEAM had the least bias, as shown by low MAE and RMSE, despite having the lowest R^2 of 0.01 (Table 3-4). On both sites we are looking at periods of high radiation and ET during the summer season, despite limited rainfall in Elandsberg during this period. Furthermore, PM underestimated ET during periods of low ET on both sites, as illustrated in Figures 3-5 and 3-6. The poor performance of the models during the wet season in Elandsberg could be related to the weather conditions, particularly since it was raining during these days (Figure 3-4). The low correlations that were recorded in our study, notably for Elandsberg wet season, are comparable to other studies that have been done in dry ecosystems (Ershadi et al., 2014; Michel et al., 2015). Vinukollu et al. (2011b) reported low correlations in grasslands and woody savannas with all the models they tested in their study. They reported Kendall's tau of 0.01, 0.32 and 0.33 in woody savanna Tonzi, 0.51, 0.27 and 0.37 in grassland Audubon, and 0.55, 0.54, 0.59 in grassland Fort Peck, for SEBS, PM-Mu, and PT-Fi models, respectively. In their extensive evaluation of SEBS, PT-JPL, PM-Mu and GLEAM models, across different ecoclimatic regions, McCabe et al. (2015) also found that the PT-based models, PT-JPL and GLEAM, performed better than the others in most ecoclimatic regions. Low correlations and accuracies of the models were also recorded as the aridity increased, such that they excluded the results of shrublands in their further analysis. Ershadi et al. (2014) evaluated the performance of PM, advection-aridity, SEBS and PT-JPL models, and showed that there is no model that consistently performed well across all biomes. Hu et al. (2015) also reported low

performance of the MOD16 ET and MET on shrublands located in semi-arid climates.

Model performance is affected by different attributes, including structural complexities, model assumptions, parameterisations, and the amount of data required. To estimate ET using these models, both meteorological data measured from the study sites and remote sensing data were used as inputs. The error and uncertainties of the data inputs are propagated into the models' outputs. For instance, the remote sensing inputs of LST and surface emissivity are instantaneous in the case, and 8-day averages in cases of vegetation indices, whereas the ground measurements of air temperature, humidity, atmospheric pressure, wind speed are daily averages. Also, MODIS products that were used as inputs in this study come with their level of uncertainty and/or error, presented as part of the datasets as reported in their user guides (Didan et al., 2015; Myneni, 2012; Wan, 2008). The MODIS products used as inputs in this study are affected by artifacts caused by clouds, atmospheric aerosols, instrument errors and uncertainties of retrieval algorithms. There is, thus, a need for these data inputs to be improved to improve the ET estimation. The spatial scale difference between MODIS image footprint of 1 km and the flux tower and LAS footprints, confounded by the heterogeneity of the landscape, the wind velocity and direction, and atmospheric stability, within the satellite footprint also contribute error and uncertainty (Ramoelo et al., 2014). As shown by the flux footprint model, and discussed in Ramoelo et al. (2014), with a measurement height of 16 m, the Skukuza flux tower footprint is approximately 1.6 km, i.e. based on the general rule of the thumb which suggests the fetch: measurement height ratio of 100 484-m: 1 m (Burba & Anderson, 2010; Smith & Cresser, 2003). This indicates that the flux tower provides a good match to the MODIS pixel size. Although flux footprint modelling gives a good estimation of the spatial discrepancy between flux tower measurements and the image pixel, it is beyond the scope of this study. The coarser the image resolution, the higher the landscape heterogeneity, and spatial mismatch, introducing errors as shown by Matthew F. McCabe and Wood (2006) who showed that while Landsat and ASTER higher accuracies in ET estimates, MODIS was less accurate. For evapotranspiration models, it is important to have an accurate estimation of Rnet which is a critical component of each of these models. Low accuracy in Rnet, as shown in our study also contributed to the error and inaccuracies of the ET estimates.

GLEAM and TsVI are PT based, which is a simplified version of the PM, with the TsVI triangle method being a relatively simple formulation that employs empirical means (using to normalise the PT parameter (ϕ) using the LST-vegetation indices triangle feature space, to estimate the evaporativefraction; it

requires fewer inputs and parameterisations required (see Table 3-2) (Fisher et al., 2008; Petropoulos et al., 2009). The simplification of the model in the estimation of EF also means that the computing complexities of surface and aerodynamic resistances are avoided, thus reducing errors and uncertainty in ET estimation (Wang & Dickinson, 2012). The main challenge of the TsVI method is the subjective determination of the wet and dry edges from the triangle feature space and the neglect of local advection in its formulation. Also, during the rainy season or in areas of low variability in vegetation cover range, the triangle feature space is hard to establish, as evidenced in Elandsberg, where it was generally outperformed by other models. In other instances, the heterogeneity of the land surface, together with atmospheric forcing complicates the establishment of the TsVI relationship. Since the TsVI feature space is established empirically, the method is site-specific. During the rainy days, like in the Elandsberg winter period and Skukuza summer period, the determination of the wet and dry edges presents a challenge, hence the non-performance of the model during this period. GLEAM, on the other hand, is more comprehensive, combining the PT equation, a soil moisture stress computation, and a Gash analytical model to compute ET as a total of transpiration from tall canopy, short vegetation, soil evaporation and canopy interception loss (Miralles et al., 2011). A plus for the GLEAM model is that in water-limited regions, atmospheric water demand is constrained by precipitation, surface soil moisture and vegetation optical depth (VOD, which is a proxy for leaf water content (Liu et al., 2013b)). Each of the model components within the GLEAM structure has its own assumptions and complexities with varying levels of error and uncertainty, which are propagated to the final ET estimate. GLEAM, like the PM used in this study, also computes interception loss separately, as shown in Miralles et al. (2011) and Mu et al. (2011). Miralles et al. (2011) assessed the GLEAM product across different biomes and showed daily average correlation (R) of 0.83. They, however, stated that the distinct seasonal cycle of evaporation in the dry regions probably balanced out the correlation coefficients positively. In addition to the known challenges of the PT equation, the main challenge in validating GLEAM ET using flux tower derived ET is the coarse spatial resolution of the global product. The MET product is derived from a scheme that is different from the other estimates, based on the energy balance budget. The daily MET product is an aggregation of 30-minute ET values obtained. This presents a challenge when, for instance, there are gaps in these 30-minute ET data, resulting in underestimation. Also, the issue of spatial heterogeneity plays a part in the inaccuracies of this course resolution ET product.

Penman-Monteith is the most robust of these models and theoretically should present the best performances compared with the other models. The results (Table 3-4) however, show that this version of PM was only good during periods

of high ET. One of the biggest challenges of the PM based models is the parameterisation of the aerodynamic and surface resistances, including upscaling stomatal to canopy resistance. LAI is an important input in the parameterisation of canopy resistance, as it is linked with the biophysical control of vegetation on ET (Fisher et al., 2008; Mu et al., 2007; Mu et al., 2011). Hu et al. (2015) explored the relationship between PM-MOD16 estimated ET and LAI, showing that the two are closely related, especially for the savannas and the deciduous broadleaf forests. Because soil water availability plays a key role in ET in semi-arid regions, it is important that models include a soil water constraint function in the model. However, in this version of PM, relative humidity and VPD were used as a proxy for soil water in the estimation of soil evaporation, hence low accuracy of the model during low ET periods. Currently, research is focused on incorporating soil water constraint function in the ET modelling, especially in dry regions. Di et al. (2015) incorporated two layers of relative soil moisture parameters in the PM model to parameterise the surface resistance and added a multiplier in the vegetation surface resistance model to cater for the influence of the relative soil moisture in the root zone. L. Sun et al. (2013) also investigated the incorporation of soil moisture in the PM-Mu method to constrain soil evaporation by using actual soil water content and the soil water content at saturation to compute the soil resistance, which they also substituted with a soil moisture index derived from the T-VI triangle method. These studies showed improved estimations of ET by the PM algorithm during water constrained periods. For the estimation of ET to cover different ecosystems, PM would have to be assessed further and modified, especially for semi-arid climatic regions.

3.6 Conclusion

Accurate estimates of ET are essential especially in semi-arid and arid regions where there is less water being competed for by different users. Different remote sensing-based models and products, of varying complexities and data input requirements, are available, and their applicability at varying ecoclimatic regions and scales is consistently under scrutiny.

This study, thus, presented an evaluation of four ET models and global products, i.e. TsVI, PM, and MET and GLEAM global products in two semi-arid eco-climates. Our results show that there is essentially no model that clearly outperforms others at the two sites. Low coefficients ranging between 0 and 0.45 were recorded on both sites, during both seasons. It was also observed that during periods of high ET at both sites, i.e. Skukuza in the wet season and Elandsberg in the dry season, PM was relatively more accurate than the other models and products, with rRMSE's of lower than 30%. In Skukuza, TsVI marginally outperformed MET during the dry period, whereas GLEAM gave the

least accurate estimates. ET estimation during the rainy season in Elandsberg was quite poor with rRMSE's of over 70%, with GLEAM being most accurate.

The conclusion, therefore, is that none of the models performed well, as shown by low R^2 and high errors in all the models. PM gave the least errors during periods of high ET on both sites, whereas modelling low ET was a challenge.

These results presented a prerequisite for the next stage of our study, in which we will investigate the error and uncertainty in the PM model simulations, inclusive input data (both remote sensing and meteorological input data), model structure, and parameterisations. In doing this, A. Ershadi et al. (2014) state that it would allow for the model diagnosis and identification of the main sources of error in ET estimation, in this case in water-scarce regions.

4 UNCERTAINTY AND SENSITIVITY OF A REMOTE SENSING-BASED PENMAN-MONTEITH MODEL TO METEOROLOGICAL AND REMOTE SENSING-BASED INPUTS

4.1 ABSTRACT[3]

In this paper, we analysed the uncertainty and sensitivity of core and intermediate input variables of a modified, remote sensing data based version of the Penman-Monteith (PM) evapotranspiration (ET) model (Mu et al., 2007; Mu et al., 2011). We used ET model simulations of two locations in South Africa, equipped with eddy covariance (EC) flux towers for validation. We derived absolute and relative uncertainties of the core meteorological and remote sensing-based, atmosphere and land surface input variables and parameters of the PM-Mu model. Uncertainties of important intermediate data components (i.e. net radiation and aerodynamic and surface resistances) were also assessed. To estimate instrument measurement uncertainties of the in situ meteorological input variables, we used reported accuracies of the manufacturers. Observational accuracies of the remote sensing input variables (land surface temperature (LST), land surface emissivity (ε_s), leaf area index (LAI), land surface albedo (α)) were derived from peer-reviewed satellite sensor validation reports to compute their uncertainties. We then combined all different uncertainty types and propagated the errors to the final model evapotranspiration estimation uncertainty. Our analysis indicated relatively high uncertainties associated with relative humidity (RH), and hence all the intermediate variables associated with RH, like vapour pressure deficit (VPD) and the surface and aerodynamic resistances in contrast to other studies who reported LAI uncertainty as the most significant. The semi-arid conditions and seasonality of the regional South African climate and high temporal frequency of the variations in VPD, air and land surface temperatures could explain observed uncertainties in this study. The results also showed the ET algorithm to be most sensitive to the air - land surface temperature difference. Accurate assessment of those in situ and remotely sensed variables is required in order to achieve reliable evapotranspiration model estimates in these generally dry regions and climates. A vast advantage of remote sensing-based ET method remains their full area coverage in contrast to classic point (station) based ET estimates.

[3] Under submission to “Agricultural and Forest Meteorology” Journal, Elsevier.

4.2 Introduction

Evapotranspiration is dependent on meteorological variables (air temperature, solar radiation, humidity, and wind speed) and biophysical characteristics of the land surface and vegetation. It is a challenging process to measure due to its high spatio-temporal variation, hence, with the advent of remote sensing technology, models of varying complexities have been developed to capture this variation (Allen et al., 2007; Bastiaanssen et al., 2005; Bowen, 1926; Monteith, 1981; Nichols et al., 2004; Su, 1999, 2002). These models propagate varying errors and uncertainties through the final output. Errors are either linked to: i) an incomplete understanding and simplified descriptions of modelled processes compared to reality, and ii) input variables and parameterisations used, the latter being dependent on the biomes and climates where they are used (Ershadi et al., 2014; McCabe et al., 2015; Michel et al., 2015; Vinukollu et al., 2011b).

While uncertainty analysis (UA) is performed to evaluate the effect of input variable and parameter uncertainties on the output uncertainties, sensitivity analysis (SA) quantifies how the uncertainty of different model inputs impacts the model output (Saltelli et al., 2004). UA and SA are important steps in evaluating environmental models as they rank the importance of input variable errors in the final result and highlight the need to assess the physical meaning of model parameters and their relative influence on the output. UA is divided into Type A (U_A), which evaluates measurement uncertainty using statistical analysis of a series of measurements, and Type B (U_B), which quantifies any other uncertainty other than the statistical analysis, including the instrument manufacturer's published accuracy and the quoted accuracies for remote sensing products (Lira 2002, Taylor 1997). SA techniques range from the simplest local (LSA, one-parameter-at-a-time (OAT) and derivative-based) to global SA (GSA, multiple parameters at a time, derivative-based or more often variance-based) techniques, from differential to Monte Carlo analysis, from measures of importance to sensitivity indices, and from regression or correlation methods to variance - based techniques (Frey & Patil, 2002; Hamby, 1995; Kucherenko & Iooss, 2017; Lilburne & Tarantola, 2009).

In evapotranspiration (ET) research, most studies have focused on the sensitivity of potential (PET) and reference (ET_o) ET model outputs to different climatic inputs, with varying outcomes. Tabari and Hosseinzadeh Talaee (2014) investigated the sensitivity of the Food and Agriculture Organisation (FAO) PM reference ET (ET_0) estimates to air temperature (Tair), wind speed (u) and sunshine hours in different climates, and their results showed that sensitivity to u and Tair decreased from arid to humid environments. In Southern Spain, ET was most sensitive to Tair in summer

causing ET overestimation, and relative humidity (RH) in winter causing ET underestimation (Estévez et al., 2009). In the Yangtze River Catchment, Gong et al. (2006) showed that the Food and Agriculture Organisation (FAO) PM derived ET_0 was most sensitive to RH, followed by solar shortwave radiation (R_{sd}), Tair and u and that sensitivities were season dependent. Using GSA, DeJonge et al. (2015) evaluated the sensitivity of the ASCE Standardised Reference Evapotranspiration ET_o estimates to input measurement instrument accuracy. Most of these studies only varied the input variables by fixed percentage bounds without taking into account the input variable limits and rarely use measurement instrument accuracy limits as a basis for comparison. The emergence of remote sensing (RS) based ET estimation presents an opportunity to investigate the impact of land cover/ land use change on ET, and how these parameters affect different ET models. Van der Kwast et al. (2009) analysed the sensitivity of SEBS modelled sensible heat flux to surface elevation, land surface temperature, albedo, NDVI and emissivity in a test site in Barrax, Spain. They reported low sensitivity of the modelled sensible heat flux (H) to the land surface parameters, except LST, attributing this result to the fact that H derivation only uses meteorological data and LST. Wang et al. (2009) performed a sensitivity analysis of SEBAL on full, half, and sparse cover conditions, based on the NDVI of the areas. They reported that ET was most sensitive to the selection of the wet- and dry- edges, temperature difference between surface and atmosphere (dT), at the full cover site, which is linked to LST, but less sensitive to NDVI and albedo; whereas it was sensitive to the selection of wet and dry spots, roughness length, c, and dT at half canopy cover, and finally at sparse canopy cover, ET was most sensitive to selection of the dry spot, c and NDVI. With the remote sensing driven PM model, no wok has been done to analyse the sensitivity of the model to the land surface parameters.

The term uncertainty analysis is often used to analyse the sensitivity of an ET model to its inputs (Westerhoff, 2015), while others use it to evaluate the performance of ET models (Paparrizos et al., 2017). Meanwhile, only a few studies have explicitly focused on how input variable uncertainty is propagated to the final ET uncertainty (Chen et al., 2018; Hofreiter & Jirka). On top of analysing the sensitivity of ET estimates to climatic inputs that has been done, the use of RS based inputs in ET modelling gives the chance to assess the sensitivity and uncertainty of ET models to land surface parameters, and hence, land use change.

Based on the results of the performance assessment of different models (Chapter 3), which showed that the PM-Mu model had no table results

during high ET periods, this study, therefore investigated the sensitivity of this model to its input variables, i.e. both measured meteorological and remote sensing-based land surface characteristics. It also quantified the uncertainty of the input variables and how these were propagated into the final ET uncertainty. The PM model is a structurally complex and data intensive model presenting a combination of the energy balance and aerodynamic components. One of the challenges of the PM method is its high data requirement and parameterisation, making it important to understand and quantify potential errors and uncertainties of the input data and how these impact the final ET output. This process will, therefore, identify the inputs that are most influential and correlated with the dependent variable in a semi-arid environment, in order to improve parameterisations that could eventually improve our results.

4.3 Methodology

4.3.1 Site description

ET was estimated using data from two eddy covariance flux tower sites located in savanna and grassland southern African ecoregions. The 2012 data were selected for both sites and considered in this study Based on the surface energy balance closure results in Chapter 2:

i. The Skukuza FLUXNET site is located in a semi-arid, subtropical savanna ecosystem in the Kruger National Park. It is characterised by low rainfall averaging 550±160 mm per annum between November and April, and temperatures range between 15.6 and 29.6 °C, with a mean of 22.6 °C. Soils in this part of the park are generally shallow, with coarse sandy to sandy-loam texture. The vegetation is mainly open woodland, with approximately 30% tree canopy cover of mixed *Acacia* and *Combretum* savanna types, of canopy height, is 5–8 m with occasional trees (mostly *Sclerocarya birrea*) reaching 10 m. The grassy and herbaceous understory comprises grasses such as *Panicum maximum, Digitaria eriantha, Eragrostis rigidor,* and *Pogonarthria squarrosa* (Scholes et al., 2003; Scholes et al., 2001).

ii. Welgegund flux tower site (26°34'10"S, 26°56'21"E) is located on a semi-arid, subtropical grazed grassland plain. It is situated approximately 100 km west of Johannesburg in South Africa. The mean annual rainfall is 540±112 mm, spreading between October and April. Temperature ranges between 0 and 30 °C with an average of 18 °C. The dominant vegetation comprises grasses, geophytes, and herbs. The dominant grass species are *Hyparrhenia hirta* and *Sporobolus pyramidalis*. Non-

grassy forbs include *Acacia sieberiana*, *Rhus rehmanniana*, *Walafrida densiflora*, *Spermacoce natalensis*, *Kohautia cynanchica*, and *Phyllanthus glaucophyllus* (Räsänen et al., 2017).

4.3.2 Penman-Monteith equation

The Penman - Monteith model as modified by Mu et al. (2007; 2011) was assessed in this study. Latent heat flux is estimated as:

$$\boldsymbol{\lambda E} = \frac{\boldsymbol{s*A+\rho*Cp*(e_{sat}-e)/r_a}}{\boldsymbol{s+\gamma*\left(1+\frac{r_s}{r_a}\right)}} \quad 12$$

where λE is the latent heat flux (Wm^{-2}) and λ is the heat of vapourisation (Jkg^{-1}), s is the slope of the curve relating saturated vapour pressure to temperature (PaK-1), A is available energy (Wm^{-2}), □ is the air density (kgm^{-3}), Cp is the specific heat capacity of air ($Jkg^{-1}K^{-1}$), γ (PaK^{-1}) is the psychrometric constant, esat is the saturation vapour pressure (kPa), e is the actual vapour pressure (kPa), where esat – e = vapour pressure deficit (VPD, kPa), ra (sm-1) is the aerodynamic resistance, and rs (sm-1) is the canopy resistance, which is the reciprocal of canopy conductance gc (gc=1/rc).

On top of estimating ET as a sum of evaporation from moist soil, interception, and transpiration, Mu et al. (2007), (Mu et al., 2011) further computed the daytime and nighttime ET separately. Instead of using NDVI to compute the fraction of vegetation cover, they used Fraction of Absorbed Photosynthetically Active Radiation (FPAR) as a surrogate of vegetation cover fraction, with another modification to the derivation of soil heat flux. Other modifications included separating dry and wet (interception) canopy surfaces, and soil surface into saturated and moist surface, as well as improving stomatal conductance, aerodynamic resistance, and boundary layer resistance estimates.

The core input variables used in this model are Tair, RH, land surface temperature (LST), surface emissivity (ε_s), leaf area index (LAI), land surface albedo (α), and were used to derive intermediate inputs like net solar radiation (Rnet), vapour pressure deficit (VPD), the slope of the saturated vapour – air temperature curve (Δ), the air and saturated air vapour pressures (e_a, e_s,) and the aerodynamic and surface resistances (r_a, r_s).

4.3.3 Uncertainty and Sensitivity analysis

Uncertainty and sensitivity analyses were performed on the PM-Mu to quantify input uncertainties and how these are propagated to the final ET uncertainties and identify the inputs and parameters that are most important in modelling ET

in a semi-arid environment. This will contribute to informing on efforts needed for improving input variable accuracies. We assessed the uncertainty of each input variable. i.e. the direct measured variable uncertainty (core input), derived input variable uncertainty (intermediate input), and remote sensing-based input variable uncertainty using Type A and Type B uncertainty methods. The total uncertainty on the model simulations, i.e. model output uncertainty, was then evaluated by uncertainty propagation using the Gaussian uncertainty analysis method.

Based on the PM-Mu model, ET is defined as a function (*f*) of meteorological point measurements of Tair and RH, and spatially explicit remote sensing estimates of LST, and land surface characteristics such as LAI, fraction of green vegetation cover (Fc)/ fraction of photosynthetically active radiation (FPAR), NDVI/ EVI and surface emissivity (ε_s), which are biome /or land cover characteristics defining parameters.

The generic model presented as:

$$\boldsymbol{ET} = \boldsymbol{f}(\boldsymbol{x_1}, \dots, \boldsymbol{x_n}) \quad 13$$

where x_1 to x_n represents the n input variables and parameters of the PM-Mu model.

The change in ET, i.e. ΔET, resulting from errors and/or uncertainties in input variables (Δx_i) is then expressed as:

$$\boldsymbol{ET} \pm \Delta\boldsymbol{ET} = \boldsymbol{f}(\boldsymbol{x_1} \pm \Delta\boldsymbol{x_1}, \dots, \boldsymbol{x_n} \pm \Delta\boldsymbol{x_n}) \quad 14$$

The study analysed the uncertainty and sensitivity of the PM-Mu input variables and outputs as shown in Figure 4-1, and aimed at:

i. Estimating uncertainty of model inputs and parameters, i.e. the meteorological and land surface characteristics, representing both point- and remote sensing-based inputs
ii. Propagating input uncertainties through to the ET model and computing output uncertainties
iii. Estimating the sensitivity indices of the model inputs.

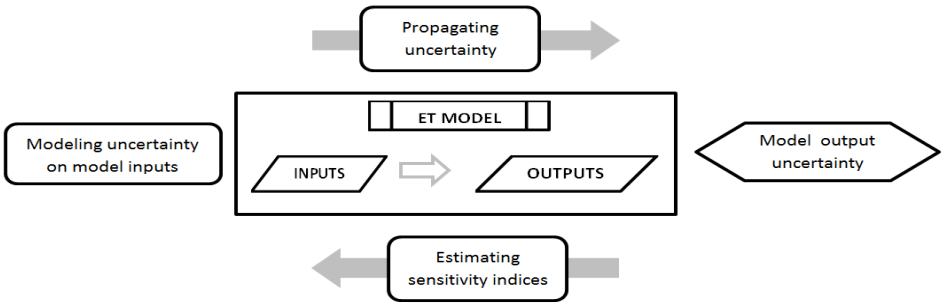

Figure 4-1: Steps of the uncertainty and sensitivity analysis of the PM-Mu ET model

Core input variable uncertainties

We estimated the uncertainty of each core input variable as a combination of Type A and Type B uncertainties. In this study, where each measured input variable was a daily mean of 30 minute recordings, we computed Type A standard uncertainty of the meteorological inputs as the standard deviation of the daily mean:

$$\boldsymbol{U_A(x_i)} = \sqrt{\frac{\sum_{i=1}^{n}(x_i-\bar{x}_i)^2}{v}} \quad 15$$

where x_i is the input value of the variable or parameter under consideration, $\bar{x}_i$ is the average value of the measured values calculated from n number of independent observations, and v is the degrees of freedom equal to n-1.

Type B standard uncertainty (U_B) was also computed for the meteorological input variables, based on the instruments manufacturer's published accuracies. The quoted accuracies of the measurement instruments are summarised in Table 4-1. They were estimated using:

$$\boldsymbol{U_B(x_i)} = \frac{\boldsymbol{a}}{\sqrt{\boldsymbol{3}}} \quad 16$$

where a is the quoted accuracy specification from the manufacturer, and includes calibration information from calibration certificates.

For meteorological data inputs, the combined standard uncertainty was then estimated as:

$$\boldsymbol{U_C(x_i)} = \sqrt{\left(\boldsymbol{U^2_{A(x_i)}} + \boldsymbol{U^2_{B(x_i)}}\right)} \quad 17$$

The combined uncertainty was then converted to relative uncertainty for detailed comparison and analysis.

Table 4-1: Quoted accuracy of meteorological instruments at the two observation sites

	Skukuza		Welgegund	
Measurement	**Sensor**	**Quoted accuracy**	**Sensor**	**Quoted accuracy**
Temperature	Campbell Scientific HMP50	0.4 °C at 15 °C, 0.5 °C at 40 °C, 0.8 °C at 60 °C	Vaisala WXT510 meteorological station (Helsinki, Finland)	0.3 °C at 20 °C, 0.4 °C at 40 °C, 0.7 °C at 60 °C
Relative humidity (at 20 °C)		±3% 0 to 90% RH, ±5% 90 to 98% RH		±3% 0 to 90% RH, ±5% 90 to 100% RH

Remote sensing-based input uncertainties

Remote sensing derived inputs have uncertainties due to a number of factors, including model algorithm structure and input variables. The uncertainties of the remotely sensed input variables used in this study (LST, εs, LAI, α) were extracted mainly from published Algorithm Theoretical Basis Documents (ATBD). Based on the quoted errors (Table 4-2), the uncertainties were then estimated using equation 16. We give a short description of each variable and associated remote sensing product below.

- *LST and surface emissivity*: these variables are essential in land surface-atmosphere studies, including estimation of evapotranspiration and atmospheric water vapour. In our study, we used the MODIS derived MOD11A1 V006 product, which is generated from the thermal infrared channels 31 (10.78 to 11.28 μm) and 32 (11.77 to 12.27 μm) using the physically-based , split-window algorithm by (Wan & Dozier, 1996). The uncertainties associated with these products are extensively discussed in the MODIS Land-Surface Temperature ATBD (Hulley et al., 2016; Wan, 1999). They indicate an absolute error of 1 K for LST which can increase up to 5 K in arid regions. For surface emissivity, the absolute accuracy is reported to be 0.02.
- *Land surface albedo*: defined as a dimensionless characteristic of the soil–plant canopy system representing the fraction of total solar energy reflected by the surface, it is expressed as the ratio of the radiant energy scattered upward by a surface in all directions to that received from all directions, integrated over the wavelengths of the solar spectrum. Surface albedo is one of the key geophysical parameters that control the surface energy budget. The MODIS bi-directional reflectance distribution function (BRDF)

and albedo product (MCD43A3 version VOO6) were used in this study. This product was derived using a kernel-driven semi empirical BRDF model using the RossThick-LiSparse kernel functions for characterizing isotropic, volume and surface scattering (Schaaf et al., 2011; Schaaf et al., 2002; Wanner et al., 1997). Studies have given an absolute accuracy of 0.02 to 0.05 as a requirement for climate modelling (Nobre et al., 1991; Sellers et al., 1995), with other validation studies (Jin et al., 2003; Wang et al., 2004) reporting errors falling within the 0.02 accuracy.

- *Leaf Area Index (LAI)*: defined as the total one-sided green leaf area per unit ground surface area, is also dimensionless. This variable measures the total amount of leaf material in an ecosystem. It is used in the estimation of biogeochemical processes like photosynthesis, evapotranspiration, and net primary production. MOD15A2 V005 product used in this study was derived using the three-dimensional radiative transfer (3D RT) model. The product ATBD reports the accuracy of the LAI product at 0.2 (Knyazikhin et al., 1999). Furthermore, a review by Fang et al. (2012) summarises uncertainties of MODIS, CYCLOPES, and GLOBCARBON LAI products under different biomes, showing relative uncertainty of 0.26 in the savanna biome for the MODIS product.

Table 4-2: A summary of remote sensing input variable errors

Input variable	Error values	Units	Reference
LST	±3.5	K	G. Hulley et al. (2016)
Surface emissivity	±0.02	-	Wan (1999)
LAI	0.2	-	Knyazikhin et al. (1999)
Albedo	0.02	-	Strahler et al. (1999)

Intermediate input uncertainty

For intermediate inputs that were derived from the core input variables, such as net radiation and surface and aerodynamic resistances, the standard uncertainties were estimated as combined standard uncertainties of their inputs, using the Gaussian error propagation method, as shown in equation 18:

$$\boldsymbol{U_C(Y_i)} = \sqrt{\sum_{\boldsymbol{i=1}}^{\boldsymbol{n}} \left(\left(\frac{\boldsymbol{\partial Y_i}}{\boldsymbol{\partial x_i}} \right)^{\boldsymbol{2}} * \left(\boldsymbol{U_C(x_i)} \right)^{\boldsymbol{2}} \right)} \quad 18$$

where $\frac{\partial Y_i}{\partial x_i}$ is the partial derivative of y with reference to input variables x_i to a_n, also called sensitivity coefficient.

Each estimated input variable uncertainty was also propagated to the final ET output uncertainty using equation 18.

4.3.4 Sensitivity analysis

One of the aims of SA is to identify and rank input variables according to their importance in modelling a particular phenomenon. This is done to identify the input variables that require more accurate measurement to reduce model output variance to a minimum. The sensitivity of the PM-Mu estimated daily ET was done by varying one input variable at a time within ±20% ranges. First, ET was computed with the initial input variables, then one variable was perturbed by 5% within ±20% whilst the rest of the inputs were held constant, every day for the whole year of 2012 and the new ET values were recorded. Then the sensitivity coefficient, S, was computed using equation 19, after which an overall average was calculated:

$$\boldsymbol{S_i} = \left(\frac{\boldsymbol{Y_i - Y_0}}{\boldsymbol{Y_0}}\right) * \mathbf{100} \qquad 19$$

where Y_i is the ET recorded when you vary one variable a time at each percentage step, and Y_0 is initial ET.

4.4 Results

Uncertainty analysis gives a range of values likely to enclose the true value, thus the confidence of the modelled values, and includes possibly all sources of error. Meanwhile, sensitivity analysis ranks the input variables according to their sensitivity to errors in a model. In our study, we quantified the uncertainty of the PM-Mu ET model input variables at two FLUXNET sites in semi-arid ecosystems, Skukuza and Welgegund, and analyse how these propagated through to the model final output uncertainty.

4.4.1 Core input variables uncertainty

Figure 4-2 illustrates the relative uncertainties for the meteorological inputs Tair and RH, for the two study sites. While Tair relative uncertainty ranged between 0.5 and 7.6% with an average 3.1±1.5% for Skukuza, and it varied between 0.9 and 10.6% with a mean of 4.0±1.7% for Welgegund. RH relative uncertainty was 8.47±0.9% for Skukuza, and 14.2±5.4% for Welgegund. As illustrated in Figure 4-2, the relative uncertainties of both Tair and RH showed strong seasonal variability, with relative uncertainties being higher during the drier months of the year, i.e. between April and September, compared to the wet months. During this period, daily temperatures tend to be highly variable throughout the day, hence the high Type A standard uncertainty. Furthermore, there was much

less variation in Tair relative uncertainty between the two sites compared to RH relative uncertainty.

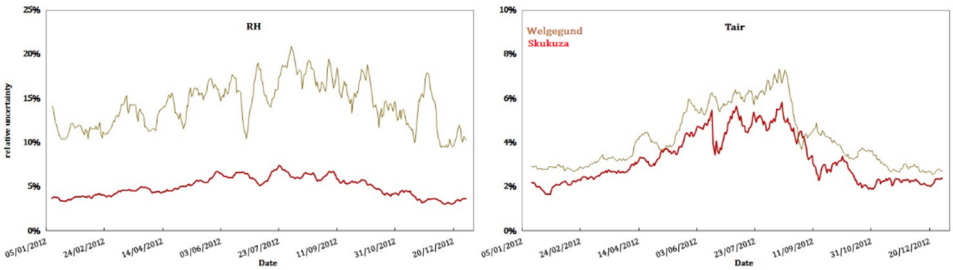

Figure 4-2: Relative uncertainty for air temperature (a), and relative humidity (b)), for the Skukuza and Welgegund flux tower sites

4.4.2 Intermediate input uncertainty

This subsection reports on how the core input uncertainties estimated above were propagated to the ET intermediate inputs, i.e. Rnet and the aerodynamic and surface resistances.

Net radiation uncertainty

Net radiation (Rnet) estimation depends on a number of atmospheric and land surface variables, including α, ε_s, ε_a, LST, and Tair. The relative uncertainty was 4.0±0.6% of the estimated 558.0±105.2 Wm^{-2} daytime Rnet in Skukuza, whereas for Welgegund, a 2.8±0.8% relative uncertainty was reported for the derived 556.4 Wm^{-2} Rnet. For Skukuza, a mean relative air temperature (Tair) uncertainty of 3.1% was associated with relative Rnet uncertainties of between 23.28±9.85% of the total Rnet uncertainty, whereas a land surface temperature (LST) error of 3.5 K contributed 59.31±12.87% to the total uncertainty. The surface emissivity (ε_s) error of 0.02 contributed a Rnet uncertainty between 4 and 7 Wm^{-2}, while the albedo (α) uncertainty contributed to an average 2.8±0.42 mm^{-2}. Similar results were realised for Welgegund, where a mean relative Tair uncertainty of 4% resulted in relative uncertainty of 30.25±10.23%, and 89.42±22.07% being attributed to the LST error of 3.5 K, showing that it was the highest source of uncertainty in Rnet estimation. Ɛs and α contributed to the mean relative uncertainties of 38.81±9.43 and 22.06±10.31%, respectively.

Aerodynamic and surface resistances

In the estimation of wet canopy evaporation, the aerodynamic resistance to evapourated water on wet canopy surface (r_a^{wc}) is a function of Tair, LAI, and RH (in the form of wet surface fraction (Fwet)); whereas the surface resistance to evapourated water on the wet canopy (r_s^{wc}) is a function of LAI and RH. Further, in plant transpiration estimation, the aerodynamic resistance to water vapour from a dry canopy surface (r_a^t) is a function of Tair only; and the canopy

resistance to transpired water (r_s^t) is estimated from LST, LAI, Tmin, and RH. In the computation of soil evaporation, both the surface (r_s^{tot}) and aerodynamic resistances (r_a^s) to water vapour from the soil surface are a function of LST and VPD (which is indirectly RH).

Our results, as illustrated in Table 4-3 (only the standard uncertainties for resistances are shown here) show that the mean standard uncertainties for r_a^{wc} were 0.0011 ms^{-1}± 6.25% and 0.001 sm^{-1} ± 0.17% for Skukuza and Welgegund, respectively. Of the total standard r_a^{wc} uncertainty, Tair contributed the highest uncertainty of average 91±5.0% and 96.02±16.54%, with low contributions from the LAI and RH uncertainties, for Skukuza and Welgegund, respectively. Meanwhile, r_s^{wc} standard uncertainties were an average 10.34±10.0 sm^{-1} and 18.02±19.0 sm^{-1}, respectively, with RH uncertainty contributing most to the total r_s^{wc} uncertainty (approximately 80%), on both sites.

Table 4-3: Aerodynamic and surface resistance standard uncertainties (sm^{-1}) contributions to each component of ET uncertainty

	Skukuza				Welgegund			
	Aerodynamic resistance		Surface resistance		Aerodynamic resistance		Surface resistance	
	Mean	Standard deviation	Mean	Standard deviation	Mean	Standard deviation	Mean	Standard deviation
Interception Evaporation (r_a^{wc}, r_s^{wc})	$1.1*10^{-3}$	$3.5*10^{-4}$	10.34	10.07	$1*10^{-3}$	$3*10^{-4}$	18.02	18.96
Transpiration (r_a^t, r_s^t)	$1.6*10^{-3}$	$7*10^{-4}$	21.68	19.68	$1.5*10^{-3}$	$4.3*10^{-4}$	30.71	26.92
Soil evaporation (r_a^s, r_s^{tot})	$3.8*10^{-3}$	$2.4*10^{-4}$	0.53	0.04	$3.8*10^{-3}$	$2.5*10^{-4}$	0.51	0.06

Table 4-4: Contribution of core and intermediate input variable relative uncertainties to each component of ET uncertainty for Skukuza. Values in brackets are VPD uncertainties

	Transpiration		Interception loss		Potential soil evaporation		Wet soil evaporation	
	Mean	Standard deviation	Mean	Standard deviation	Mean	Standard deviation	Mean	Standard deviation
Total standard uncertainty ($mmday^{-1}$)	0.33	0.41	0.038	0.14	0.89	0.34	0.12	0.22
% RH (VPD)	14.63	8.71	6.37	1.45	(21.49)	13.37	-9.71	-2.66
% Fc (1-Fc)	1.36	1.02	0.67	0.28	-0.85	-0.38		
% Fwet (1-Fwet)	9.64	3.31	0.97	0.05	-2.69	-5.19	12.92	4.49
% r_a^s					1.93	0.8	2.02	0.74
% r_s^{tot}					1.29	0.49	1.25	0.45
% r_a^t	0.89	0.08						
% r_s^t	2.42	5.03						
% r_a^{wc}			0.97	0.05				
% r_s^{wc}			21.46	5.97				

In the estimation of r_a^t standard uncertainty, the values ranged between 0.00019 and 0.0038 sm^{-1}, and 0.00031 and 0.0032 sm^{-1} (low average relative uncertainties of 0.81±0.36% and 0.84±0.22%) for Skukuza and Welgegund, respectively. These low values indicate that Tair uncertainties have an insignificant effect on the estimation of r_a^t uncertainty. Total standard r_s^t uncertainty ranged from 0 to 90 sm^{-1} (mean relative uncertainty of 8.82±2.71%) for Skukuza; whereas for Welgegund, it was between 20 and 146 sm^{-1}, (average relative uncertainty of 8.4±1.7%). The r_a^s relative uncertainties were on average around 2% for both sites. Finally, r_s^{tot} standard uncertainty ranged from 0.45 to 0.73 sm^{-1}, and 0.35 to 0.77 sm^{-1}, for Skukuza and Welgegund, respectively, an average 1% relative uncertainty for both sites. Of the total uncertainty, LST uncertainty contributed the most of the two input variables with an average of 58% and 63%, whereas 5.25% of the total r_s^{tot} uncertainty was attributed to VPD uncertainty, for Skukuza and Welgegund, respectively.

Uncertainty in Evapotranspiration

The final estimate of ET uncertainty is a result of uncertainties propagated from the measured and remote sensing input variables, through intermediate parameters, up to the final ET uncertainty. The standard uncertainty was computed for each ET component, i.e. evaporation from intercepted rainfall (wet canopy), transpiration and soil evaporation, and ultimately combined to give the total ET uncertainty.

In Skukuza (Table 4-4), of the 0.038 mmday^{-1} wet canopy evaporation standard uncertainty, r_s^{wc} uncertainty contributed the highest with 21.46±5.97%, with VPD also having a relatively significant impact of 6.37±1.45% while the rest of the inputs (r_a^{wc}, Fc and Fwet) contributed very little. In addition, of the 0.33 mmday^{-1} transpiration uncertainty, 14.63±8.71% of it was attributed to VPD uncertainty and 9.64±% to Fwet uncertainty. Wet soil evaporation uncertainty of 0.11 mm day^{-1} was made of 12.3% of Fwet uncertainty, 9.7% of VPD uncertainty, and very low contributions from the rest of the inputs. Lastly, VPD uncertainty contributed the highest to the potential soil evaporation uncertainty of 21.5%.

Table 4-5: Contribution of core and intermediate input variable relative uncertainties to each component of ET uncertainty for Welgegund

	Transpiration		**Potential soil evaporation**	
	Mean	**Standard deviation**	**Mean**	**Standard deviation**
total uncertainty	0.13	0.28	1.05	0.29
% Tair contribution				
% RH (VPD)	26.93	15.13	(46.11)	(53.05)
% Fc (1-Fc)	3.85	3.10	(1.27)	(0.81)
% Fwet (1-Fwet)	0	0	0	0
% ras			1.97	0.46
rtot			1.45	0.25
ra	0.87	0.12		
rs	8.98	1.67		

In Welgegund (Table 4-5), ET estimation was only the sum of potential soil evaporation and transpiration and so were the uncertainties, since wet soil evaporation and wet canopy evaporation gave zero values and did not contribute to the final ET. The potential soil evaporation standard uncertainty of 1.05 mmday^{-1} was mainly a result of VPD which contributed 46.11%, while other inputs had very low contributions. Transpiration standard uncertainty of 0.13 mmday^{-1} mostly resulted from the VPD that contributed 26.93±15.13% while other inputs had significantly low contributions.

The total ET mean relative uncertainty for Skukuza was 76.19±30.82%. The total uncertainty for Welgegund was similar to that of Skukuza, with a mean relative uncertainty of 81.1±17.57%. In both sites, the highest uncertainty was attributed to soil evaporation, which contributed 76.74±19.13% of the 1.38±0.51 mmday^{-1} in Skukuza, and 90.93±32.46% of the 1.62±0.36 mmday^{-1} in

Welgegund; subsequently plant transpiration uncertainty with mean 23.06±18.83%, and 18.21±18.62%, for Skukuza and Welgegund, respectively. On both sites, the wet canopy evaporation uncertainty was very low, which corresponded with this portion of evapotranspiration.

4.4.3 Sensitivity of PM-Mu model to core input variables

A sensitivity of the ET output to input variables was done on the PM-Mu model to determine which input variable contributes the most to ET output variation. The percentage change in ET with respect to the percentage change in input variables at the study sites is summarised in Table 4-6 and illustrated in Figure 4-3.

Table 4-6: Sensitivity of ET to input variables

Station	Input variables	% change in ET with respect to % change in input variables					
		-20	**-10**	**-5**	**5**	**10**	**20**
Skukuza	Tair		-92.25	-64.80	38.60		
	LST		55.08	39.56	-50.56	-77.45	
	RH	-0.57	-0.30	-0.16	0.17	0.35	0.75
	εa		12.06	6.03	-6.03	-12.06	
	LAI	1.28	0.47	0.19	-0.12	-0.16	-0.02
	α	6.16	3.08	1.54	-1.54	-3.08	-6.16
Welgegund	Tair		-84.17	-47.71	51.12	93.29	
	LST		84.75	44.15	-57.83	-63.15	
	RH	-0.37	-0.19	-0.10	0.10	0.20	0.43
	εa		9.42	4.69	-4.69	-9.38	
	LAI	0.50	0.12	0.03	0.03	0.13	0.48
	α	5.00	2.50	1.25	-1.25	-2.50	-5.00

In the savanna biome, the PM-Mu model was mainly sensitive to LST and Tair. A change of -10% and -5% in Tair resulted in a 92% and 65% ET decrease, respectively, whereas an increase of 5% increased ET by 39%. In contrast, an LST decrease by the same values resulted in ET increasing by 55% and 40%, respectively. On the other hand, an LST increase of 5% and 10% resulted in an ET decrease of 51% and 77%, respectively. ε_a changes from -20% to 0% gave ET increase of +10% generated ET increase and decrease of 12%, respectively, and α changes of -20% to +20% decreased ET by between 6.16 and -6.16%. ET had the lowest sensitivities to RH and LAI, with the computed parameter variations producing ET variations mostly inferior to 3%.

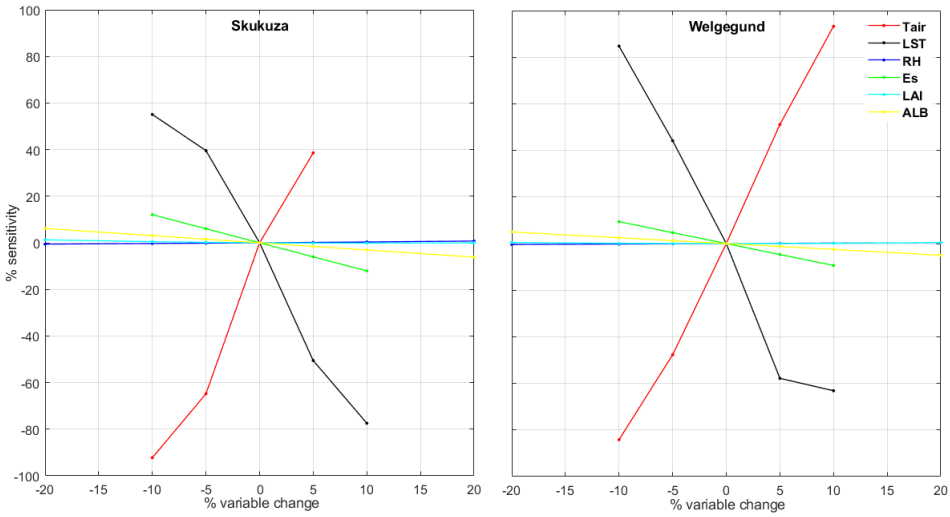

Figure 4-3: Sensitivity of PM-Mu ET model to input variables

The grassland biome results were quite comparable to the savanna biome results, and again ET was mostly sensitive to Tair and LST. The percentage change in ET in relation to Tair decrease of -10% and -5% were -84% and -48%, while an increase of the same magnitudes showed an increase of 51% and 93%, respectively. Similarly, an LST decrease of the same magnitudes showed ET increased by 85% and 44%, respectively, and an increase of 5% and 10% resulted in an ET decrease of 58% and 63%, respectively. ET was least sensitive to RH, Lai, and α, with ET variations generally below 2.5%.

4.5 Discussion

In this study, we evaluated how input variable uncertainty was propagated in the PM-Mu algorithm to the final ET uncertainty, along with the analysis of the sensitivity of the ET output to the different input variable uncertainties. Our study only concentrated on the uncertainty associated with the input variables including uncertainty propagation, and not on the model algorithms used to compute the intermediate variables and the final ET product.

The measured meteorological input variable uncertainties were estimated as a combination of Type A and B uncertainties, whereas for the remote sensing-based inputs, values from literature were used to compute Type B uncertainties. Another essential assumption made was that there is no correlation between the input variables. This, in reality, might not be fully true, an example being the possible relationship between Tair and RH. A sensitivity analysis of ET to both the measured and remote sensing estimated input variables was also done.

4.5.1 Input variable and intermediate parameter uncertainty

Core input variables

The mean relative uncertainties for air temperature (Tair) were within similar ranges for the two sites, i.e. 3% and 4%, for Skukuza and Welgegund, respectively, with the variable showing slight seasonal uncertainty variation during the year. The cooler, drier season exhibited higher relative uncertainties compared with the hotter, wetter season on both sites. This is explained by high diurnal temperature ranges, and thus, high Type A standard uncertainties during the dry, cooler months. In contrast, relative humidity (RH) relative uncertainty showed rather lower variability throughout the year compared to Tair, especially for Skukuza. This was probably due to more stable RH readings throughout the day, resulting in less variation in estimated Type A uncertainty. Welgegund RH relative uncertainties were significantly higher than Skukuza uncertainties, indicating a higher diurnal variation of RH measurements at this site compared to the Skukuza site.

Our results are consistent with the ranges reported in other studies that have been conducted, albeit for different purposes. In most cases, Tair and RH uncertainties have been evaluated simultaneously. For instance, Muniz et al. (2014) ascertained uncertainty of air temperature and relative humidity measured by thermography and found a standard Tair uncertainty of between 0 and 2 °C, and 0 and 5% for RH, in their study to ascertain uncertainty of air temperature measured by thermography. In their case, though, they only considered Type B uncertainties, whereas we took into account Type A uncertainty, which is the variation of temperature over time. In addition, Lin and Hubbard (2004) reported that the uncertainty of derived dew point temperature ranged from 1.8 to 3.3 °C. Comparing our results with other studies, like the ones discussed above is a challenge because of the different metrics used in each study.

It is important to have an understanding of uncertainties associated with remote sensing products that are used in simulating ET, as shown in this study. These uncertainties are normally estimated and included in the ATB documents, with further research being carried out per biome. For example, the absolute quoted accuracy for LST is 1 K and 0.02 for ε_s, in the MODIS ATBD document (Wan, 1999). However, these accuracies vary with the land cover type and the type of uncertainties included in the estimations (Hulley et al., 2012), and should be investigated in detail.

Intermediate data components

The core input variable uncertainties had varying effects on the uncertainties of intermediate parameters like net solar radiation, and the aerodynamic and

surface resistances. There was little variation in Rnet uncertainty in the grassland and savanna sites, with the relative uncertainties modelledd at 4% and 3% for Skukuza and Welgegund, respectively. We noted that on both asites, LST uncertainty contributed the highest to the Rnet uncertainty, with ε_s and Tair uncertainties also contributing significantly. Contrasting with other studies, our total Rnet uncertainties are much different. For example, we recorded much lower Rnet uncertainties than those reported by Mira et al. (2016), who reported overall uncertainties of between 15% and 20% in varying sites of rain-fed to irrigated meadows and crops in the Mediterranean region of Rhône Valley, South Eastern France. In addition, they found that the main contribution to the total uncertainty was equally distributed between the measured incoming short and longwave radiations (at 5% and 8%, respectively) with LST contributing the least uncertainty.

The aerodynamic resistance (r_a^{wc}, r_a^t, r_a^s) relative uncertainties were consistent at an average of 0.8, 0.5, and 2%, respectively, throughout the year, at both sites. Considering these low uncertainties, their contribution to the ET uncertainties was significantly low as well. These results concur with findings of Ershadi et al. (2015), who also showed that aerodynamic resistances play a relatively minor role in ET estimation in the PM model. Furthermore, it has been shown that changes in the parameterisation of aerodynamic resistance in the PM model produce minor improvements to the model output (Bailey & Davies, 1981; Irmak & Mutiibwa, 2009). Compared to the aerodynamic resistances, relative surface resistance uncertainties were quite significant. Given that surface resistances (r_s^{wc}, r_s^t, r_s^{tot}) have a significant contribution to ET estimation, the corresponding uncertainties also have a significant impact on standard uncertainties of ET. This was also reported by Ershadi et al. (2015), who determined that surface resistance parameterisation significantly affects PM model performance.

Uncertainty in PM-Mu ET estimation

The final ET uncertainty is a product of all the input variable uncertainties that were propagated through the PM-Mu model. In our study, we only investigated the uncertainty associated with the input variables, and not with the algorithms used to compute the intermediate inputs and the final ET model. Soil evaporation uncertainty contributed the most to the final ET uncertainty in our study areas, with wet canopy evaporation uncertainty contributing slightly less.

In both biomes, our results show that RH uncertainty, including RH, used to compute VPD, Fwet and the different resistances, contributed the highest to the uncertainties of all the ET components. These results are in agreement with a study by Langensiepen et al. (2009) who reported that VPD is one of the principal meteorological variables in ET estimation using the PM model.

Consequently, any error in the humidity and temperature measurement significantly impacts VPD uncertainty, and hence, increases the overall uncertainty.

The overall mean relative ET uncertainty in our study was around 80% for both biomes, as measured from the propagation of input uncertainties. Nichols et al. (2004) used a similar approach to quantify propagated ET uncertainty of a number of ET estimation methods including the Penman method, in a riparian area of the Middle Rio Grande Basin in New Mexico. They used different values of input variable errors and obtained a much lower relative ET uncertainty of only 10% on the Penman method. This notable difference is due to a number of issues, including the methods and eco-climates under investigation, the difference in the determination of the individual input uncertainties, and the number of input variables and parameters considered in the propagation. Our uncertainties were a product of U_A and U_B estimates propagated from the core inputs, through intermediate parameters, through to the final uncertainty product. Nichols et al. (2004)used predefined input uncertainty values from the manufacturers, for example, they used Rnet uncertainty of 15%, while we reported a low Rnet uncertainty of 3 and 4% for our sites. Ferguson et al. (2010) evaluated the uncertainty contributions of input variables to the final ET output. They show the overall contributions of α and ε_s to ET uncertainties were minor, whereas LAI contributed quite significantly.

4.5.2 Sensitivity of PM-Mu ET estimates to input variables

It is always a challenge to compare results on sensitivity analysis with other studies because of the difference between models, datasets, and procedures being used to estimate the sensitivity coefficients. Also, these are applied under different eco-climatic conditions under investigation. In our study, we used the simple one-at-a-time local sensitivity analysis method to estimate the sensitivity coefficients. Based on the maximum value of each input, we perturbed each of the input variables within the ±20% range. Our results show that PM-Mu is most sensitive to Tair and LST, thus making them the most influential input variables in ET estimation in southern Africa using the PM-Mu method. They also show that the land surface parameters have little effect on the PM method in these regions. These results are consistent with other studies in similar semi-arid/ arid regions, where they reported the PM model is most sensitive to Tair (Eslamian et al., 2011; Debnath et al., 2015). In a comprehensive sensitivity analysis assessment of the PM and Priestley-Taylor models to various inputs in different climates in Australia, Guo et al. (2017a) showed that Tair was the most important variable. In an arid region of India, Goyal (2004) concluded that PET is most sensitive to potential changes in temperature, with solar radiation being

the least sensitive. This result is explained by the fact that in dry environments air has a high capacity to hold water vapour, which can then transfer energy to the land surface. Fisher et al. (2013) investigated the error caused by LST variations on the SEBS model at AmeriFlux sites across the USA and reported that higher LST uncertainty resulted in increased ET uncertainty.

Other studies in similar climates are, however, in contrast with our results of PM-Mu estimated ET being most sensitive to air and land surface temperatures. Tabari and Hosseinzadeh Talaee (2014) observed that ET_0 was more sensitive to wind speed in a semi-arid climate, with less sensitivity to Tair and sunshine hours. Garcia et al. (2004) also reported that wind speed is a critical variable in ET_0 estimation in arid and semi-arid climates. They reasoned that this is because of the importance of the aerodynamic term under dry and high wind speed conditions. Gong et al. (2006) reported that reference ET was most sensitive to the RH variations, followed by solar radiation in the Changjiang basin in China.

4.6 Conclusion

We conducted a comprehensive uncertainty and sensitivity analysis of the PM-Mu model with regards to both in situ and remote sensing-based input variables, in both savanna and grassland biomes of southern Africa. We only assessed the input variable uncertainties and quantified how these were propagated to the final ET uncertainty and not the uncertainties related to the model algorithms used. We found an overall ET uncertainty of approximately 80% in both biomes. This final propagated uncertainty is considerably larger than those reported in other studies. A number of reasons have been highlighted, including the number of input variables assessed for their uncertainty contribution, the assumption that there is no correlation between these input variables and the uncertainty analysis method used that gives the total uncertainty as a combination of Type A and Type B uncertainties. The highest contributor to the final ET uncertainty in our study was relative humidity uncertainty. This highlights the importance of accurate input data collection in ET estimation, as any errors are propagated to the final product. In contrast, the PM model was most sensitive to air and land surface temperatures, indicating the importance of these input variables to ET estimation using the PM-Mu model in our study areas. However, the sensitivity of the PM-Mu model to land surface parameters was quite low. Besides the importance of these variables in ET estimation using the PM method, these results show the impact of temperature due to climate change would have on ET.

Uncertainty and sensitivity studies are fundamental in land surface modelling as they are needed to understand the dynamics of the models and what role the input variables play in model outputs. For instance, in our study, although RH

uncertainty contributed the highest to the final ET uncertainty, air and land surface temperatures played the most significant role in remote sensing-based ET estimation using the PM-Mu model.

5 A REMOTE SENSING-BASED ANALYSIS OF WATER USE AND PRODUCTIVITY ACROSS SOUTH AFRICAN LANDSCAPES

5.1 ABSTRACT

With global water resources facing scarcity, degradation, and overuse, and arable land limited, the focus is shifting towards improving water resource management through increasing water productivity. The maturity of remote sensing-based products of evapotranspiration and other variables gives the opportunity to explore how these products can be applied to improve water resource use and management. Hence, water productivity mapping is currently under development, with the aim to identify water productivity gaps and providing solutions to improve. This study explored the applicability of the WaPOR platform to monitor water productivity and its components, of different land use/ land cover classes across the South African landscape. A performance assessment was done on the WaPOR precipitation and evapotranspiration using ground data from two locations. With R^2 of less than 0.2, results showed that the performance of WaPOR precipitation was quite poor, whereas ET performed reasonably with R^2 of 0.52 and 0.39 for the two sites. An initial analysis of the water use and productivity of different land use/ land cover classes shows that the WaPOR products can adequately show the regional spatial and temporal variability of water use, for example, they can clearly show the effect of the 2014-2016 drought on water use (ET), primary production, and water productivity. Also, a trend across most of the different land uses/ land classes assessed shows that the vegetation uses more water than precipitation in these areas.

5.2 Background

Globally, water resources continue to be threatened by scarcity, degradation, and overuse, while population and income growth increase demands for water consumption for food production. Further, competition for water in other sectors (urbanisation, industrialisation and ecological reserve), and climate and global change contribute to increasing pressure on these scarce resources (Scheierling et al., 2014). Agriculture is the largest water consumer – irrigated agriculture covers about 19% of agricultural area (Thenkabail et al., 2010) – accounting for 70% of total water use (Molden et al., 2007). In South Africa, an already water-stressed country, 40% of the available water is used for agricultural production, of which 60% is for irrigated agriculture while the remainder 60% is allocated to other users (environmental, industrial, urban and domestic uses) (Maila et al., 2018). It is therefore crucial to, first, assess water use and productivity by the different sectors, and then to find ways to use water more efficiently to improve water productivity, especially in irrigated and rainfed agriculture. Increasing water productivity is an important element in improving sustainable water management for agriculture, food security and healthy ecosystem functioning (Xueliang Cai et al., 2011; Cook et al., 2006). It has been estimated that three-quarters of the additional food we need to balance the growing population could be met by increasing the productivity of low-yield farming systems by up to 80% of the productivity that high-yield farming systems obtain from comparable land (Molden et al., 2007). In areas with large yield gaps, there is a huge scope for improvement (Cai et al., 2011; De Fraiture & Wichelns, 2010). In that respect, the highest potential water productivity gains can be achieved in low-yielding rainfed areas in pockets of poverty across much of sub-Saharan Africa and South Asia (Johan Rockström et al., 2010). As many of the world's poorest people live in currently low-yielding rainfed rural areas, improving the productivity of water and land in these areas would result in multiple benefits.

In its broadest sense, water productivity reflects the objectives of producing more food, and the associated income, livelihood and ecological benefits, at the lowest social and environmental cost per unit of water used possible (Molden et al., 2007). Water productivity is defined as the output per unit water used, either physical (crop yield, biomass produced) or economic outputs (money) per unit water applied or consumed (evapotranspiration) (Hsiao et al., 2007; Kijne et al., 2003; Molden et al., 2010). Water productivity is often loosely interchanged with water use efficiency, a term sometimes defined as the ratio between effective water use and actual water withdrawn for irrigation. Although some studies argue rightly that water productivity is not the only component in improving agricultural productivity, water scarcity, aggravated by

the stiff competition between water users, have prompted the United Nations to conclude that water, instead of arable land, and is fast becoming the main constraint to increased food production (Dubois, 2011; Tscharntke et al., 2012). However, improving water productivity is only feasible when other stresses like nutrient deficiency, pest, and weed infestations have been alleviated (Bouman, 2007). In some instances, such as in South Africa water-stressed region, land expansion is no longer a viable solution in increasing food production, hence, the focus should be on efforts to increase water productivity (Godfray & Garnett, 2014; Pretty et al., 2018).

Remote sensing-based evapotranspiration (ET) modelling and prediction is a mature technology, with the available models continually being calibrated, validated and adapted to different ecosystems, climates and management systems, and applied at various temporal and spatial scales. Considering the current urgency of the water crisis, more focus needs to be on transferring these remote sensing techniques to operational applications in water resource monitoring and management. Water productivity mapping of different crops is currently under development at different scales, with different WP tools being applied to monitor water use per land use and improve on water resource management. Some of the work done to map water productivity includes the use of different sensors to map WP for different crops in Galaba in the Syr Darya river basin in Central Asia (Biradar et al., 2008; Cai & Sharma, 2010; Cai et al., 2009; Platonov et al., 2008). They derived crop yield empirically by relating crop spectral information to measurements of LAI, biomass, and yield, and water use using the Simplified Surface Energy Balance model. Meanwhile, Zwart et al. (2010) developed a WATer PROductivity (WATPRO) model for wheat using remote sensing inputs. By combining the dry matter production model from Monteith's (1972) theoretical framework and an energy balance based evapotranspiration model, they ensured the omission of the evaporativefraction and atmospheric transmissivity. Using Sentinel 2 and Landsat 8, Nyolei et al. (2019) applied the SEBAL ET model, locally calibrated LAI map and land use map to map WP in the Makanya river catchment in Tanzania. Other WP projects include the Futurewater Water Productivity pilot project involving smallholder farmers in the Gaza region of Mozambique (den Besten et al., 2017). They employed unmanned aerial vehicles (UAV) and AQUACROP, a crop water productivity model, to assess yield and WP for maize. They demonstrated the feasibility of using UAV technology to monitor WP at farm level. On the same thread, the Food and Agriculture Organisation (FAO) of the United Nations is running a portal to monitor Water Productivity through Open-access of Remotely sensed derived data (WaPOR), to assess land and water productivity, identify water productivity gaps, in a bid to propose solutions to reduce these gaps and to contribute to a sustainable increase of agricultural

production. This portal covers Africa and the Near East, with a few designated pilot project areas in the Nile, Niger, Awash, and Jordan/ Latini river basins. Products from this portal are now being used in different studies, including monitoring water use in agriculture (Tantawy, 2019), comparison with other estimation methods (Javadian et al., 2019) and as inputs in groundwater studies (Nhamo et al., 2019).

The objectives of this chapter are, therefore, to assess water productivity across different land use/ land cover classes on the South African landscape, including natural vegetation and agricultural land. Under natural vegetation, grasslands and forests will be targeted, whilst subsistence and commercial agricultural lands will also be assessed. We will evaluate the different inputs of the Water Productivity through Open access of Remotely sensed derived data (WaPOR) WP (gross and net WP), including land cover, ET and above-ground biomass (AGBP) against the SA based and tested products.

5.3 Methodology

5.3.1 FAO WaPOR platform

The FAO Water Productivity Open-access portal (WaPOR) is a tool that has been developed under the FAO project aimed at monitoring water productivity, identifying water productivity gaps and proposing solutions. The ultimate goal is to reduce these gaps, and thus, contribute to a sustainable increase in agricultural production through the use of satellite remote sensing technology. This initiative was driven by the fact that agriculture is a major water user, hence, the need to carefully monitor agricultural water productivity, and ultimately finding means to improve it. Different datasets are available for analysis at three spatial scales, i.e. 30 m scale sub-national for selected pilot sites, 100 m for the pilot countries, and 250 m for the rest of Africa, at annual, decadal and daily time scales. Table 5-1 gives the datasets that are available on the platform that will be analysed in this paper. The derivation of each of these variables is described in detail in (FAO, 2018).

Table 5-1: Data extracted from the WaPOR platform

Dataset	Unit	Temporal resolution	Method used
Precipitation	mm	annual, decadal, daily	Obtained from the CHIRPS dataset, which estimates precipitation from global models which use satellite observations and ground based measurements
Actual Evapotranspiration (ET)	mm	annual, decadal	Penman-Monteith model as described by W. Bastiaanssen et al. (2012) on ETLook
Net Primary Production (NPP)	gm^{-2}	Annual, decadal	Derived using a method detailed in Veroustraete et al. (2002)
Above Ground Biomass Production (AGBP)	$kgDMha^{-1}$	annual	Obtained by converting NPP using the AGBP Over Total biomass production conversion factor which accounts for the division between the above and below ground components. Conversion factor fixed at 0.65
Net Biomass Water Productivity (NBWP)	kgm^{-3}	annual, decadal	Ratio of above-ground biomass production to evapotranspiration
Gross Biomass Water Productivity (GBWP)	kgm^{-3}	annual, decadal	Ratio of above-ground biomass production to transpiration

5.3.2 Study area

The 1.22 million km^2 of the South African land area, of which 79.8% is agricultural land, 7.62% is forest, and the remainder classified as other land. These are further subdivided into 73 different land cover classes, including natural and cultivated forest, vines, orchards, sugarcane, and annual crops (Thompson, 2019). The aim of this study is to assess the use of the WaPOR database to monitor water productivity of different land use/land cover classes, based on the South African National Land Cover map. Initially, the FLUXNET sites were assessed, with a few more sites randomly selected (these are initial results of the study, hence they cover a few sites), as shown below. These sites cover a range of land use/ land cover classes, including natural vegetation (Kruger National Park, Welgegund, Elandsberg, and Dukuduku Forest), agriculture (plantation, subsistence, and rainfed and irrigated commercial).

Skukuza FLUXNET site (Kruger National Park)

Covering almost 2 million hectares, the Kruger National Park (KNP) is located on the north-eastern border of South Africa and Mozambique. It is in a subtropical climate characterised by wet, hot summers, and dry, warm winters. Mean annual precipitation ranges between 440 mm in the north and 750 mm in the south significant inter-annual variability. Meanwhile, temperature ranges between 15.6 and 29.6 °C, with a mean of 22.6 °C. The park is bound by the Limpopo River in the north and the Crocodile River in the south, with several other flowing through from west to east, including the Sabie, Oliphants, Letaba and Luvuvhu Rivers. The park is rich in biodiversity, with flora comprising 1903 species, of which 400 are tree and shrub species and 220 kinds of grass. Four vegetation types characterise the park, i.e. the well-wooded south-west with tree species including the red bushwillow (*Combretum apiculatum Sond.*), knobthorn (*Acacia nigrescens Oliv.*), tamboti (*Spirostachys Africana Sonder*) and marula (*Sclerocarya birrea [A. Rich.] Hochst*.). The south-east is grassier and heavily grazed, with trees like knobthorn, leadwood (*Combretum imberbe Wawra*) and marula. On the other hand, the north of the Oliphants River is poorly grassed, with the main tree species being the mopane (*Colophospermum mopane*) and red bushwillow. The north-eastern region is dominated by mopane shrubs. This park houses 147 mammal species and 492 birds. There are local communities along the border of the KNP who use the communal rangelands for livestock ranching, crop agricultural activities, and fuel energy.

Elandsberg Nature Reserve

A South African National Heritage Site, and a Contractual Nature Reserve, Elandsberg Private Nature Reserve is situated near the town of Hermon in the valley of the Berg River, Western Cape Province. It is situated on the west-facing foot slopes of the Elandskloof mountain range, with an area of about 2 000 ha. The reserve is in a winter rainfall region, with dry summers typical of Mediterranean type climate, receiving a mean annual rainfall of 660 mm. The temperatures range between an absolute 2 and 43 °C. Lying within the West Coast Renosterveld of the fynbos biome, it is home to at least 820 plant species. The dominant vegetation types include the Swartland Alluvial Fynbos on deeper, sandy soils interspersed with patches of Swartland Shale Renosterveld on more stony, shale-derived soils.

Welgegund

Welgegund farm is located within an elevated plateau known as the SA Highveld in the North West Province, about 25 km north-west of Potchefstroom. It is situated in a semi-arid climate, grassland biome. The mean annual rainfall in the area is 540 mm, and temperatures range between 0 and 30 °C with an average of 18 °C. 1300±300 Cattle graze on an area of approximately 6000 ha, with the

carrying capacity quite low. The dominant vegetation comprises grasses, geophytes, and herbs. The dominant grass species are *Hyparrhenia hirta* and *Sporobolus pyramidalis*. Non-grassy forbs include *Acacia sieberiana*, *Rhus rehmanniana*, *Walafrida densiflora*, *Spermacoce natalensis*, *Kohautia cynanchica*, and *Phyllanthus glaucophyllus*.

Dukuduku Forest and surrounding lands

Dukuduku forest is an indigenous forest located between Mtubatuba and St. Lucia towns in northern KwaZulu-Natal Province. It is part of the iSmangaliso Wetland Park, a UNESCO world heritage site, comprising the St Lucia estuary, the largest estuarine system in Africa (Whitfield & Taylor, 2009). The climate is subtropical with warm, moist summers and mild winters, and mean annual temperature exceeding 21 °C. Due to deforestation, this forest has shrunk from 6000 ha, when it was declared a protected area in the early 1950's, to 3200 ha in 2013. A 29% loss of the forest has been reported to be due to its conversion to small farms and squatter camps between 1992 and 2005 (Ndlovu, 2013). The area is dominated by various natural indigenous vegetation species including rare tree species like *Syzygium cordatum, Cussonia zuluensis, Ficus natalensis, Canthium inerme, Strychnos madagascariensis, Strychnos spinosa, Apodytes dimidiate, Ozoroa engleri, Barringtonia racemosa, Albizia adianthifolia, Ekebergia capensis, Harpephyllum caffrum, Hymenocardia ulmoides, Sclercarya birrea,* and *Trichilia dregeana*. On the western and southern borders, the forest is surrounded by sugar and Eucalyptus plantations, and villages that practise subsistence farming on the eastern border.

5.3.3 Evaluation of WaPOR products

Performance of WaPOR precipitation and evapotranspiration products

Using ground measured data from the Skukuza and Welgegund FLUXNET sites, the accuracy of the WaPOR precipitation and evapotranspiration was evaluated using the coefficient of determination (R^2), bias, mean absolute error (MAE), root mean square error (RMSE), and relative RMSE (rRMSE).

Assessment of WaPOR products

Apart from the sites that have already described and investigated in this thesis (i.e. Skukuza and Welgegund flux tower sites, and Elandasberg), extra sites were randomly selected from around South Africa based on climate and land cover/ land use, as described in Section 5.2.1. Decadal and annual values of Precipitation, Evapotranspiration (ET), NPP, AGBP, NBWP and GBWP from 2009 to 2018, were extracted from the WaPOR platform for analysis. The measured precipitation and ET data from the Skukuza and Welgegund eddy covariance flux tower sites were then used to evaluate the extracted decadal WaPOR products.

Furthermore, annual precipitation, ET, NPP, GPP, NBWP, and GBWP were analysed per site.

5.4 Results and discussion

Water use varies across significantly across different land use/land cover and vegetation types, depending on a number of factors that include water availability, soil characteristics, and agricultural management systems. This section presents the results of the performance assessment of the WaPOR precipitation and ET products which was done using the Skukuza and Welgegund eddy covariance system data. Unfortunately, we could not get the field yield (biomass) values to be able to compute WP and compare these with the modelled values. Subsequently, the different components of precipitation, ET, NPP, AGBP, NBWP, and GBWP of each land use/ land cover class were analysed.

5.4.1 Performance of the WaPOR precipitation and ET

Before any modelled remote sensing-based products can be used and applied with confidence, they should be tested against ground measured data. Here the precipitation and ET products were tested using measured data from Skukuza (savanna) and Welgegund (grassland) eddy covariance flux tower systems.

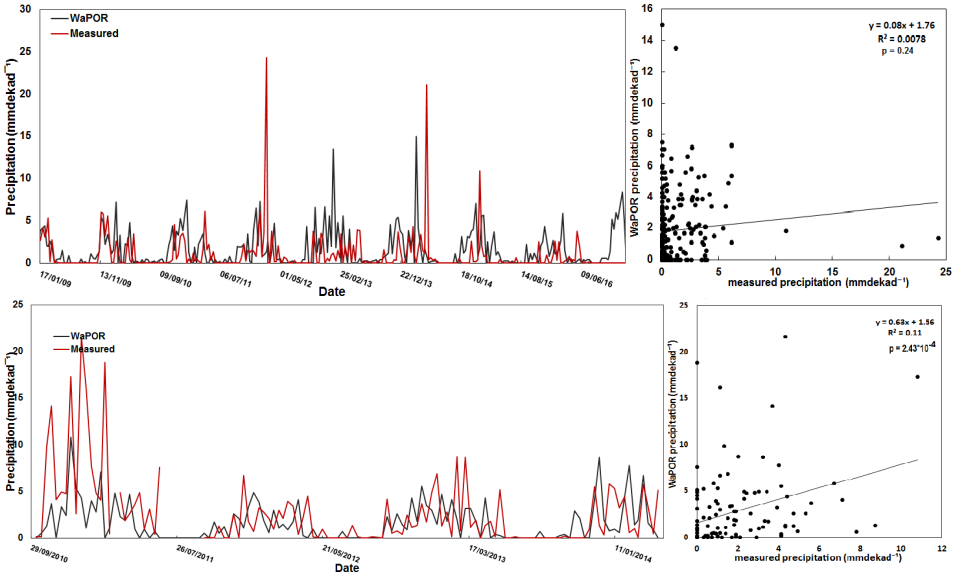

Figure 5-1: Decadal measured and WaPOR precipitation time series (left) and scatterplot (right) comparisons for Skukuza (top), Welgegund (bottom)

The WaPOR precipitation estimates followed the trend of the measured precipitation, managing to estimate precipitation at the designated rainfall intervals (Figure 5-1). However, the estimation accuracy was very low, as shown by the low R^2 of 0.0078 and 0.11 for the two sites. Meanwhile, the correlation between the estimated and measured precipitation was statistically significant for Welgegund (p-value = $2.43*10^{-4}$), whereas it was insignificant for Skukuza (p-value = 2.37). Moreover, the WaPOR precipitation estimates could not simulate high precipitation events.

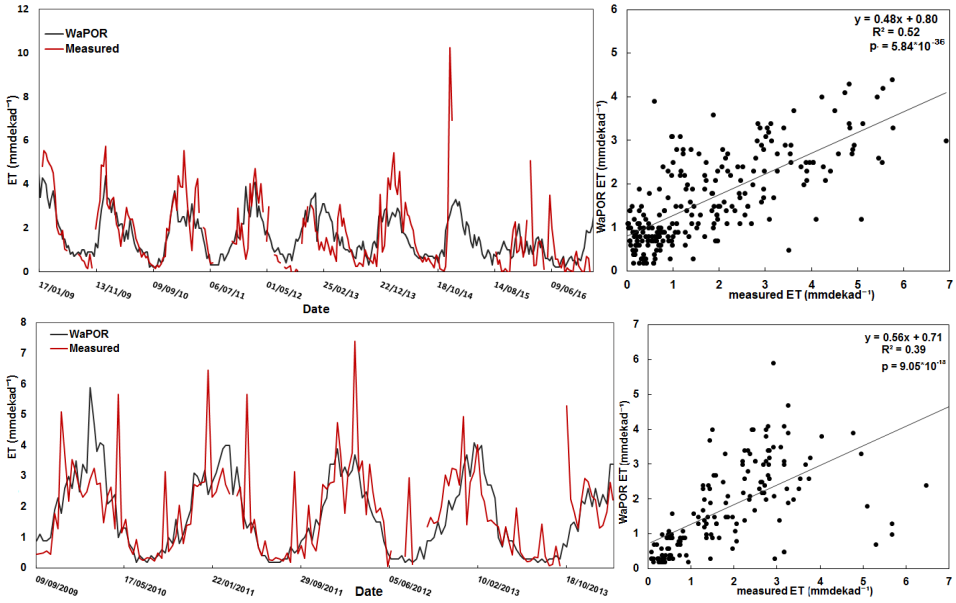

Figure 5-2: Decadal measured and WaPOR ET time series (left) and scatterplot (right) comparisons for Skukuza (top), Welgegund (bottom)

Figure 5-2 shows that the seasonal trend of WaPOR ET was observed following the measured ET. With R^2 of 0.52 and 0.39 for the savanna and grassland sites, respectively, the statistics (Table 5-2) indicate the WaPOR decadal ET performed better in the savanna than the grassland biome. For Skukuza, particularly, the WaPOR ET performed better than the PM-Mu used earlier in Chapter 3. The periods of low ET are characterized by a more perfect fit between the EC and WaPOR ET for both sites. Furthermore, for Welgegund, the fit extends to the periods of higher ET. The main reason could be that WaPOR PM included soil moisture measurements to constrain the model, whereas PM-Mu used in Chapter 3 only used RH and VPD as soil moisture proxy. Conversely, WaPOR PM indicates a general underestimation of ET during periods of higher ET in Skukuza. This result concurs with previous results of this work in Chapter 3, which shows a saturation of PM-Mu ET at some point.

Table 5-2: Statistics summary of eddy covariance derived and WaPOR ET estimates

	Skukuza	Welgegund
Bias	0.11	0.15
MAE	0.78	0.83
RMSE	1.06	1.24
rRMSE	60.35	67.14

Another evaluation of the MOD16 8-day ET using the Skukuza EC data by Dzikiti et al. (2019) gave an RMSE of 1.19 mmday^{-8}, which is comparable to the 1.06 mmdekad^{-1} reported in this study. Meanwhile, Gomis-Cebolla et al. (2019) also showed that PM had an RMSE averaging 1.25 mmday^{-1} in their study in the Amazonia, with the conclusion that this model overestimated ET.

5.4.2 Evaluation of WaPOR water use across different land use/ land cover classes

We evaluated water use and water productivity for different land use/ land cover classes across South Africa using the WaPOR products. Table 5-3 shows that the Dukuduku forest and surrounding land uses on the eastern part of South Africa recorded the highest precipitation amount over the 10 year period with an average of 884 mmyear^{-1}. Within the same area, the communal area receives the highest precipitation, as shown in Figure 5-3. Welgegund received the lowest precipitation averaging 537±78 mmyear^{-1}, although not significantly different from Elandsberg 542±146 mmyear^{-1}. Moreover, 2015 recorded the lowest precipitation in all the areas around South Africa, except for the high precipitation Dukuduku area, which experienced low precipitation the previous year. Also, the winter rainfall Elandsberg experienced a severe drought in 2018.

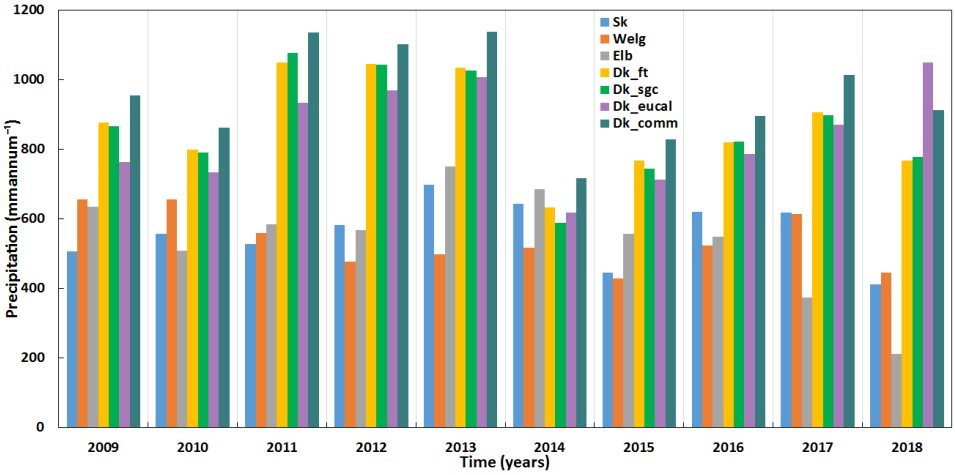

Figure 5-3: Mean annual precipitation variation across different biomes and land uses in South Africa

It can be observed that the multiyear average evapotranspiration was higher than precipitation at all the sites, except the Dukuduku communal area, which lost 94% of the multiyear average rainfall of 956 mmyear^{-1} through evapotranspiration, and Skukuza which lost almost the same amount of water that fell as rainfall. Higher ET than precipitation is encountered due to a number of factors, based on location and land use. For example, the Welgegund flux tower is located on a commercial farm, where they cultivate pastures and sunflower for grazing. The rainfall is supplemented by irrigation, hence more water is available for loss through ET, resulting in higher ET compared to rainfall. The low precipitation recorded in 2014-2015 is followed by a dip in ET in 2015, especially for Skukuza and the Dukuduku Eucalyptus plantation.

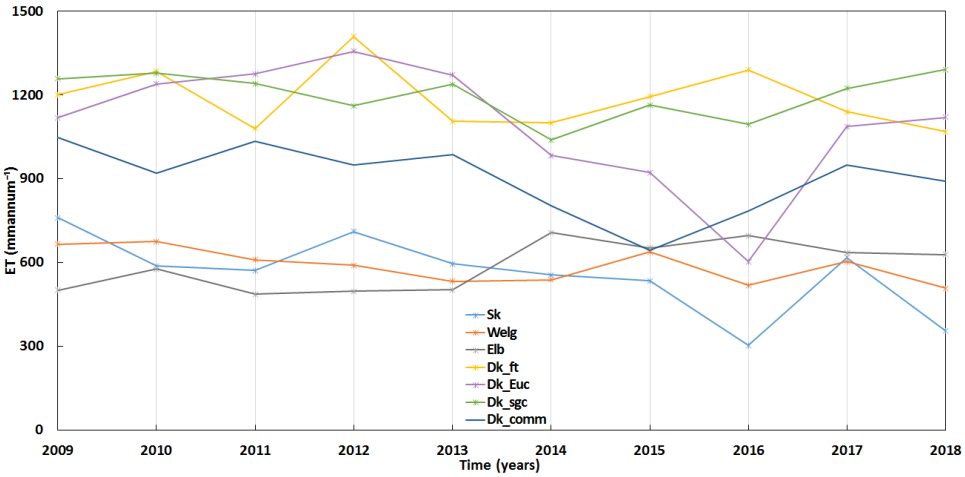

Figure 5-4: Time series ET of different biomes and land uses

Consequently, although with similar precipitation amounts, the ET to precipitation ratios in the Dukuduku area vary from 1.39 at the sugarcane plantations, 1.37 at the natural forest, and 1.3 at the Eucalyptus plantation. A plausible reason for the higher than unity ET/precipitation ratio in the Eucalyptus and natural plantations could be because they have deep root systems that tap into the groundwater. On the other hand, the results point out that sugarcane production uses more water than plantations, resulting in the highest ET/precipitation ratio. An extension to drier regions of the country also shows higher ET than precipitation, with both having a 1.09 ratio. Skukuza was the exception, losing an equal amount of water as received.

The estimated ET for the Eucalyptus plantation in our study concurs with other studies done in South Africa, which stated that Eucalyptus ET varies between 1100 and 1200 mm per year (Dyeet al., 2007). However, while our results show an overall high mean annual water loss for the natural forest compared to the Eucalyptus forest, contrasting results are reported in other studies where these plantations consume more water than the baseline vegetation (Gush et al., 2002, Gush 2006, Dye et al., 2007). The discrepancy in our results is likely because of the age of the Eucalyptus trees observed, where there they have not fully matured the deep root system (Dye, 1999). This is further illustrated by the low ET recorded during the 2016 period (Figure 5-4), which came after two years of lower than the mean annual precipitation (Figure 5-3). Mean annual precipitation may not vary too much in an area, except during extreme events, vegetation water use varies quite a lot depending on the type and maturity stage. In our study, we, however, did not determine the age of the Eucalyptus plantation, and so the results are taken as generic. Meanwhile, a study in the

Brazilian Eucalyptus plantation during a dry (779 mmyear^{-1}) and wet (939 mmyear^{-1}) year showed lower ET than our results (Ren et al., 2019).

As summarised by Sun et al., (2013), the spatial distribution of AGB is affected by a number of environmental factors, categorised into meteorological (air temperature, relative humidity, precipitation), topographic (longitude, latitude, altitude, slope, aspect), and soil (soil moisture, soil temperature, soil nutrient, soil texture, soil organic matter). Our results in Figure 5-6 show a positive relationship between precipitation and NPP, i.e. high NPP corresponds with high rainfall, and the opposite being true. However, a slight lag in NPP increase is highlighted in line with the precipitation events. It was observed that there is little distinction between Elandsberg fynbos biome and Skukuza savanna NPP (1.1±0.77 gm^{-2} and 1.07±0.40 kgDMha^{-1}) and AGBP (5799.4±1748.6 gm^{-2} and 5672.2±353.24 kgDMha^{-1}). A clear distinction between AGBP from the high rainfall Dukuduku area and the low rainfall areas is clearly visible in Figure 5-5. Moreover, in the Dukuduku area, the natural forest had the highest biomass production of all the land uses.

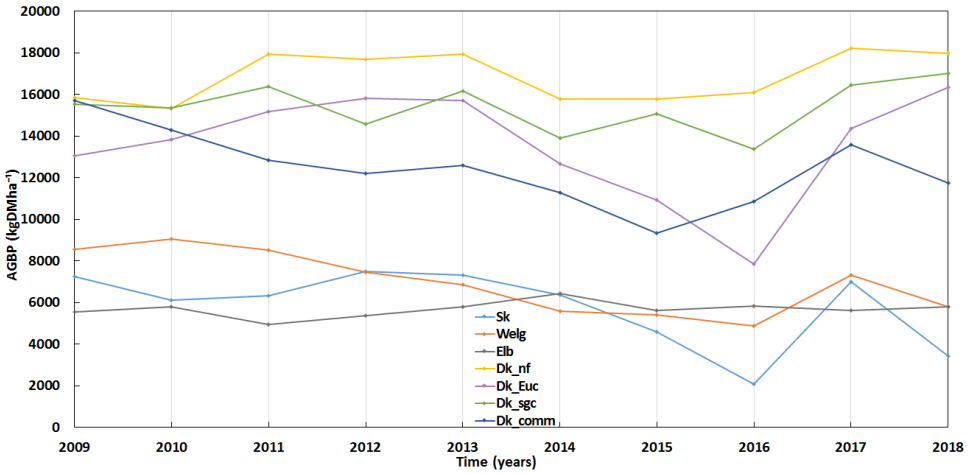

Figure 5-5: Time series AGBP of different biomes and land uses

ET versus AGBP correlation was high, with R^2 between 0.48 and 0.86 for all the sites. An exception was the Dukuduku natural forest which had the poorest correlation of 0.1, indicating that other factors other than water availability affect AGBP. Our results are in line with other studies by Scholes et al., (2002) and House and Hall (2001) who also confirmed the almost linear relationship between biomass and precipitation and/or water availability in the savanna biome.

A number of studies have been carried out to investigate AGBP on the southern part of the Kruger National Park, including using destructive harvesting data

collection to develop an allometric equation to estimate AGBP (Colgan et al., 2013). Their results showed that individual tree biomass ranged between 0.2 and 4531 $kgha^{-1}$. A more detailed investigation of the savanna AGBP mapping was investigated by Naidoo et al., (2015) and Mathieu et al., (2013), who used finer resolution active SAR data. Moreover, Odipo et al., (2016) explored the potential of high resolution TLS-derived canopy cover and height metrics to estimate plot-level aboveground biomass (AGB) and extrapolated to a landscape-wide biomass estimation using multi-temporal SAR. Their results gave AGB ranging between 19.7±5.2 tha^{-1} to 34.2 ± 30.78 tha^{-1}. Their results gave AGB ranging between 19.7±5.2 tha^{-1} to 34.2±30.78 tha^{-1}. One of the challenges in comparison to these studies is the metrics used in each of the studies. For example, the above studies were investigating woody (tree) biomass, whereas the WaPOR product only considers C3 crop types, and does not cater for crop type variations. However, this dataset is very useful for cereal crops like wheat, maize, and wheat, but certainly would need modifications for it to be applied for other crops like root, tuber and bulb crops, as described in FAO and IHE (2019).

Gross biomass water productivity provides insights on the impact of vegetation development on consumptive water use and thus on the area (catchment) water balance, whereas net biomass water productivity is a useful parameter in monitoring how effectively vegetation (particularly crops) uses water to develop biomass (and thus yield). WP analyses in Table 5-3 show a clear distinction between, first, the different biomes and climatic zones, second, the different land uses across the natural vegetation and agricultural areas. For example, with the highest NPP and AGBP, the Dukuduku natural forest recorded the highest gross and net biomass water productivities.

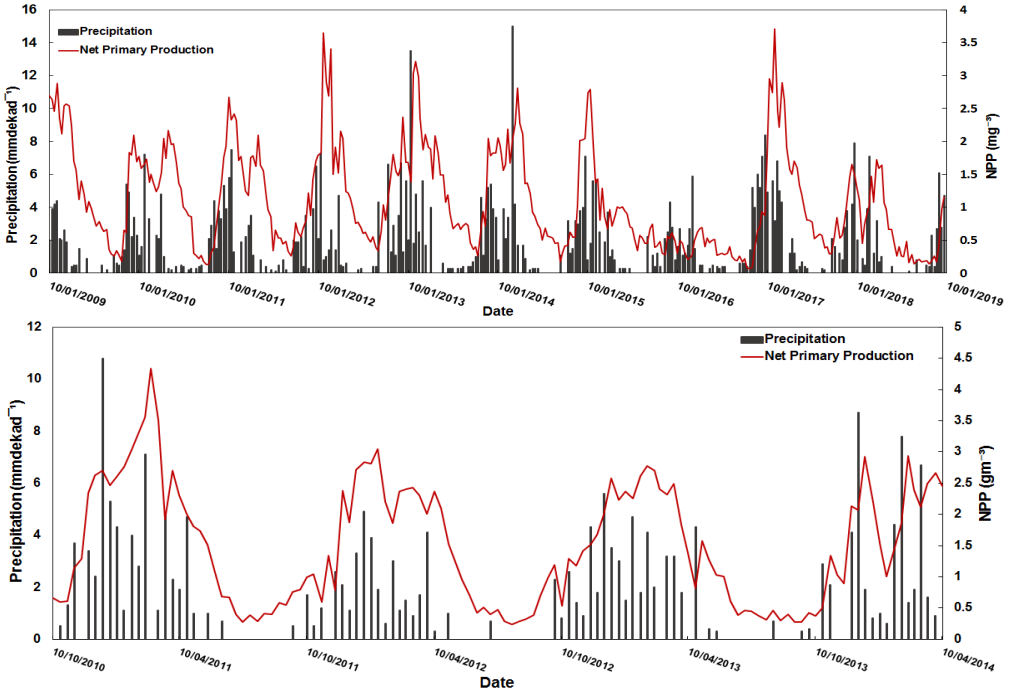

Figure 5-6: Time series comparison of precipitation and NPP Skukuza (top) and Welgegund (bottom)

On the other hand, although with much lower consumptive water use, Dukuduku communal area recorded quite high water productivity compared to the surrounding eucalyptus and sugarcane plantations. In the low precipitation areas, all the three sampled areas, Welgegund (1.45±0.95 kgm^{-3}), Skukuza (1.35±0.12 kgm^{-3}) and Elandsberg (1.27±0.13 kgm^{-3}) actually had quite comparable net biomass water productivity.

A comparison with studies within the WaPOR project shows that our results have lower WP for sugarcane (1.38±0.04) compared to the irrigated Ethiopian sugarcane (6.13 kgm^{-3}). Other studies across South Africa recorded Eucalyptus WP between 0.0008 and 0.0123 m^3m^{-3} water consumed (Albaugh et al., 2013). Furthermore, in the Argentinian Entre Rios region, another study on Eucalyptus WP (1.20 kgm^{-3}) showed values that were much lower than those recorded in the Dukuduku plantation.

Table 5-3: Multi-year annual average values of 2009-2018 WaPOR biomass and water use components for different land uses across South Africa

Site/ Area	Land use/ land cover	Precipitation	Evapo-transpiration	Net Primary Production	Above Ground Biomass Production	Net Biomass Water Productivity	Gross Biomass Water Productivity
Skukuza	Natural vegetation (savanna)	560.8±83.32	559.43±133.03	1.1±0.77	5799.4±1748.6	1.35±0.12	1.02±0.15
Welgegund	Pasture (grassland)	537.4±77.95	588.44±57.99	1.32±0.96	6941.9±1404.31	1.45±0.95	1.17±0.17
Elandsberg	Natural vegetation (fynbos)	542.0±146.38	588.81±82.03	1.07±0.40	5672.2±353.24	1.27±0.13	0.98±0.11
Dukuduku forest	Natural vegetation (forest)	869.6±132.95	1187.55±105.82	3.20±0.80	16860.5±1116.08	1.61±0.25	1.43±0.18
Dukuduku Plantation	Commercial Eucalyptus plantation	844.69±135.56	1097.79±209.12	2.57±0.81	13576.4±2476.29	1.37±0.14	1.24±0.10
Dukuduku sugarcane	Commercial rainfed	863.4±144.77	1198.99±78.17	2.92±0.94	15386.9±1110.96	1.38±0.04	1.28±0.05
Dukuduku communal	Subsistence agriculture	956.2±133.49	901.34±118.61	2.36±0.77	12440.9±1723.68	1.50±0.10	1.38±0.10

5.5 Conclusion

The WaPOR platform provides different datasets covering primary production, biomass, and water availability, use, and productivity. These data products are critical not only in assessing and monitoring water productivity of different land use/ land cover classes, but can be used to identify biomass (yield) and WP gaps, and applying management practices to improve WP and hence, yield. Also, these datasets can be used as input data to research on the catchment water balance, especially in areas of scarce in situ data.

Evaluating the performance of these data under different biomes and/or land uses is a critical step in their production and further application. The main focus of this study was to assess biomass and water productivity variation between biomes and land uses across the South African landscape, making it a preliminary study to using the WaPOR platform to further investigate agricultural water productivity. Firstly, an evaluation of the precipitation and ET data against ground measured data showed a good correlation between the two datasets. These results give confidence in using and applying the WaPOR products in our region. However, to be applied in cases of crops other than C3/ C4 cereals, the suggested modifications would have to be implemented for more accurate results. Furthermore, this study is still ongoing to assess water use/ water productivity of a variety of land use/ land classes, with the main focus being the agricultural areas.

With the challenges facing water availability and food production, water productivity mapping using remote sensing and modelling techniques assist in

identifying areas of low WP, which in many instances translates to low biomass and/or yield. Obtaining such information is important in ensuring sustainable management strategies would be employed to reduce water use and increase biomass (yield). This would further ensure increased food production.

With precision agriculture gaining momentum around the world, water use/ WP mapping are necessary tools to identify, even within field, areas of low WP, in order to further investigate the reasons for low crop productivity in order to come up with mitigating actions.

6 SYNTHESIS AND FINAL REMARKS

6.1 Summary

Efficient use of water resources in (semi-)arid regions is increasingly becoming critical due to population increase and income growth leading to higher demand for water for consumption and food production, and competition for water with other sectors (urbanisation, mining, industrialisation, and ecological reserve). Hence, accurate estimation of all hydrological cycle components, including evapotranspiration is important. Deemed the most complex component of the water cycle, evapotranspiration is a critical process linking the water and the energy cycles. Thus, it has been a subject of study since the eighteenth century, with numerous techniques having been developed and tested under varying biomes and climatic conditions, including direct measurement and modelling techniques. The aim of this thesis was, therefore, to evaluate remote sensing-based evapotranspiration estimates in a semi-arid ecosystem, and apply remote sensing-based ET estimates in water use/ water productivity assessment.

This chapter will summarise the findings of this thesis and highlight the main contribution to science.

6.1.1 Eddy covariance data quality assessment

The Skukuza eddy covariance flux tower, located in the Kruger National Park, has been operational since February 2000. This long-running dataset continues to contribute immensely to the study of the carbon, energy and water dynamics of the semi-arid African savanna ecosystem (Archibald et al., 2009; Kutsch et al., 2008; Nickless et al., 2011; Williams et al., 2009). In the meantime, so much work has been done to evaluate the quality of these EC data worldwide, including identifying the sources of error. However, the Skukuza flux data have not been subjected to this process, which is crucial especially if these data are to be used in the atmosphere and land surface model cal/val. Furthermore, it is important to understand the partitioning of solar energy in such an environment characterized by high temperatures and low, sporadic precipitation. This section of the thesis was important in identifying the long-running Skukuza eddy covariance system data, assess their quality, identify windows of compromised data, and possible reasons for loss of quality. Therefore, in Chapter 2, the quality of 15 years of EC data from the Skukuza flux tower was assessed using the ordinary least squares (OLS) and the energy balance ratio (EBR) methods. This was a critical step in our study, not only to present the EBR information of these data but also to screen which periods had high-quality data to be used for further evaluation of the remote sensing-based ET models. During the assessment, those periods (years) with large data gaps and poor data quality, i.e. with an EBR of less than 0.5, were discarded and not included in the subsequent analysis. To add substance to our analysis, the EC data were divided

between day- and nighttime, and seasonal, and the effect of weather conditions on the SEBC. While the mean multi-year EBR was 0.93, 60% of the yearly EBR was within the 10-30% error reported on other FLUXNET sites worldwide, and the remainder 40% recorded a higher EBR. In this study, the heat storage terms (soil and canopy heat storage, and energy storage by photosynthesis and respiration) were excluded. Furthermore, an investigation of the effect of friction velocity highlighted its effect on EBR, which was in essence linked to the time of day. The effect of friction velocity on the imbalance was ascertained, highlighting its link to the time of day. The seasonal variation of EBR showed low surface energy imbalance during the wet season compared to the dry season.

Generally, the variations in surface energy availability and partitioning depend on solar radiation, air temperature, precipitation and/or soil moisture. Additionally, vegetation dynamics provide an explanation for the partitioning of surface energy. Results obtained in Chapter 2 highlight that in (semi-)arid areas solar radiation is not a limiting factor to latent heat flux, but water availability (precipitation and/or soil moisture), unlike in temperate regions where solar radiation is. The wet season is characterised by high precipitation amount and high temperatures, hence latent heat flux was more dominant than sensible heat flux. Vegetation development, i.e. flowering and leaf emergence is influenced by precipitation, and as it peaks, latent heat flux also peaks whilst sensible heat flux reaches the minimum. On the other hand, the dry season is characterised by lower solar radiation, little to no precipitation, leaf senescence and tree defoliation, resulting in sensible heat flux rising to its maximum and latent heat flux hitting its bottom. Regardless of the time of year and available solar radiation, the results also showed that an increase in vapour pressure deficit is characterised by a rise in sensible heat flux and a reduction in latent heat flux. The challenges of maintaining such a delicate system running for a long time could also be identified in this study. These include the measuring instruments breaking down and needing to be fixed and/or replaced, the effect of weather on measurements, and the change of instruments from one type to another as was the case in this system. The biggest challenge has been the expertise and sourcing funding to maintain the system running.

6.1.2 Model assessment and intercomparison

The objective of Chapter 3 was to identify the best performing ET model and/or product in semi-arid environments like South Africa. Based on the results of the EBR analysis in Chapter 2, EC data with the best EBR was selected for use in the evaluation of ET models, which in this instance was 2012 with the best EBR of 1.01. In addition to the tropical climate savanna biome Skukuza flux tower site, another ET dataset from the Mediterranean climate fynbos biome region

(Elandsberg Nature Reserve) of the south-western part of South Africa was used in this evaluation.

The models tested in this section include the Penman-Monteith model (PM-Mu) modified by Mu et al. (2007); Mu et al. (2011) and the Priestley-Taylor based land surface temperature-vegetation index triangle method (Ts-VI), the Priestley-Taylor based GLEAM (Martens et al., 2017; Miralles et al., 2011) and the Soil-Vegetation-Atmosphere-Transfer (SVAT) model Tiled ECMWF (European Centre for Medium-Range Weather Forecasts) Surface Scheme of Exchange processes at the Land surface (TESSEL) based LSA-SAF MET (N. Ghilain et al., 2011; Ghilain et al., 2012; Ghilain et al., 2014) products. Using the statistical methods like the relative root mean square error (rRMSE), mean absolute error (MAE) and bias, all the results showed a general underestimation of ET, except during the wet season in the fynbos biome. PM-Mu method was the best performing during periods of high ET for both sites, although there was no outstanding difference between the other model and products. The PM-Mu error statistics fall within the globally observed error of up to 30% during these periods of high ET. This is further seconded by the coefficient of determination (R^2), which showed variable results. Periods of low ET showed Ts-VI performed the better compared to the other models/ products on in the savanna biome, with GLEAM outperforming the rest of the models in the fynbos biome.

The variation between the model performances is attributed to factors like structural complexities, model assumptions, parameterisations, amount of data required, and atmospheric and land surface characteristics. The MODIS products, together with in situ measurements, used as inputs to the models they have their errors and uncertainties that have been investigated and recorded in the ATBD and product documents. Another source of error discussed was the flux footprint, i.e. for the 16 m measuring the height of the Skukuza EC system the footprint of 1.6 km, which, although is almost similar to the MODIS pixel size of 1 km, is a function of landscape heterogeneity, atmospheric stability, and wind velocity and direction.

The Ts-VI method is a version of the PT model, which parameterises the PT parameter (φPT) in order to estimate the evaporativefraction (EF) using the triangular feature space of the LST-VI scatterplot. One of the biggest advantages of this method is that it does not require ancillary data, i.e. it is the least data intensive of the models that were tested in this study. Its reliability depends on the accurate identification of the wet and dry edges in the Ts-VI feature space, which is reliant on the heterogeneity of the land surface under investigation, from full vegetation cover to bare soil surface. In areas and during periods of high land surface homogeneity, it is challenging for the triangle shape to form convincingly in the Ts-VI scatterplot, hence the identification of the wet and dry

is also difficult. The Ts-VI method is not transferable to another area and time without violating the main assumption of uniform atmospheric forcing across the image. This is further compromised by the spatial resolution of the images being used to define the triangle feature space; the coarser the resolution the wider the area used to determine the dry and wet edges. Meanwhile, the GLEAM product of Martens et al. (2017); Miralles et al. (2011) also uses the PT as the base model for computing potential ET before using different modules, the stress module, soil water module and the interception module, to estimate actual ET. This 0.25° spatial resolution product estimates different components of ET (i.e. intercepted rainfall evaporation, soil evaporation and transpiration) for tall vegetation, short vegetation (including grasses) and bare soil, with the ET being an average of all the fractions of the four land cover types available in each grid cell. One of the greatest advantages of this product is the use of microwave sensors to estimate soil moisture and vegetation optical depth that are used to constrain PT estimated potential ET. The LSA SAF ET product uses the TESSEL SVAT scheme, which is based on the surface energy budget for ET model development. Like the GLEAM product, the LSA SAF ET is an average of all the tiles (land cover) within each pixel. The daily ET in this product is an aggregation of 30-minute ET estimates, and this results in ET underestimation, especially during times when there are data gaps, for instance when there are clouds. Although it is available in fine temporal resolutions of 30-minute and daily, the spatial resolution is very course at 3 km. The highlight of this section was the comparable performance of PM-Mu during periods of high ET, and vice-versa during periods of low ET. The parameterisation of aerodynamic and surface resistances is a challenge, including the upscaling stomatal to canopy resistance. In this version of Mu modified version of PM, VPD and minimum air temperature were used to constraint canopy resistance, with LAI used in upscaling stomatal to canopy resistance. While the GLEAM and LAS SAF ET products use soil moisture to constrain soil evaporation in their modelling, the PM-Mu method used relative humidity and VPD as a proxy for soil water availability in soil evaporation. This, among other factors, was seen as the main contribution to the poor performance of the model during dry periods. Several modifications have been made to this model to include soil moisture constraints in the estimation of ET in dry ecosystems, with results showing improved ET estimates (Di et al., 2015; Sun et al., 2013).

6.1.3 Uncertainty and sensitivity analysis of the PM-Mu model

Uncertainty and sensitivity analyses are critical steps of the modelling process, particularly in hydrological modelling. Although error and/or uncertainty are an integral component of the ET modelling process, this component is usually not investigated and reported on. Hence, Chapter 4 focused on identifying and

quantifying different sources of error and/or uncertainty in the PM-Mu ET model and how these impact the final modelled ET product. This study only focused on the core input variables uncertainty, i.e. measured meteorological input (air temperature and relative humidity) and remote sensing derived land surface parameter uncertainty, and their propagation through the intermediate parameters (land surface temperature, LAI, surface albedo, and emissivity) to the final ET uncertainty. Moreover, the sensitivity of the PM-Mu model to these input variables was also investigated.

The results showed that Tair and RH uncertainties followed a seasonal trend, being higher during the warm, dry season and lower during the hotter, wet season. However, this variation was more significant for Tair uncertainty, which could be explained by higher Type A uncertainty during this period, which is defined by high daytime temperatures and low nighttime temperature. Compared to air temperature, land surface temperature, LAI, surface albedo, and emissivity, relative humidity uncertainty contributed the highest to the final ET uncertainty in our study sites. Any errors associated with relative humidity could lead to high uncertainty in the final estimated ET. This variable is an input in the derivation of a number of intermediate parameters, like vapour pressure deficit, Fwet, aerodynamic and surface resistances, and hence any uncertainty in RH measurements would contribute significantly the final ET uncertainty. The overall evapotranspiration relative uncertainty reported in this research was 79%, after propagating all the input uncertainties.

On the other hand, the PM-Mu model was most sensitive to air and land surface temperatures, with surface emissivity and albedo also showing some slight significance to ET estimation. One main assumption made in this study was the non-correlation between the model input variables. Also, the study focused on model input variable uncertainty and sensitivity analysis and did not investigate the different algorithms used to compute the intermediate variables.

In some instances, some studies use the term uncertainty analysis to investigate the performance of the ET models against measured ET, and not to evaluate the impact of error associated with input variables on the modelled ET error. Whereas in other instances, uncertainty and sensitivity terms are used interchangeably. Hence, it is important to have a clear definition of these terms.

6.1.4 Using remote sensing techniques to monitor biomass production and water productivity

Freshwater resources are under immense pressure as competition between different users continues to increase. These include an ever growing population, which results in increased agricultural production, urbanization and

industrialization, and the need to maintain a safe ecological reserve. Global and climate change also add pressure to an already strained resource. Water-scarce regions have an even bigger challenge to produce more food with little water. Moreover, expanding croplands not being an option, hence, the onus is on improving agricultural water productivity.

In Chapter 5, therefore, we assessed water productivity, and its components, of different land use classes, under different climates in South Africa, using the WaPOR platform. Regions of high and low precipitation, including Dukuduku natural forests and surrounding commercial Eucalyptus and sugarcane plantations, and a communal area, Skukuza natural vegetation, Welgegund commercial farm (pasture), and Elandsberg Nature Reserve, were evaluated. Precipitation and ET products were validated using eddy covariance data from the Skukuza and Welgegund flux towers. Comparable results were recorded for the measured/ WaPOR ET correlation, with Skukuza (R^2 0.52, RMSE 1.06) performing better than Welgegund (R^2 0.39, RMSE 1.24). The WaPOR PM model underestimated ET during periods of high ET in Skukuza, while in Welgegund it gave a more perfect fit in low ET. Also, although the correlations were higher during high ET, the model showed some saturation. In an earlier study in Chapter 3, lower ET periods presented better correlations at the Skukuza site, although the PM-Mu model performed better during the high ET periods. However, although the temporal trends were similar, the measured/WaPOR precipitation correlations were very low at both sites.

The spatial variation of the different components was captured. Starting with precipitation, the Dukuduku forest area recorded the highest precipitation, compared to the north-eastern located Skukuza, central Welgegund farm, and the south-western Elandsberg Nature Reserve. It follows that ET followed the same pattern, together with the NPP and AGBP.

Mapping and monitoring water productivity is essential not only in the agriculture space, but in the overall water resources management. WP for different crops has been investigated across different climates, giving a range of values for each crop. For example, a difference between irrigated and rainfed WP has been reported. WP is reported in different terms, either as biomass (yield) or economic output per unit water consumed (ET) or applied.

Reported data on water productivity with respect to evapotranspiration (WPET) show considerable variation, e.g. wheat 0.6-1.9 kgm^{-3}, maize 1.2-2.3 kgm^{-3}, rice 0.5-1.1 kgm^{-3}, forage sorghum 7-8 kgm^{-3}, and potato tubers 6.2-11.6 kgm^{-3}, with incidental outliers obtained under experimental conditions. Data on field-level water productivity per unit of water applied (WPirrig), as reported in the literature, are lower than WPET and vary over an even wider range. For

example, grain WPirrig for rice varied from 0.05 to 0.6 kgm^{-3}, for sorghum from 0.05 to 0.3 kgm3 and for maize from 0.2 to 0.8 kgm^{-3}. The variability occurs because data were collected in different environments and under different crop management conditions. These affected the yield and the amount of water supplied (Kijne et al., forthcoming).

6.2 Final remarks and recommendations

This research work evaluated the performance of remote sensing derived ET estimates from different models, and the application of these estimates in monitoring water use and productivity in a semi-arid climate under different biomes. Before embarking on utilizing any ground based measured data, including eddy covariance data, to calibrate and/or validate climate and land surface models, it is crucial to understand the amount of error associated with these 'trusted data'.

This was illustrated first in Chapter 2, where we analysed the surface energy balance closure for the long-running Skukuza eddy covariance flux tower data, secondly where we investigated the effect of input variable uncertainty to modelled ET uncertainty and sensitivity. We could not use the Welgegund eddy covariance system data at this stage because they only became available at a later stage, hence their use in Chapters 4 and 5. Our results showed that the surface energy closure imbalance varies in time due to a number of factors, including instrument malfunction, and unstable weather conditions like clouds, rain, and strong winds. We, however, did not include the different storage terms (soil heat and canopy air) when evaluating the surface energy balance closure. To understand how these storage terms impact the energy balance in this ecosystem, further studies would be necessary. Including the quality of these ground data is a critical step in validation exercises, if not to understand the error associated with the ground data, but to apply correction techniques to improve the reliability of our baseline datasets.

Validation of remote sensing-based ET modelling techniques has been, and is still being, done under different climates, biomes, timescales and spatial scales. The results of these studies, including ours (Chapter 3), vary, and hence the main message is that there is no model that outperforms others in ET estimation across the climates and biomes. Also, these models are continually being modified to improve ET estimation, especially in semi-arid regions, including the introduction of soil moisture to constrain the models. With such advancement in the evaluation and application of available ET models, it is important to understand the accuracy of the inputs used in modelling ET and the confidence levels of these models based on the input variables used and the model

parameterisations. Further research could investigate how different parameterisations of the intermediate inputs affect the output.

Data with very high spatial and temporal resolutions from more advanced Earth observation technologies, for example, the unmanned aerial vehicles (UAV) and Cubesats, being introduced, gives the research fraternity the platform to explore new in-depth descriptions of the evaporative process at finer scales. However, McCabe et al. (2019) go on further to state that it is time to challenge the understanding of the evaporativeprocess beyond the already developed and tested models. Furthermore, with the advancement in remote sensing-based modelling of the Earth's surface, including ET, more research is geared towards application techniques. For example, there is a serious shift toward precision agriculture, to increase yield with fewer resources, including land, water, and nutrient use. Moreover, platforms like the WaPOR need to be available at finer scales to more areas, including South Africa, to assist in monitoring water use and productivity, with the aim to improve water use and productivity.

References

Albaugh, J. M., Dye, P. J., & King, J. S. (2013). Eucalyptus and water use in South Africa. *International Journal of Forestry Research, 2013*.

Allen, R., Irmak, A., Trezza, R., Hendrickx, J. M. H., Bastiaanssen, W., & Kjaersgaard, J. (2011). Satellite‐based ET estimation in agriculture using SEBAL and METRIC. *Hydrological Processes, 25*(26), 4011-4027.

Allen, R. G., Howell, T. A., Pruitt, W. O., Walter, I. A., & Jensen, M. E. (1991). Lysimeters for evapotranspiration and environmental measurements.

Allen, R. G., Tasumi, M., Morse, A., Trezza, R., Wright, J. L., Bastiaanssen, W., Kramber, W., Lorite, I., & Robison, C. W. (2007). Satellite-based energy balance for mapping evapotranspiration with internalized calibration (METRIC)—Applications. *Journal of Irrigation and Drainage Engineering, 133*(4), 395-406.

Ambas, V. T., & Baltas, E. (2012). SENSITIVITY ANALYSIS OF DIFFERENT EVAPOTRANSPIRATION METHODS USING A NEW SENSITIVITY COEFFICIENT. *GLOBAL NEST JOURNAL, 14*(3), 335-343.

Anderson, M., Norman, J., Diak, G., Kustas, W., & Mecikalski, J. (1997). A two-source time-integrated model for estimating surface fluxes using thermal infrared remote sensing.

Anderson, M. C., Norman, J. M., Mecikalski, J. R., Otkin, J. A., & Kustas, W. P. (2007). A climatological study of evapotranspiration and moisture stress across the continental United States based on thermal remote sensing: 1. Model formulation. *Journal of Geophysical Research: Atmospheres, 112*(D10).

Arain, M., Black, T., Barr, A. G., Griffis, T., Morgenstern, K., & Nesic, Z. (2003). Year‐round observations of the energy and water vapour fluxes above a boreal black spruce forest. *Hydrological Processes, 17*(18), 3581-3600.

Arboleda, A., Ghilain, N., & Gellens-Meulenberghs, F. (2005). *The LSA-SAF evapotranspiration product-first results with MSG.* Paper presented at the Proceedings of the 2005 EUMETSAT meteorological satellite data user's conference, Dubrovnik, Croatia, 19th-23th September.

Archibald, S., & Scholes, R. J. (2007). Leaf green‐up in a semi‐arid African savanna‐separating tree and grass responses to environmental cues. *Journal of Vegetation Science, 18*(4), 583-594.

Archibald, S. A., Kirton, A., Merwe, M. R., Scholes, R. J., Williams, C. A., & Hanan, N. (2009). Drivers of inter-annual variability in Net Ecosystem Exchange in a semi-arid savanna ecosystem, South Africa. *Biogeosciences, 6*(2), 251-266.

Asner, G. P., Archer, S., Hughes, R. F., Ansley, R. J., & Wessman, C. A. (2003). Net changes in regional woody vegetation cover and carbon storage in Texas drylands, 1937–1999. *Global Change Biology, 9*(3), 316-335.

Aubinet, M., Grelle, A., Ibrom, A., Rannik, Ü., Moncrieff, J., Foken, T., Kowalski, A. S., Martin, P. H., Berbigier, P., & Bernhofer, C. (1999). Estimates of the annual net carbon and water exchange of forests: the EUROFLUX methodology. *Advances in Ecological Research, 30*, 113-175.

Bagayoko, F., Yonkeu, S., Elbers, J., & van de Giesen, N. (2007). Energy partitioning over the West African savanna: Multi-year evaporation and surface conductance measurements in Eastern Burkina Faso. *Journal of Hydrology, 334*(3), 545-559.

Bai, Y., Zhang, J., Zhang, S., Koju, U. A., Yao, F., & Igbawua, T. (2017). Using precipitation, vertical root distribution, and satellite‐retrieved vegetation information to parameterize water stress in a Penman‐Monteith approach to evapotranspiration modeling under Mediterranean climate. *Journal of Advances in Modeling Earth Systems, 9*(1), 168-192.

Bailey, W., & Davies, J. (1981). Evaporation from soybeans. *Boundary-Layer Meteorology, 20*(4), 417-428.

Baldocchi, D. (2008). 'Breathing'of the terrestrial biosphere: lessons learned from a global network of carbon dioxide flux measurement systems. *Australian Journal of Botany, 56*(1), 1-26.

Baldocchi, D., Falge, E., Gu, L., Olson, R., Hollinger, D., Running, S., Anthoni, P., Bernhofer, C., Davis, K., & Evans, R. (2001). FLUXNET: A new tool to study the temporal and spatial variability of ecosystem-scale carbon dioxide, water vapor, and energy flux densities. *Bulletin of the American Meteorological Society, 82*(11), 2415-2434.

Baldocchi, D. D. (2003). Assessing the eddy covariance technique for evaluating carbon dioxide exchange rates of ecosystems: past, present and future. *Global Change Biology, 9*(4), 479-492.

Barr, A. G., van der Kamp, G., Black, T. A., McCaughey, J. H., & Nesic, Z. (2012). Energy balance closure at the BERMS flux towers in relation to the water balance of the White Gull Creek watershed 1999–2009. *Land-Atmosphere Interactions: Advances in Measurement, Analysis, and Modeling – A Tribute to T. Andrew Black, 153*(0), 3-13. doi: http://dx.doi.org/10.1016/j.agrformet.2011.05.017.

Bastiaanssen, W., Cheema, M., Immerzeel, W., Miltenburg, I., & Pelgrum, H. (2012). Surface energy balance and actual evapotranspiration of the transboundary Indus Basin estimated from satellite measurements and the ETLook model. *Water Resources Research, 48*(11).

Bastiaanssen, W. G. M., Menenti, M., Feddes, R. A., & Holtslag, A. A. M. (1998a). A remote sensing surface energy balance algorithm for land (SEBAL). 1. Formulation. *Journal of Hydrology, 212*, 198-212.

Bastiaanssen, W. G. M., Noordman, E. J. M., Pelgrum, H., Davids, G., Thoreson, B. P., & Allen, R. G. (2005). SEBAL model with remotely sensed data to improve water-resources management under actual field conditions. *Journal of Irrigation and Drainage Engineering, 131*(1), 85-93.

Bastiaanssen, W. G. M., Pelgrum, H., Wang, J., Ma, Y., Moreno, J. F., Roerink, G. J., & Van der Wal, T. (1998b). A remote sensing surface energy balance algorithm for land (SEBAL).: Part 2: Validation. *Journal of Hydrology, 212*, 213-229.

Biradar, C. M., Thenkabail, P. S., Platonov, A., Xiao, X., Geerken, R., Noojipady, P., Turral, H., & Vithanage, J. (2008). Water productivity mapping methods using remote sensing. *Journal of Applied Remote Sensing, 2*(1), 023544.

Blanken, P. D., Black, T. A., Yang, P. C., Neumann, H. H., Nesic, Z., Staebler, R., Den Hartog, G., Novak, M. D., & Lee, X. (1997). Energy balance and canopy conductance of a boreal aspen forest: partitioning overstory and understory components. *Journal of Geophysical Research: Atmospheres (1984–2012), 102*(D24), 28915-28927.

Blonquist, J., Tanner, B., & Bugbee, B. (2009). Evaluation of measurement accuracy and comparison of two new and three traditional net radiometers. *Agricultural and Forest Meteorology, 149*(10), 1709-1721.

Bouchet, R. J. (1963). Evapotranspiration réelle et potentielle, signification climatique. *IAHS Publ, 62*, 134-142.

Bouman, B. (2007). A conceptual framework for the improvement of crop water productivity at different spatial scales. *Agricultural systems, 93*(1-3), 43-60.

Bowen, I. S. (1926). The ratio of heat losses by conduction and by evaporation from any water surface. *Physical Review, 27*(6), 779.

Brugnach, M., Pahl-Wostl, C., Lindenschmidt, K., Janssen, J., Filatova, T., Mouton, A., Holtz, G., Van der Keur, P., & Gaber, N. (2008). Chapter four complexity and uncertainty: rethinking the modelling activity. *Developments in Integrated Environmental Assessment, 3*, 49-68.

Brutsaert, W. (2009). *Hydrology: an introduction* (Vol. 4th). New York: Cambridge University Press.

Burba, G., & Anderson, D. (2010). A brief practical guide to eddy covariance flux measurements: principles and workflow examples for scientific and industrial applications: Li-Cor Biosciences.

Cai, X., Molden, D., Mainuddin, M., Sharma, B., Ahmad, M.-u.-D., & Karimi, P. (2011). Producing more food with less water in a changing world:

assessment of water productivity in 10 major river basins. *Water international, 36*(1), 42-62.

Cai, X., & Sharma, B. R. (2010). Integrating remote sensing, census and weather data for an assessment of rice yield, water consumption and water productivity in the Indo-Gangetic river basin. *Agricultural Water Management, 97*(2), 309-316.

Cai, X., Thenkabail, P. S., Biradar, C. M., Platonov, A., Gumma, M., Dheeravath, V., Cohen, Y., Goldshleger, N., Ben-Dor, E., & Alchanatis, V. (2009). Water productivity mapping using remote sensing data of various resolutions to support. *Journal of Applied Remote Sensing, 3*(1), 033557.

Cammalleri, C., Anderson, M., Gao, F., Hain, C., & Kustas, W. (2014). Mapping daily evapotranspiration at field scales over rainfed and irrigated agricultural areas using remote sensing data fusion. *Agricultural and Forest Meteorology, 186*, 1-11.

Cap-Net. (2014). *Tutorial on basic principles on Integrated Water Resources Management.* Retrieved from http://www.cap-net.org/documents/2014/06/iwrmt-tutorial-on-basic-principles-of-iwrm.pdf.

Carlson, T. (2007). An overview of the" triangle method" for estimating surface evapotranspiration and soil moisture from satellite imagery. *Sensors, 7*(8), 1612-1629.

Chang, Y., Qin, D., Ding, Y., Zhao, Q., & Zhang, S. (2018). A modified MOD16 algorithm to estimate evapotranspiration over alpine meadow on the Tibetan Plateau, China. *Journal of Hydrology, 561*, 16-30. doi: https://doi.org/10.1016/j.jhydrol.2018.03.054

Chen, L.-H., Chen, J., & Chen, C. (2018). Effect of Environmental Measurement Uncertainty on Prediction of Evapotranspiration. *Atmosphere, 9*(10), 400.

Chen, S., Chen, J., Lin, G., Zhang, W., Miao, H., Wei, L., Huang, J., & Han, X. (2009). Energy balance and partition in Inner Mongolia steppe ecosystems with different land use types. *Agricultural and Forest Meteorology, 149*(11), 1800-1809.

Chirouze, J., Boulet, G., Jarlan, L., Fieuzal, R., Rodriguez, J., Ezzahar, J., Raki, S. E., Bigeard, G., Merlin, O., & Garatuza-Payan, J. (2014). Intercomparison of four remote-sensing-based energy balance methods to retrieve surface evapotranspiration and water stress of irrigated fields in semi-arid climate. *Hydrology and Earth System Sciences Discussions*(18), 1165-1188.

Cleugh, H. A., Leuning, R., Mu, Q., & Running, S. W. (2007). Regional evaporation estimates from flux tower and MODIS satellite data. *Remote Sensing of Environment, 106*(3), 285-304.

Colaizzi, P. D., Agam, N., Tolk, J. A., Evett, S. R., Howell, T. A., Gowda, P. H., O'Shaughnessy, S. A., Kustas, W. P., & Anderson, M. C. (2014). Two source energy balance model to calculate E, T, and ET: Comparison of Priestley-Taylor and Penman-Monteith formulations and two time scaling methods. *Trans. Asabe, 57*(2), 479-498.

Colgan, M. S., Asner, G. P., & Swemmer, T. (2013). Harvesting tree biomass at the stand level to assess the accuracy of field and airborne biomass estimation in savannas. *Ecological Applications, 23*(5), 1170-1184.

Cook, S., Gichuki, F., & Turral, H. (2006). *Agricultural water productivity: issues, concepts and approaches*. Retrieved from

Dalton, J. (1802). *Experiments and observations to determine whether the quantity of rain and dew is equal to the quantity of water carried off by the rivers and raised by evaporation: With an enquiry into the origin of springs*: R. & W. Dean.

De Fraiture, C., & Wichelns, D. (2010). Satisfying future water demands for agriculture. *Agricultural Water Management, 97*(4), 502-511.

DeJonge, K. C., Ahmadi, M., Ascough Ii, J. C., & Kinzli, K.-D. (2015). Sensitivity analysis of reference evapotranspiration to sensor accuracy. *Computers and Electronics in Agriculture, 110*, 176-186. doi:http://dx.doi.org/10.1016/j.compag.2014.11.013

den Besten, N., Simons, G., & Hunink, J. (2017). Water Productivity assessment using Flying Sensors and Crop Modelling. Pilot study for Maize in Mozambique.

Dhungel, R., Allen, R. G., Trezza, R., & Robison, C. W. (2014). Comparison of latent heat flux using aerodynamic methods and using the Penman–Monteith method with satellite-based surface energy balance. *Remote Sensing, 6*(9), 8844-8877.

Dhungel, R., Allen, R. G., Trezza, R., & Robison, C. W. (2016). Evapotranspiration between satellite overpasses: methodology and case study in agricultural dominant semi‐arid areas. *Meteorological Applications, 23*(4), 714-730.

Di, S.-C., Li, Z.-L., Tang, R., Wu, H., Tang, B.-H., & Lu, J. (2015). Integrating two layers of soil moisture parameters into the MOD16 algorithm to improve evapotranspiration estimations. *International Journal of Remote Sensing*(ahead-of-print), 1-19.

Didan, K., Munoz, A. B., Solano, R., & Huete, A. (2015). MODIS vegetation index user's guide (MOD13 series). *University of Arizona: Vegetation Index and Phenology Lab*.

Dubois, O. (2011). *The state of the world's land and water resources for food and agriculture: managing systems at risk*: Earthscan.

Dutra, E., Balsamo, G., Viterbo, P., Miranda, P. M. A., Beljaars, A., Schär, C., & Elder, K. (2010). An improved snow scheme for the ECMWF land surface model: description and offline validation. *Journal of Hydrometeorology, 11*(4), 899-916.

Dzikiti, S., Jovanovic, N. Z., Bugan, R. D., Ramoelo, A., Majozi, N. P., Nickless, A., Cho, M. A., Le Maitre, D. C., Ntshidi, Z., & Pienaar, H. H. (2019). Comparison of two remote sensing models for estimating evapotranspiration: algorithm evaluation and application in seasonally arid ecosystems in South Africa. *Journal of Arid Land, 11*(4), 495-512.

Ershadi, A., McCabe, M., Evans, J., & Wood, E. (2015). Impact of model structure and parameterization on Penman–Monteith type evaporation models. *Journal of Hydrology, 525*, 521-535.

Ershadi, A., McCabe, M. F., Evans, J. P., Chaney, N. W., & Wood, E. F. (2014). Multi-site evaluation of terrestrial evaporation models using FLUXNET data. *Agricultural and Forest Meteorology, 187*, 46-61.

Estévez, J., Gavilán, P., & Berengena, J. (2009). Sensitivity analysis of a Penman–Monteith type equation to estimate reference evapotranspiration in southern Spain. *Hydrological Processes, 23*(23), 3342-3353.

Eugster, W., & Senn, W. (1995). A cospectral correction model for measurement of turbulent NO2 flux. *Boundary-Layer Meteorology, 74*(4), 321-340.

Falge, E., Reth, S., Brüggemann, N., Butterbach-Bahl, K., Goldberg, V., Oltchev, A., Schaaf, S., Spindler, G., Stiller, B., & Queck, R. (2005). Comparison of surface energy exchange models with eddy flux data in forest and grassland ecosystems of Germany. *Ecological Modelling, 188*(2), 174-216.

Fang, H., Wei, S., Jiang, C., & Scipal, K. (2012). Theoretical uncertainty analysis of global MODIS, CYCLOPES, and GLOBCARBON LAI products using a triple collocation method. *Remote Sensing of Environment, 124*, 610-621. doi: https://doi.org/10.1016/j.rse.2012.06.013

FAO. (2018). *WaPOR Database Methodology: Level 1. Remote Sensing for Water Productivity Technical Report: Methodology Series.* . Retrieved from FAO Rome: doi:https://wapor.apps.fao.org/home/WAPOR_2/1

Ferguson, C. R., Sheffield, J., Wood, E. F., & Gao, H. (2010). Quantifying uncertainty in a remote sensing-based estimate of evapotranspiration over continental USA. *International Journal of Remote Sensing, 31*(14), 3821-3865.

Finnigan, J. J., Clement, R., Malhi, Y., Leuning, R., & Cleugh, H. (2003). A re-evaluation of long-term flux measurement techniques part I: averaging and coordinate rotation. *Boundary-Layer Meteorology, 107*(1), 1-48

Fisher, J. B., Lee, J. H., Hulley, G., Hughes, C., Mallick, K., & Hook, S. (2013, 8 September 2013). *Uncertainty in evapotranspiration from uncertainty in*

land surface temperature. Paper presented at the 27th Conference on Hydrology.

Fisher, J. B., Tu, K. P., & Baldocchi, D. D. (2008). Global estimates of the land–atmosphere water flux based on monthly AVHRR and ISLSCP-II data, validated at 16 FLUXNET sites. *Remote Sensing of Environment, 112*(3), 901-919.

Foken, T., Mauder, M., Liebethal, C., Wimmer, F., Beyrich, F., Leps, J.-P., Raasch, S., DeBruin, H. A. R., Meijninger, W. M. L., & Bange, J. (2010). Energy balance closure for the LITFASS-2003 experiment. *Theoretical and Applied Climatology, 101*(1-2), 149-160.

Franssen, H. J., Stöckli, R., Lehner, I., Rotenberg, E., & Seneviratne, S. I. (2010). Energy balance closure of eddy-covariance data: A multisite analysis for European FLUXNET stations. *Agricultural and Forest Meteorology, 150*(12), 1553-1567.

Frey, C. H., & Patil, S. R. (2002). Identification and review of sensitivity analysis methods. *Risk analysis, 22*(3), 553-578.

Garcia, M., Raes, D., Allen, R., & Herbas, C. (2004). Dynamics of reference evapotranspiration in the Bolivian highlands (Altiplano). *Agricultural and Forest Meteorology, 125*(1), 67-82. doi: https://doi.org/10.1016/j.agrformet.2004.03.005

Gash, J., & Dolman, A. (2003). Sonic anemometer (co) sine response and flux measurement: I. The potential for (co) sine error to affect sonic anemometer-based flux measurements. *Agricultural and Forest Meteorology, 119*(3-4), 195-207.

GCOS. (2009). Implementation plan for the global observing system for climate in support of the UNFCCC (2010 Update).

Gebler, S., Hendricks Franssen, H.-J., Pütz, T., Post, H., Schmidt, M., & Vereecken, H. (2015). Actual evapotranspiration and precipitation measured by lysimeters: a comparison with eddy covariance and tipping bucket. *Hydrology and Earth System Sciences, 19*(5), 2145-2161.

GEO. (2010). *GEO Task US-09-01a: Critical Earth Observations Priorities for Water Societal Benefit Area (SBA). Final SBA Report*. Retrieved from https://sbageotask.larc.nasa.gov/water.html

Ghilain, N., Arboleda, A., & Gellens-Meulenberghs, F. (2011). Evapotranspiration modelling at large scale using near-real time MSG SEVIRI derived data. *Hydrology and Earth System Sciences, 15*, 771-786.

Ghilain, N., Arboleda, A., Sepulcre-Canto, G., Batelaan, O., Ardo, J., & Gellens-Meulenberghs, F. (2012). Improving evapotranspiration in a land surface model using biophysical variables derived from MSG/SEVIRI satellite.

Ghilain, N., De Roo, F., & Gellens-Meulenberghs, F. (2014). Evapotranspiration monitoring with Meteosat Second Generation satellites: improvement opportunities from moderate spatial resolution satellites for vegetation. *International Journal of Remote Sensing, 35*(7), 2654-2670.

Gibson, L. A., Jarmain, C., Su, Z., & Eckardt, F. E. (2013). Review: Estimating evapotranspiration using remote sensing and the Surface Energy Balance System–A South African perspective. *Water SA, 39*(4), 477-484.

Glenn, E. P., Huete, A. R., Nagler, P. L., Hirschboeck, K. K., & Brown, P. (2007). Integrating remote sensing and ground methods to estimate evapotranspiration. *Critical Reviews in Plant Sciences, 26*(3), 139-168.

Glenn, E. P., Nagler, P. L., & Huete, A. R. (2010). Vegetation index methods for estimating evapotranspiration by remote sensing. *Surveys in Geophysics, 31*(6), 531-555.

Godfray, H. C. J., & Garnett, T. (2014). Food security and sustainable intensification. *Philosophical transactions of the Royal Society B: biological sciences, 369*(1639), 20120273.

Gong, L., Xu, C.-y., Chen, D., Halldin, S., & Chen, Y. D. (2006). Sensitivity of the Penman–Monteith reference evapotranspiration to key climatic variables in the Changjiang (Yangtze River) basin. *Journal of Hydrology, 329*(3), 620-629.

Goulden, M. L., Munger, J. W., Fan, S. M., Daube, B. C., & Wofsy, S. C. (1996). Measurements of carbon sequestration by long‐term eddy covariance: Methods and a critical evaluation of accuracy. *Global Change Biology, 2*(3), 169-182.

Goward, S. N., Cruickshanks, G. D., & Hope, A. S. (1985). Observed relation between thermal emission and reflected spectral radiance of a complex vegetated landscape. *Remote Sensing of Environment, 18*(2), 137-146.

Goyal, R. (2004). Sensitivity of evapotranspiration to global warming: a case study of arid zone of Rajasthan (India). *Agricultural Water Management, 69*(1), 1-11.

Gu, L., Meyers, T., Pallardy, S. G., Hanson, P. J., Yang, B., Heuer, M., Hosman, K. P., Riggs, J. S., Sluss, D., & Wullschleger, S. D. (2006). Direct and indirect effects of atmospheric conditions and soil moisture on surface energy partitioning revealed by a prolonged drought at a temperate forest site. *Journal of Geophysical Research: Atmospheres (1984–2012), 111*(D16).

Guo, D., Westra, S., & Maier, H. (2017a). Sensitivity of potential evapotranspiration to changes in climate variables for different Australian climatic zones.

Guo, D., Westra, S., & Maier, H. R. (2017b). Sensitivity of potential evapotranspiration to changes in climate variables for different

Australian climatic zones. *Hydrology and Earth System Sciences, 21*(4), 2107-2126.

Ha, W., Kolb, T. E., Springer, A. E., Dore, S., O'Donnell, F. C., Martinez Morales, R., Masek Lopez, S., & Koch, G. W. (2015). Evapotranspiration comparisons between eddy covariance measurements and meteorological and remote‐sensing‐based models in disturbed ponderosa pine forests. *Ecohydrology, 8*(7), 1335-1350.

Hamby, D. M. (1994). A review of techniques for parameter sensitivity analysis of environmental models. *Environmental monitoring and assessment, 32*(2), 135-154.

Hamby, D. M. (1995). A comparison of sensitivity analysis techniques. *Health physics, 68*(2), 195-204.

Hammerle, A., Haslwanter, A., Tappeiner, U., Cernusca, A., & Wohlfahrt, G. (2008). Leaf area controls on energy partitioning of a temperate mountain grassland. *Biogeosciences, 5*(2), 421-431. doi:10.5194/bg-5-421-2008

Hargreaves, G. H., & Samani, Z. A. (1982). Estimating potential evapotranspiration. *Journal of the Irrigation and Drainage Division, 108*(3), 225-230.

Hemakumara, H. M., Chandrapala, L., & Moene, A. F. (2003). Evapotranspiration fluxes over mixed vegetation areas measured from large aperture scintillometer. *Agricultural Water Management, 58*(2), 109-122. doi: https://doi.org/10.1016/S0378-3774(02)00131-2

Hillel, D. (1982). *Introduction to soil physics* (Vol. 364): Academic press New York.

Hofreiter, M., & Jirka, V. Uncertainty Analysis of Evapotranspiration Estimates in Ecosystems. *Asian Review of Mechnical Engineering, 1*, 46.

Honaker, J., King, G., & Blackwell, M. (2011). Amelia II: A program for missing data. *Journal of statistical software, 45*(7), 1-47.

House, J. I., Colin Prentice, I., & Le Quere, C. (2002). Maximum impacts of future reforestation or deforestation on atmospheric CO2. *Global Change Biology, 8*(11), 1047-1052.

Hsiao, T. C., Steduto, P., & Fereres, E. (2007). A systematic and quantitative approach to improve water use efficiency in agriculture. *Irrigation Science, 25*(3), 209-231.

Hu, G., Jia, L., & Menenti, M. (2015). Comparison of MOD16 and LSA-SAF MSG evapotranspiration products over Europe for 2011. *Remote Sensing of Environment, 156*, 510-526.

Hulley, G., Malakar, N., Hughes, T., Islam, T., & Hook, S. (2016). Moderate resolution imaging spectroradiometer (MODIS) MOD21 land surface temperature and emissivity algorithm theoretical basis document.

Hulley, G. C., Hughes, C. G., & Hook, S. J. (2012). Quantifying uncertainties in land surface temperature and emissivity retrievals from ASTER and MODIS thermal infrared data. *Journal of Geophysical Research: Atmospheres, 117*(D23).

Irmak, S., & Mutiibwa, D. (2009). On the dynamics of stomatal resistance: Relationships between stomatal behavior and micrometeorological variables and performance of Jarvis-type parameterization. *Transactions of the ASABE, 52*(6), 1923-1939.

Jarmain, C., Everson, C. S., Savage, M. J., Mengistu, M. G., Clulow, A. D., Walker, S., & Gush, M. B. (2009a). *Refining tools for evaporation monitoring in support of water resources management*: Water Research Commission Pretoria.

Jarmain, C., Mengitsu, M., Jewitt, G. P. W., Kongo, V., & Bastiaanssen, W. (2009b). A methodology for near-real time spatial estimation of evaporation. *Water Research Commission, Report*(1751-1), 09.

Javadian, M., Behrangi, A., Gholizadeh, M., & Tajrishy, M. (2019). METRIC and WaPOR Estimates of Evapotranspiration over the Lake Urmia Basin: Comparative Analysis and Composite Assessment. *Water, 11*(8), 1647.

Jewitt, G. (2006). Integrating blue and green water flows for water resources management and planning. *Physics and Chemistry of the Earth, Parts A/B/C, 31*(15), 753-762.

Jia, X., Zha, T. S., Wu, B., Zhang, Y. Q., Gong, J. N., Qin, S. G., Chen, G. P., Qian, D., Kellomäki, S., & Peltola, H. (2014). Biophysical controls on net ecosystem CO₂ exchange over a semiarid shrubland in northwest China. *Biogeosciences, 11*(17), 4679-4693. doi:10.5194/bg-11-4679-2014

Jiang, L., & Islam, S. (1999). A methodology for estimation of surface evapotranspiration over large areas using remote sensing observations. *Geophysical Research Letters, 26*(17), 2773-2776.

Jiang, L., & Islam, S. (2001). Estimation of surface evaporation map over southern Great Plains using remote sensing data. *Water Resources Research, 37*(2), 329-340.

Jiang, L., & Islam, S. (2003). An intercomparison of regional latent heat flux estimation using remote sensing data. *International Journal of Remote Sensing, 24*(11), 2221-2236.

Jin, Y., Schaaf, C. B., Woodcock, C. E., Gao, F., Li, X., Strahler, A. H., Lucht, W., & Liang, S. (2003). Consistency of MODIS surface bidirectional reflectance distribution function and albedo retrievals: 2. Validation. *Journal of Geophysical Research: Atmospheres, 108*(D5).

Jovanovic, N., Dzikiti, S., Le Maitre, D., Roberts, W., Ramoelo, A., & Majozi, N. P. (2013). *Monitoring of water availability using geo-spatial data and earth observations – Technical report*. Retrieved from Pretoria:

Jovanovic, N., Garcia, C. L., Bugan, R. D. H., Teich, I., & Rodriguez, C. M. G. (2014). Validation of remotely-sensed evapotranspiration and NDWI using ground measurements at Riverlands, South Africa. *Water SA, 40*(2), 211-220.

Kalma, J. D., McVicar, T. R., & McCabe, M. F. (2008). Estimating land surface evaporation: A review of methods using remotely sensed surface temperature data. *Surveys in Geophysics, 29*(4-5), 421-469.

Khan, M. S., Liaqat, U. W., Baik, J., & Choi, M. (2018). Stand-alone uncertainty characterization of GLEAM, GLDAS and MOD16 evapotranspiration products using an extended triple collocation approach. *Agricultural and Forest Meteorology, 252*, 256-268. doi:https://doi.org/10.1016/j.agrformet.2018.01.022

Kijne, J. W., Barker, R., & Molden, D. J. (2003). *Water productivity in agriculture: limits and opportunities for improvement* (Vol. 1): Cabi.

Klaasse, A., Bastiaanssen, W., Bosch, J., Jarmain, C., & De Wit, M. (2008). Water use efficiency of table and wine grapes in Western Cape, South Africa: The spatial and temporal variation of water use efficiency in grape cultivation using remote sensing technology. *Report to the Department of Agriculture, Western Cape, South Africa*.

Klaasse, A., & Jarmain, C. (2011). GrapeLook: Improving Agricultural Water Management using Satellite Earth Observation. *Agriculture, Articles, Earth Observation, Water Availability*.

Kljun, N., Calanca, P., Rotach, M. W., & Schmid, H. P. (2004). A Simple Parameterisation for Flux Footprint Predictions. *Boundary-Layer Meteorology, 112*(3), 503-523. doi:10.1023/b:boun.0000030653.71031.96

Knyazikhin, Y., Glassy, J., Privette, J., Tian, Y., Lotsch, A., Zhang, Y., Wang, Y., Morisette, J., Votava, P., & Myneni, R. (1999). MODIS leaf area index (LAI) and fraction of photosynthetically active radiation absorbed by vegetation (FPAR) product (MOD15) algorithm theoretical basis document. *Theoretical Basis Document, NASA Goddard Space Flight Center, Greenbelt, MD, 20771*.

Kolle, O., & Rebmann, C. (2007). EddySoft: Dokumentation of a Software Package to Acquire and Process Eddy Covariance Data.

Kormann, R., & Meixner, F. X. (2001). An analytical footprint model for non-neutral stratification. *Boundary-Layer Meteorology, 99*(2), 207-224.

Kruger, A., Makamo, L., & Shongwe, S. (2002). An analysis of Skukuza climate data. *Koedoe, 45*(1), 87-92.

Kucherenko, S., & Iooss, B. (2017). Derivative-based global sensitivity measures. *Handbook of uncertainty quantification*, 1241-1263.

Kurc, S. A., & Small, E. E. (2004). Dynamics of evapotranspiration in semiarid grassland and shrubland ecosystems during the summer monsoon season, central New Mexico. *Water Resources Research, 40*(9).

Kutsch, W., Hanan, N., Scholes, R., McHugh, I., Kubheka, W., Eckhardt, H., & Williams, C. (2008). Response of carbon fluxes to water relations in a savanna ecosystem in South Africa. *Biogeosciences Discussions, 5*(3), 2197-2235.

Langensiepen, M., Fuchs, M., Bergamaschi, H., Moreshet, S., Cohen, Y., Wolff, P., Jutzi, S. C., Cohen, S., Rosa, L. M. G., Li, Y., & Fricke, T. (2009). Quantifying the uncertainties of transpiration calculations with the Penman–Monteith equation under different climate and optimum water supply conditions. *Agricultural and Forest Meteorology, 149*(6), 1063-1072. doi:https://doi.org/10.1016/j.agrformet.2009.01.001

Law, B., Falge, E., Gu, L. v., Baldocchi, D., Bakwin, P., Berbigier, P., Davis, K., Dolman, A., Falk, M., & Fuentes, J. (2002). Environmental controls over carbon dioxide and water vapor exchange of terrestrial vegetation. *Agricultural and Forest Meteorology, 113*(1-4), 97-120.

Lee, X., & Hu, X. (2002). Forest-air fluxes of carbon, water and energy over non-flat terrain. *Boundary-Layer Meteorology, 103*(2), 277-301.

Leuning, R., Denmead, O., Lang, A., & Ohtaki, E. (1982). Effects of heat and water vapor transport on eddy covariance measurement of CO 2 fluxes. *Boundary-Layer Meteorology, 23*(2), 209-222.

Leuning, R., Zhang, Y., Rajaud, A., Cleugh, H., & Tu, K. (2008). A simple surface conductance model to estimate regional evaporation using MODIS leaf area index and the Penman ‐ Monteith equation. *Water Resources Research, 44*(10).

Li, S.-G., Eugster, W., Asanuma, J., Kotani, A., Davaa, G., Oyunbaatar, D., & Sugita, M. (2006). Energy partitioning and its biophysical controls above a grazing steppe in central Mongolia. *Agricultural and Forest Meteorology, 137*(1), 89-106.

Li, Y., Liu, S., Wang, S., Miao, Y., & Chen, B. (2014). Comparative study on methods for computing soil heat storage and energy balance in arid and semi-arid areas. *Journal of Meteorological Research, 28*, 308-322.

Li, Z. L., Tang, R., Wan, Z., Bi, Y., Zhou, C., Tang, B., Yan, G., & Zhang, X. (2009). A review of current methodologies for regional evapotranspiration estimation from remotely sensed data. *Sensors, 9*(5), 3801-3853.

Lilburne, L., & Tarantola, S. (2009). Sensitivity analysis of spatial models. *International Journal of Geographical Information Science, 23*(2), 151-168.

Lin, X., & Hubbard, K. (2004). Uncertainties of derived dewpoint temperature and relative humidity. *Journal of Applied Meteorology, 43*(5), 821-825.

Liou, Y.-A., & Kar, S. (2014). Evapotranspiration estimation with remote sensing and various surface energy balance algorithms—A review. *Energies, 7*(5), 2821-2849.

Liu, S. M., Xu, Z. W., Wang, W. Z., Jia, Z. Z., Zhu, M. J., Bai, J., & Wang, J. M. (2011). A comparison of eddy-covariance and large aperture scintillometer measurements with respect to the energy balance closure problem. *Hydrology and Earth System Sciences, 15*(4), 1291-1306.

Liu, S. M., Xu, Z. W., Zhu, Z. L., Jia, Z. Z., & Zhu, M. J. (2013a). Measurements of evapotranspiration from eddy-covariance systems and large aperture scintillometers in the Hai River Basin, China. *Journal of Hydrology, 487*, 24-38. doi:https://doi.org/10.1016/j.jhydrol.2013.02.025

Liu, Y. Y., van Dijk, A. I. J. M., McCabe, M. F., Evans, J. P., & de Jeu, R. A. M. (2013b). Global vegetation biomass change (1988-2008) and attribution to environmental and human drivers. *Global Ecology and Biogeography, 22*(6), 692-705. doi:10.1111/geb.12024

Long, D., & Singh, V. P. (2010). Integration of the GG model with SEBAL to produce time series of evapotranspiration of high spatial resolution at watershed scales. *Journal of Geophysical Research: Atmospheres, 115*(D21).

López-Urrea, R., Martín de Santa Olalla, F., Fabeiro, C., & Moratalla, A. (2006). Testing evapotranspiration equations using lysimeter observations in a semiarid climate. *Agricultural Water Management, 85*(1), 15-26. doi:https://doi.org/10.1016/j.agwat.2006.03.014

Ma, W., Ma, Y., & Ishikawa, H. (2014). Evaluation of the SEBS for upscaling the evapotranspiration based on in-situ observations over the Tibetan Plateau. *Atmospheric Research, 138*, 91-97.

Ma, Y., Wang, Y., Wu, R., Hu, Z., Yang, K., Li, M., Ma, W., Zhong, L., Sun, F., & Chen, X. (2009). Recent advances on the study of atmosphere-land interaction observations on the Tibetan Plateau. *Hydrology and Earth System Sciences, 13*(7), 1103-1111.

Maidment, R. I., Grimes, D., Allan, R. P., Tarnavsky, E., Stringer, M., Hewison, T., Roebeling, R., & Black, E. (2014). The 30 year TAMSAT African rainfall climatology and time series (TARCAT) data set. *Journal of Geophysical Research: Atmospheres, 119*(18), 10,619-610,644.

Maila, D., Crawford, J., Mathebula, V., Naidoo, N., & Visser, W. (2018). *National water accounts for South Africa systems, methods and initial results*.

Mallick, K., Jarvis, A., Fisher, J. B., Tu, K. P., Boegh, E., & Niyogi, D. (2012). Latent Heat Flux and Canopy Conductance Based on Penman–Monteith, Priestley–Taylor Equation, and Bouchet's Complementary

Hypothesis. *Journal of Hydrometeorology, 14*(2), 419-442. doi:10.1175/JHM-D-12-0117.1

Marshall, M., Tu, K., Funk, C., Michaelsen, J., Williams, P., Williams, C., Ardo, J., Boucher, M., Cappelaere, B., & De Grandcourt, A. (2013). Improving operational land surface model canopy evapotranspiration in Africa using a direct remote sensing approach.

Martens, B., Gonzalez Miralles, D., Lievens, H., Van Der Schalie, R., De Jeu, R. A., Fernández-Prieto, D., Beck, H. E., Dorigo, W., & Verhoest, N. (2017). GLEAM v3: Satellite-based land evaporation and root-zone soil moisture. *Geoscientific Model Development, 10*(5), 1903-1925.

Mathieu, R., Naidoo, L., Cho, M. A., Leblon, B., Main, R., Wessels, K., Asner, G. P., Buckley, J., Van Aardt, J., & Erasmus, B. F. (2013). Toward structural assessment of semi-arid African savannahs and woodlands: The potential of multitemporal polarimetric RADARSAT-2 fine beam images. *Remote Sensing of Environment, 138*, 215-231.

Mauder, M., Jegede, O. O., Okogbue, E. C., Wimmer, F., & Foken, T. (2007). Surface energy balance measurements at a tropical site in West Africa during the transition from dry to wet season. *Theoretical and Applied Climatology, 89*(3-4), 171-183.

McCabe, M. F., Ershadi, A., Jimenez, C., Miralles, D. G., Michel, D., & Wood, E. F. (2015). The GEWEX LandFlux project: evaluation of model evaporation using tower-based and globally-gridded forcing data. *Geoscientific Model Development Discussions, 8*(8), 6809-6866.

McCabe, M. F., Miralles, D. G., Holmes, T. R., & Fisher, J. B. (2019). Advances in the Remote Sensing of Terrestrial Evaporation: Multidisciplinary Digital Publishing Institute.

McCabe, M. F., & Wood, E. F. (2006). Scale influences on the remote estimation of evapotranspiration using multiple satellite sensors. *Remote Sensing of Environment, 105*(4), 271-285.

Meijninger, W., Beyrich, F., Lüdi, A., Kohsiek, W., & Bruin, H. D. (2006). Scintillometer-based turbulent fluxes of sensible and latent heat over a heterogeneous land surface–a contribution to LITFASS-2003. *Boundary-Layer Meteorology, 121*(1), 89-110.

Michel, D., Jiménez, C., Miralles, D. G., Jung, M., Hirschi, M., Ershadi, A., Martens, B., McCabe, M. F., Fisher, J. B., & Mu, Q. (2015). The WACMOS-ET project–Part 1: Tower-scale evaluation of four remote sensing-based evapotranspiration algorithms.

Mira, M., Olioso, A., Gallego-Elvira, B., Courault, D., Garrigues, S., Marloie, O., Hagolle, O., Guillevic, P., & Boulet, G. (2016). Uncertainty assessment of surface net radiation derived from Landsat images. *Remote Sensing of*

Environment, 175, 251-270. doi:http://dx.doi.org/10.1016/j.rse.2015.12.054

Miralles, D. G., De Jeu, R. A. M., Gash, J. H., Holmes, T. R. H., & Dolman, A. J. (2011). An application of GLEAM to estimating global evaporation. *Hydrology and Earth System Sciences Discussions, 8*(1), 1-27.

Miralles, D. G., Jiménez, C., Jung, M., Michel, D., Ershadi, A., McCabe, M. F., Hirschi, M., Martens, B., Dolman, A. J., Fisher, J. B., Mu, Q., Seneviratne, S. I., Wood, E. F., & Fernández-Prieto, D. (2016). The WACMOS-ET project – Part 2: Evaluation of global terrestrial evaporation data sets. *Hydrol. Earth Syst. Sci., 20*(2), 823-842. doi:10.5194/hess-20-823-2016

Molden, D., Oweis, T., Steduto, P., Bindraban, P., Hanjra, M. A., & Kijne, J. (2010). Improving agricultural water productivity: Between optimism and caution. *Agricultural Water Management, 97*(4), 528-535. doi:https://doi.org/10.1016/j.agwat.2009.03.023

Molden, D., Oweis, T. Y., Pasquale, S., Kijne, J. W., Hanjra, M. A., Bindraban, P. S., Bouman, B. A., Cook, S., Erenstein, O., & Farahani, H. (2007). *Pathways for increasing agricultural water productivity*.

Monteith, J. (1963). Gas exchange in plant communities. *Environmental control of plant growth, 95*, 112.

Monteith, J. (1972). Solar radiation and productivity in tropical ecosystems. *Journal of applied ecology, 9*(3), 747-766.

Monteith, J. L. (1965, 1965). *Evaporation and environment.* Paper presented at the Symp. Soc. Exp. Biol.

Monteith, J. L. (1981). Evaporation and surface temperature. *Quarterly Journal of the Royal Meteorological Society, 107*(451), 1-27.

Monteith, J. L., & Unsworth, M. H. (2013). Chapter 16 - Micrometeorology: (i) Turbulent Transfer, Profiles, and Fluxes. In J. L. Monteith & M. H. Unsworth (Eds.), *Principles of Environmental Physics (Fourth Edition)* (pp. 289-320). Boston: Academic Press.

Mu, Q., Heinsch, F. A., Zhao, M., & Running, S. W. (2007). Development of a global evapotranspiration algorithm based on MODIS and global meteorology data. *Remote Sensing of Environment, 111*(4), 519-536.

Mu, Q., Zhao, M., & Running, S. W. (2011). Improvements to a MODIS global terrestrial evapotranspiration algorithm. *Remote Sensing of Environment, 115*(8), 1781-1800.

Muniz, P. R., Kalid, R. d. A., Cani, S. P., & Magalhães, R. d. S. (2014). *Handy method to estimate uncertainty of temperature measurement by infrared thermography*.

Nagler, P. L., Cleverly, J., Glenn, E., Lampkin, D., Huete, A., & Wan, Z. (2005). Predicting riparian evapotranspiration from MODIS vegetation indices and meteorological data. *Remote Sensing of Environment, 94*(1), 17-30.

Naidoo, L., Mathieu, R., Main, R., Kleynhans, W., Wessels, K., Asner, G., & Leblon, B. (2015). Savannah woody structure modelling and mapping using multi-frequency (X-, C-and L-band) Synthetic Aperture Radar data. *ISPRS Journal of Photogrammetry and Remote Sensing, 105*, 234-250.

Ndlovu, N. B. (2013). *Quantifying indigenous forest change in Dukuduku from 1960 to 2008 using GIS and remote sensing techniques to support sustainable forest management planning.* Stellenbosch: Stellenbosch University.

Nhamo, L., Ebrahim, G. Y., Mabhaudhi, T., Mpandeli, S., Magombeyi, M., Chitakira, M., Magidi, J., & Sibanda, M. (2019). An assessment of groundwater use in irrigated agriculture using multi-spectral remote sensing. *Physics and Chemistry of the Earth, Parts A/B/C*, 102810.

Nichols, J., Eichinger, W., Cooper, D., Prueger, J., Hipps, L., Neale, C., & Bawazir, A. (2004). Comparison of evaporation estimation methods for a riparian area. *College of Engineering, University of Iowa: Iowa City, IA, USA*.

Nickless, A., Archibald, S., Van der Merwe, M. R., Scholes, R., Williams, C., & Hanan, N. (2011). Estimation of net ecosystem exchange at the Skukuza flux site, Kruger National Park, South Africa.

Nobre, C. A., Sellers, P. J., & Shukla, J. (1991). Amazonian deforestation and regional climate change. *Journal of Climate, 4*(10), 957-988.

Norman, J., Kustas, W., Prueger, J., & Diak, G. (2000). Surface flux estimation using radiometric temperature: A dual‐temperature‐difference method to minimize measurement errors. *Water Resources Research, 36*(8), 2263-2274.

Nyolei, D., Nsaali, M., Minaya, V., van Griensven, A., Mbilinyi, B., Diels, J., Hessels, T., & Kahimba, F. (2019). High resolution mapping of agricultural water productivity using SEBAL in a cultivated African catchment, Tanzania. *Physics and Chemistry of the Earth, Parts A/B/C, 112*, 36-49.

Odipo, V. O., Nickless, A., Berger, C., Baade, J., Urbazaev, M., Walther, C., & Schmullius, C. (2016). Assessment of aboveground woody biomass dynamics using terrestrial laser scanner and L-band ALOS PALSAR data in South African savanna. *Forests, 7*(12), 294.

Paparrizos, S., Maris, F., & Matzarakis, A. (2017). Sensitivity analysis and comparison of various potential evapotranspiration formulae for selected Greek areas with different climate conditions. *Theoretical and Applied Climatology, 128*(3-4), 745-759.

Paul, G., Gowda, P. H., Prasad, P. V., Howell, T. A., Aiken, R. M., & Neale, C. M. (2014). Investigating the influence of roughness length for heat transport (z oh) on the performance of SEBAL in semi-arid irrigated and dryland agricultural systems. *Journal of Hydrology, 509*, 231-244.

Peacock, C. E., & Hess, T. M. (2004). Estimating evapotranspiration from a reed bed using the Bowen ratio energy balance method. *Hydrological Processes, 18*(2), 247-260. doi:doi:10.1002/hyp.1373

Pegram, G., & Bárdossy, A. (2013). Downscaling Regional Circulation Model rainfall to gauge sites using recorrelation and circulation pattern dependent quantile–quantile transforms for quantifying climate change. *Journal of Hydrology, 504*, 142-159.

Penman, H. L. (1948). Natural evaporation from open water, bare soil and grass. *Proceedings of the Royal Society of London.Series A.Mathematical and Physical Sciences, 193*(1032), 120-145.

Perez, P. J., Castellvi, F., Ibañez, M., & Rosell, J. I. (1999). Assessment of reliability of Bowen ratio method for partitioning fluxes. *Agricultural and Forest Meteorology, 97*(3), 141-150. doi:https://doi.org/10.1016/S0168-1923(99)00080-5

Petropoulos, G., Carlson, T. N., Wooster, M. J., & Islam, S. (2009). A review of Ts/VI remote sensing based methods for the retrieval of land surface energy fluxes and soil surface moisture. *Progress in Physical Geography, 33*(2), 224-250.

Platonov, A., Thenkabail, P. S., Biradar, C. M., Cai, X., Gumma, M., Dheeravath, V., Cohen, Y., Alchanatis, V., Goldshlager, N., & Ben-Dor, E. (2008). Water productivity mapping (WPM) using Landsat ETM+ data for the irrigated croplands of the Syrdarya River basin in Central Asia. *Sensors, 8*(12), 8156-8180.

Pretty, J., Benton, T. G., Bharucha, Z. P., Dicks, L. V., Flora, C. B., Godfray, H. C. J., Goulson, D., Hartley, S., Lampkin, N., & Morris, C. (2018). Global assessment of agricultural system redesign for sustainable intensification. *Nature Sustainability, 1*(8), 441-446.

Priestley, C., & Taylor, R. (1972). On the assessment of surface heat flux and evaporation using large-scale parameters. *Monthly Weather Review, 100*(2), 81-92.

Ramoelo, A., Majozi, N., Mathieu, R., Jovanovic, N., Nickless, A., & Dzikiti, S. (2014). Validation of Global Evapotranspiration Product (MOD16) using Flux Tower Data in the African Savanna, South Africa. *Remote Sensing, 6*(8), 7406-7423.

Räsänen, M., Aurela, M., Vakkari, V., Beukes, J. P., Tuovinen, J.-P., Van Zyl, P. G., Josipovic, M., Venter, A. D., Jaars, K., & Siebert, S. J. (2017). Carbon balance of a grazed savanna grassland ecosystem in South Africa. *Biogeosciences, 14*(5), 1039.

Ren, S., White, D., Xiang, D., Short, T., Xiao, W., Chen, J., Deng, Z., & Yang, Z. (2019). Simple model of evapotranspiration by Eucalyptus plantations for data poor areas and tested using water balance data from a small

catchment in Guangxi, China. *Australian Forestry, 82*(sup1), 66-79.

Rockström, J., & Gordon, L. (2001). Assessment of green water flows to sustain major biomes of the world: implications for future ecohydrological landscape management. *Physics and Chemistry of the Earth, Part B: Hydrology, Oceans and Atmosphere, 26*(11), 843-851.

Rockström, J., Karlberg, L., Wani, S. P., Barron, J., Hatibu, N., Oweis, T., Bruggeman, A., Farahani, J., & Qiang, Z. (2010). Managing water in rainfed agriculture—The need for a paradigm shift. *Agricultural Water Management, 97*(4), 543-550.

Roerink, G. J., Su, Z., & Menenti, M. (2000). S-SEBI: A simple remote sensing algorithm to estimate the surface energy balance. *Physics and Chemistry of the Earth, Part B: Hydrology, Oceans and Atmosphere, 25*(2), 147-157. doi:https://doi.org/10.1016/S1464-1909(99)00128-8

Rohwer, C. (1931). *Evaporation from free water surfaces*: US Department of Agriculture.

Saint-Geours, N., & Lilburne, L. (2010). *Comparison of three spatial sensitivity analysis techniques.* Paper presented at the Proceedings of the Ninth International Symposium on Spatial Accuracy Assessment in Natural Resources and Environmental Sciences.

Sala, O., Lauenroth, W., & Parton, W. (1992). Long‐term soil water dynamics in the shortgrass steppe. *Ecology, 73*(4), 1175-1181.

Saltelli, A., Tarantola, S., Campolongo, F., & Ratto, M. (2004). *Sensitivity analysis in practice: a guide to assessing scientific models*: Wiley.

Sánchez, J. M., Caselles, V., & Rubio, E. M. (2010). Analysis of the energy balance closure over a FLUXNET boreal forest in Finland. *Hydrology and Earth System Sciences, 14*(8), 1487-1497.

Saux-Picart, S., Ottlé, C., Perrier, A., Decharme, B., Coudert, B., Zribi, M., Boulain, N., Cappelaere, B., & Ramier, D. (2009). SEtHyS_Savannah: A multiple source land surface model applied to Sahelian landscapes. *Agricultural and Forest Meteorology, 149*(9), 1421-1432. doi:10.1016/j.agrformet.2009.03.013

Schaaf, C., Liu, J., Gao, F., & Strahler, A. H. (2011). MODIS albedo and reflectance anisotropy products from Aqua and Terra. *Land Remote Sensing and Global Environmental Change: NASA's Earth Observing System and the Science of ASTER and MODIS, 11*, 549-561.

Schaaf, C. B., Gao, F., Strahler, A. H., Lucht, W., Li, X., Tsang, T., Strugnell, N. C., Zhang, X., Jin, Y., & Muller, J.-P. (2002). First operational BRDF, albedo nadir reflectance products from MODIS. *Remote Sensing of Environment, 83*(1-2), 135-148.

Scheierling, S. M., Treguer, D. O., Booker, J. F., & Decker, E. (2014). *How to Assess Agricultural Water Productivity? Looking for Water in the Agricultural Productivity and Efficiency Literature. Policy Research Working Paper*. Retrieved from Washington, DC:

Schmid, H. (1994). Source areas for scalars and scalar fluxes. *Boundary-Layer Meteorology, 67*(3), 293-318.

Scholes, R. J., Bond, W. J., & Eckhardt, H. C. (2003). *Vegetation dynamics in the Kruger ecosystem*: The Kruger Experience. Island Press.

Scholes, R. J., Gureja, N., Giannecchinni, M., Dovie, D., Wilson, B., Davidson, N., Piggott, K., McLoughlin, C., Van der Velde, K., & Freeman, A. (2001). The environment and vegetation of the flux measurement site near Skukuza, Kruger National Park. *Koedoe-African Protected Area Conservation and Science, 44*(1), 73-83.

Sellers, P., Meeson, B., Hall, F., Asrar, G., Murphy, R., Schiffer, R., Bretherton, F., Dickinson, R., Ellingson, R., & Field, C. (1995). Remote sensing of the land surface for studies of global change: Models—algorithms—experiments. *Remote Sensing of Environment, 51*(1), 3-26.

Semmens, K. A., Anderson, M. C., Kustas, W. P., Gao, F., Alfieri, J. G., McKee, L., Prueger, J. H., Hain, C. R., Cammalleri, C., & Yang, Y. (2016). Monitoring daily evapotranspiration over two California vineyards using Landsat 8 in a multi-sensor data fusion approach. *Remote Sensing of Environment, 185*, 155-170.

Senay, G., Gowda, P. H., Bohms, S., Howell, T., Friedrichs, M., Marek, T., & Verdin, J. (2014). Evaluating the SSEBop approach for evapotranspiration mapping with landsat data using lysimetric observations in the semi-arid Texas High Plains. *Hydrology and Earth System Sciences Discussions, 11*(1), 723-756.

Senay, G., Verdin, J., Lietzow, R., & Melesse, A. M. (2008). Global daily reference evapotranspiration modeling and evaluation 1. *JAWRA Journal of the American Water Resources Association, 44*(4), 969-979.

Shine, K. P. (1984). Parametrization of the shortwave flux over high albedo surfaces as a function of cloud thickness and surface albedo. *Quarterly Journal of the Royal Meteorological Society, 110*(465), 747-764.

Shugart, H. H., Macko, S. A., Lesolle, P., Szuba, T. A., Mukelabai, M. M., Dowty, P., & Swap, R. J. (2004). The SAFARI 2000–Kalahari transect wet season campaign of year 2000. *Global Change Biology, 10*(3), 273-280.

Singh, R. K., & Senay, G. B. (2015). Comparison of four different energy balance models for estimating evapotranspiration in the Midwestern United States. *Water, 8*(1), 9.

Smith, K. A., & Cresser, M. S. (2003). *Soil and environmental analysis: modern instrumental techniques*: CRC Press.

Song, L., Kustas, W. P., Liu, S., Colaizzi, P. D., Nieto, H., Xu, Z., Ma, Y., Li, M., Xu, T., & Agam, N. (2016). Applications of a thermal-based two-source energy balance model using Priestley-Taylor approach for surface temperature partitioning under advective conditions. *Journal of Hydrology, 540*, 574-587.

Stisen, S., Sandholt, I., Nørgaard, A., Fensholt, R., & Jensen, K. H. (2008). Combining the triangle method with thermal inertia to estimate regional evapotranspiration—Applied to MSG-SEVIRI data in the Senegal River basin. *Remote Sensing of Environment, 112*(3), 1242-1255.

Strahler, A. H., Muller, J., Lucht, W., Schaaf, C., Tsang, T., Gao, F., Li, X., Lewis, P., & Barnsley, M. J. (1999). MODIS BRDF/albedo product: algorithm theoretical basis document version 5.0. *MODIS documentation, 23*(4), 42-47.

Stull, R. B. (2012). *An introduction to boundary layer meteorology* (Vol. 13): Springer Science & Business Media.

Su, H.-B., Schmid, H. P., Grimmond, C. S. B., Vogel, C. S., & Oliphant, A. J. (2004). Spectral characteristics and correction of long-term eddy-covariance measurements over two mixed hardwood forests in non-flat terrain. *Boundary-Layer Meteorology, 110*(2), 213-253.

Su, Z. (1999). The Surface Energy Balance System (SEBS) for estimation of turbulent heat fluxes. *Hydrology and Earth System Sciences, 6*(1), 85-100.

Su, Z. (2002). The Surface Energy Balance System (SEBS) for estimation of turbulent heat fluxes. *Hydrology and Earth System Sciences Discussions, 6*(1), 85-100.

Sun, L., Liang, S., Yuan, W., & Chen, Z. (2013). Improving a Penman–Monteith evapotranspiration model by incorporating soil moisture control on soil evaporation in semiarid areas. *International Journal of Digital Earth*(ahead-of-print), 1-23.

Sun, Z., Gebremichael, M., Ardö, J., Nickless, A., Caquet, B., Merboldh, L., & Kutschi, W. (2012). Estimation of daily evapotranspiration over Africa using MODIS/Terra and SEVIRI/MSG data. *Atmospheric Research, 112*(0), 35-44. doi:10.1016/j.atmosres.2012.04.005

Szilagyi, J., Parlange, M. B., & Katul, G. G. (2014). Assessment of the Priestley-Taylor parameter value from ERA-Interim global reanalysis data. *J. Hydrol. Environ. Res, 2*(1), 1-7.

Tabari, H., & Hosseinzadeh Talaee, P. (2014). Sensitivity of evapotranspiration to climatic change in different climates. *Global and Planetary Change, 115*, 16-23. doi:https://doi.org/10.1016/j.gloplacha.2014.01.006

Tang, R., Li, Z.-L., & Tang, B. (2010). An application of the< i> T</i>< sub> s</sub>–VI triangle method with enhanced edges determination for evapotranspiration estimation from MODIS data in arid and semi-arid regions: Implementation and validation. *Remote Sensing of Environment, 114*(3), 540-551.

Tantawy, I. (2019). The application of the FAO WaPOR data portal to monitor efficient water use in agriculture: A case study on the Eastern Nile River Basin.

Thenkabail, P. S., Hanjra, M. A., Dheeravath, V., & Gumma, M. (2010). A Holistic View of Global Croplands and Their Water Use for Ensuring Global Food Security in the 21st Century through Advanced Remote Sensing and Non-remote Sensing Approaches. *Remote Sensing, 2*(1), 211-261. doi:10.3390/rs2010211

Thompson, M. W. (2019). *South African National Land-Cover 2018 Report and Accuracy Assessment*. Retrieved from South Africa:

Trambauer, P., Dutra, E., Maskey, S., Werner, M., Pappenberger, F., van Beek, L. P. H., & Uhlenbrook, S. (2014). Comparison of different evaporation estimates over the African continent. *Hydrol. Earth Syst. Sci., 18*(1), 193-212. doi:10.5194/hess-18-193-2014

Trenberth, K. E., Fasullo, J. T., & Kiehl, J. (2009). Earth's Global Energy Budget. *Bulletin of the American Meteorological Society, 90*(3), 311-324. doi:10.1175/2008bams2634.1

Trenberth, K. E., Smith, L., Qian, T., Dai, A., & Fasullo, J. (2007). Estimates of the global water budget and its annual cycle using observational and model data. *Journal of Hydrometeorology, 8*(4), 758-769.

Tscharntke, T., Clough, Y., Wanger, T. C., Jackson, L., Motzke, I., Perfecto, I., Vandermeer, J., & Whitbread, A. (2012). Global food security, biodiversity conservation and the future of agricultural intensification. *Biological conservation, 151*(1), 53-59.

Twine, T. E., Kustas, W. P., Norman, J. M., Cook, D. R., Houser, P., Meyers, T. P., Prueger, J. H., Starks, P. J., & Wesely, M. L. (2000). Correcting eddy-covariance flux underestimates over a grassland. *Agricultural and Forest Meteorology, 103*(3), 279-300.

UNESCO, & Earthscan. (2009). *The United Nations World Water Development Report 3: Water in a changing World*. Retrieved from Paris, France: http://unesdoc.unesco.org/images/0018/001819/181993e.pdf

Van der Kwast, J., Timmermans, W., Gieske, A., Su, Z., Olioso, A., Jia, L., Elbers, J., Karssenberg, D., De Jong, S., & de Jong, S. (2009). Evaluation of the Surface Energy Balance System (SEBS) applied to ASTER imagery with flux-measurements at the SPARC 2004 site (Barrax, Spain). *Hydrology and Earth System Sciences Discussions, 6*(1), 1165-1196.

Veroustraete, F., Sabbe, H., & Eerens, H. (2002). Estimation of carbon mass fluxes over Europe using the C-Fix model and Euroflux data. *Remote Sensing of Environment, 83*(3), 376-399.

Vinukollu, R. K., Meynadier, R., Sheffield, J., & Wood, E. F. (2011a). Multi‐model, multi‐sensor estimates of global evapotranspiration: climatology, uncertainties and trends. *Hydrological Processes*.

Vinukollu, R. K., Wood, E. F., Ferguson, C. R., & Fisher, J. B. (2011b). Global estimates of evapotranspiration for climate studies using multi-sensor remote sensing data: Evaluation of three process-based approaches. *Remote Sensing of Environment, 115*(3), 801-823.

Von Randow, C., Manzi, A. O., Kruijt, B., De Oliveira, P. J., Zanchi, F. B., Silva, R. L., Hodnett, M. G., Gash, J. H. C., Elbers, J. A., & Waterloo, M. J. (2004). Comparative measurements and seasonal variations in energy and carbon exchange over forest and pasture in South West Amazonia. *Theoretical and Applied Climatology, 78*(1-3), 5-26.

Wan, Z. (1999). MODIS land-surface temperature algorithm theoretical basis document (LST ATBD). *Institute for Computational Earth System Science, Santa Barbara, 75*.

Wan, Z. (2008). New refinements and validation of the MODIS land-surface temperature/emissivity products. *Remote Sensing of Environment, 112*(1), 59-74.

Wan, Z., & Dozier, J. (1996). A generalized split-window algorithm for retrieving land-surface temperature from space. *Geoscience and Remote Sensing, IEEE Transactions on, 34*(4), 892-905.

Wang, J., Sammis, T., Gutschick, V., Gebremichael, M., & Miller, D. (2009). Sensitivity analysis of the surface energy balance algorithm for land (SEBAL). *Transactions of the ASABE, 52*(3), 801-811.

Wang, K., & Dickinson, R. E. (2012). A review of global terrestrial evapotranspiration: Observation, modeling, climatology, and climatic variability. *Reviews of Geophysics, 50*(2), RG2005.

Wang, K., Li, Z., & Cribb, M. (2006). Estimation of evaporative fraction from a combination of day and night land surface temperatures and NDVI: A new method to determine the Priestley–Taylor parameter. *Remote Sensing of Environment, 102*(3), 293-305.

Wang, K., Liu, J., Zhou, X., Sparrow, M., Ma, M., Sun, Z., & Jiang, W. (2004). Validation of the MODIS global land surface albedo product using ground measurements in a semidesert region on the Tibetan Plateau. *Journal of Geophysical Research: Atmospheres, 109*(D5).

Wang, X.-G., Wang, W., Huang, D., Yong, B., & Chen, X. (2014). Modifying SEBAL model based on the trapezoidal relationship between land surface

temperature and vegetation index for actual evapotranspiration estimation. *Remote Sensing, 6*(7), 5909-5937.

Wanner, W., Strahler, A., Hu, B., Lewis, P., Muller, J. P., Li, X., Schaaf, C. B., & Barnsley, M. (1997). Global retrieval of bidirectional reflectance and albedo over land from EOS MODIS and MISR data: Theory and algorithm. *Journal of Geophysical Research: Atmospheres, 102*(D14), 17143-17161.

Were, A., Villagarcía, L., Domingo, F., Alados-Arboledas, L., & Puigdefábregas, J. (2007). Analysis of effective resistance calculation methods and their effect on modelling evapotranspiration in two different patches of vegetation in semi-arid SE Spain. *Hydrology and Earth System Sciences Discussions, 11*(5), 1529-1542.

Westerhoff, R. S. (2015). Using uncertainty of Penman and Penman–Monteith methods in combined satellite and ground-based evapotranspiration estimates. *Remote Sensing of Environment, 169*, 102-112. doi:http://dx.doi.org/10.1016/j.rse.2015.07.021

Whitfield, A., & Taylor, R. (2009). A review of the importance of freshwater inflow to the future conservation of Lake St Lucia. *Aquatic Conservation: Marine and Freshwater Ecosystems, 19*(7), 838-848.

Wilczak, J. M., Oncley, S. P., & Stage, S. A. (2001). Sonic anemometer tilt correction algorithms. *Boundary-Layer Meteorology, 99*(1), 127-150.

Williams, C. A., Hanan, N., Scholes, R. J., & Kutsch, W. (2009). Complexity in water and carbon dioxide fluxes following rain pulses in an African savanna. *Oecologia, 161*(3), 469-480.

Wilson, K., Goldstein, A., Falge, E., Aubinet, M., Baldocchi, D., Berbigier, P., Bernhofer, C., Ceulemans, R., Dolman, H., & Field, C. (2002). Energy balance closure at FLUXNET sites. *Agricultural and Forest Meteorology, 113*(1), 223-243.

Wofsy, S., Goulden, M., Munger, J., Fan, S.-M., Bakwin, P., Daube, B., Bassow, S., & Bazzaz, F. (1993). Net exchange of CO2 in a mid-latitude forest. *Science, 260*(5112), 1314-1317.

Xin, X., & Liu, Q. (2010). The Two-layer Surface Energy Balance Parameterization Scheme (TSEBPS) for estimation of land surface heat fluxes. *Hydrology and Earth System Sciences, 14*(3), 491-504.

Yang, Y., Long, D., Guan, H., Liang, W., Simmons, C., & Batelaan, O. (2015a). Comparison of three dual‐source remote sensing evapotranspiration models during the MUSOEXE‐12 campaign: Revisit of model physics. *Water Resources Research, 51*(5), 3145-3165.

Yang, Y., Su, H., Zhang, R., Tian, J., & Li, L. (2015b). An enhanced two-source evapotranspiration model for land (ETEML): Algorithm and evaluation. *Remote Sensing of Environment, 168*, 54-65.

Yao, Y., Liang, S., Cheng, J., Liu, S., Fisher, J. B., Zhang, X., Jia, K., Zhao, X., Qin, Q., & Zhao, B. (2013). MODIS-driven estimation of terrestrial latent heat flux in China based on a modified Priestley–Taylor algorithm. *Agricultural and Forest Meteorology, 171*, 187-202.

Yao, Y., Liang, S., Zhao, S., Zhang, Y., Qin, Q., Cheng, J., Jia, K., Xie, X., Zhang, N., & Liu, M. (2014). Validation and application of the modified satellite-based Priestley-Taylor algorithm for mapping terrestrial evapotranspiration. *Remote Sensing, 6*(1), 880-904.

Yuling, F. U. (2005). Energy balance closure at ChinaFLUX sites.

Zhang, K., Kimball, J. S., & Running, S. W. (2016). A review of remote sensing based actual evapotranspiration estimation. *Wiley Interdisciplinary Reviews: Water, 3*(6), 834-853.

Zuo, J.-q., Wang, J.-m., Huang, J.-p., Li, W., Wang, G., & Ren, H. (2011). Estimation of ground heat flux and its impact on the surface energy budget for a semi-arid grassland. *Sci Cold Arid Region, 3*, 41-50.

Zwart, S. J., Bastiaanssen, W. G., de Fraiture, C., & Molden, D. J. (2010a). WATPRO: A remote sensing based model for mapping water productivity of wheat. *Agricultural Water Management, 97*(10), 1628-1636.

Zwart, S. J., & Bastiaanssen, W. G. M. (2004). Review of measured crop water productivity values for irrigated wheat, rice, cotton and maize. *Agricultural Water Management, 69*(2), 115-133. doi:https://doi.org/10.1016/j.agwat.2004.04.007

Zwart, S. J., Bastiaanssen, W. G. M., de Fraiture, C., & Molden, D. J. (2010b). A global benchmark map of water productivity for rainfed and irrigated wheat. *Agricultural Water Management, 97*(10), 1617-1627. doi:https://doi.org/10.1016/j.agwat.2010.05.018

Zwart, S. J., & Leclert, L. M. (2010). A remote sensing-based irrigation performance assessment: a case study of the Office du Niger in Mali. *Irrigation Science, 28*(5), 371-385.

Publications

Dzikiti S., Jovanovic N. Z., Bugan R. D. H., Ramoelo A, **Majozi N. P.**, Nickless A., Cho M. A, Le Maitre D. C., Ntshidi Z., Pienaar H. H. 2019. Comparison of two remote sensing models for estimating evapotranspiration: algorithm evaluation and application in seasonally arid ecosystems in South Africa. Journal of Arid Lands, 11(4), 495-512.

Majozi N. P., Mannaerts C. M., Ramoelo A., Mathieu R., Mudau A.E., Verhoef W. 2017. An intercomparison of satellite-based daily evapotranspiration estimates under different eco-climatic regions in South Africa. Remote Sensing, 9 (4), 307.

Majozi N. P., Mannaerts C. M., Ramoelo A., Mathieu R., Nickless A., Verhoef W. 2017. Analysing surface energy balance closure and partitioning over a semi-arid savanna FLUXNET site in Skukuza, Kruger National Park, South Africa. Hydrology and Earth System Sciences, 21(7), 3401.

Ramoelo A., **Majozi N. P.**, Mathieu R., Jovanovic N., Nickless A., Dzikiti S. 2014. Validation of Global evapotranspiration product (MOD16) using flux tower data in the African savanna, South Africa. Remote Sensing, 6(8), 7406-7423.

Conferences

Majozi N. P., Mannaerts C. M., Ramoelo A., Mathieu R., Mudau A.E., Verhoef W. 2017. Parameterizing net radiation for evapotranspiration modelling using remote sensing data. 37th International Symposium on Remote Sensing of Environment. CSIR, Pretoria, South Africa. Oral presentation.

Majozi N. P., Mannaerts C. M., Ramoelo A., Mathieu R., Nickless A., Verhoef W. 2015. Evaluation of Remote sensing - derived daily evapotranspiration estimates under contrasting natural ecosystems in South Africa. Earth Observation for Water Cycle Science. ESA-ESRIN, Italy. Poster presentation.

Majozi N. P., Mannaerts C. M., Ramoelo A., Mathieu R., Nickless A., Verhoef W. 2015. Analyzing surface energy balance partitioning and closure over a semi-arid savanna FLUXNET site in Skukuza, Kruger National Park, South Africa. Emerging Researchers Symposium. CSIR, Pretoria, South Africa. Poster presentation.